ФИЗИКА ЭЛЕМЕНТАРНЫХ ЧАСТИЦ И АТОМНОГО ЯДРА
2009. Т. 40. ВЫП. 3

FINITE-SIZE EFFECT ON TWO-PARTICLE PRODUCTION IN CONTINUOUS AND DISCRETE SPECTRUM

*R. Lednický**

Joint Institute for Nuclear Research, Dubna
Institute of Physics ASCR, Prague, Czech Republic

INTRODUCTION 596

FORMALISM 600

APPROXIMATE DESCRIPTION OF THE $\pi^+\pi^-$ PRODUCTION 606

CORRELATION FEMTOSCOPY — BASIC ASSUMPTIONS 611
- Noninteracting Nonidentical Particles: Space-Time Coherence. 611
- Noninteracting Identical Particles: QS Correlations. 614
- Interacting Particles: FSI Correlations. 619

ONE-CHANNEL WAVE FUNCTIONS 630
- Continuous Spectrum. 630
- Discrete Spectrum. 638
- Universality. 642
- The n Dependence. 644

TWO-CHANNEL WAVE FUNCTIONS 646
- Continuous Spectrum in Both Channels. 646
- Discrete Spectrum in the α Channel. 649
- Universality. 651

FINITE-SIZE EFFECT IN THE DIRAC EXPERIMENT 653
- $\pi^+\pi^-$ System. 653
- $\pi^-\pi^-$ and $\pi^+\pi^+$ Systems. 663

CONCLUSIONS 667

REFERENCES 673

*E-mail: lednicky@fzu.cz

ФИЗИКА ЭЛЕМЕНТАРНЫХ ЧАСТИЦ И АТОМНОГО ЯДРА
2009. Т. 40. ВЫП. 3

FINITE-SIZE EFFECT ON TWO-PARTICLE PRODUCTION IN CONTINUOUS AND DISCRETE SPECTRUM

R. Lednický[*]

Joint Institute for Nuclear Research, Dubna
Institute of Physics ASCR, Prague, Czech Republic

The formalism allowing one to account for the effect of a finite space-time extent of particle-production region is given. Its applications to the lifetime measurement of hadronic atoms produced by a high-energy beam in a thin target, as well as to the femtoscopy techniques widely used to measure space-time characteristics of the production processes, are discussed. Particularly, it is found that the neglect of the finite-size effect on the pionium lifetime measurement in the DIRAC experiment at CERN could lead to the lifetime overestimation comparable with the 10% statistical error. The theoretical systematic errors arising in the calculation of the finite-size effect due to the neglect of nonequal emission times in the pair center-of-mass system, the space-time coherence and the residual charge are shown to be negligible.

Изложен формализм, позволяющий учесть эффект конечных пространственно-временных размеров области генерации частиц. Обсуждается применение этого формализма к измерению времени жизни адронных атомов, образованных при взаимодействии пучка частиц высокой энергии с тонкой мишенью, а также к измерению пространственно-временных характеристик процессов генерации частиц с помощью фемтоскопических методов. В частности, показано, что пренебрежение эффектом конечных размеров при измерении времени жизни пиония в эксперименте DIRAC в CERN может привести к завышению времени жизни, сравнимому с 10 %-й статистической ошибкой. Показано, что при вычислении эффекта конечных размеров можно пренебречь неодинаковостью времен эмиссии в системе центра масс двух частиц, пространственно-временной когерентностью и остаточным зарядом.

PACS: 03.65; 25.75; 36.10

INTRODUCTION

The determination, on a percent level accuracy, of the breakup probability of the $\pi^+\pi^-$ atoms produced by a high-energy beam in a thin target is of principle importance for a precise lifetime measurement of these atoms in the DIRAC experiment at CERN [1–4]. This experiment aims to measure the lifetime τ_{10} of the $\pi^+\pi^-$ atoms in the ground state with 10% precision. As this lifetime of the

[*]E-mail: lednicky@fzu.cz

order of 10^{-15} s is determined by the probability of the annihilation $\pi^+\pi^- \to \pi^0\pi^0$: $1/\tau_{10} \sim |a_0^0 - a_0^2|^2$, the DIRAC measurement enables one to determine the absolute value of the difference $a_0^0 - a_0^2$ of the s-wave isoscalar and isotensor $\pi\pi$-scattering lengths to 5%. This represents a factor of 4 improvement of the accuracy achieved in previous studies [5] and is comparable with the precision of the most recent experiments E865 at BNL [6] and NA48/2 at CERN [7]. The former is based on a study of K_{e4} decays and yields the statistical error of 6% in a_0^0; this measurement essentially exploits other experimental data together with dispersion relations (Roy equations), the systematic and theoretical errors being estimated on the level of several percent. The latter studied the cusp effect at the $\pi^+\pi^-$ threshold in the distribution of the $2\pi^0$ effective mass in $K^\pm \to \pi^\pm\pi^0\pi^0$ decays and yields $|a_0^0 - a_0^2|$ with a few percent statistical precision and $\sim 5\%$ theoretical error. Both these measurements are in agreement with the preliminary DIRAC result based on $\sim 40\%$ of the collected statistics [4], as well as with the prediction of the standard chiral perturbation theory [8].

It should be stressed that the theoretical prediction for the difference $a_0^0 - a_0^2$ depends on the structure of the QCD vacuum. Thus, on the standard assumption of a strong quark condensate one has $a_0^0 - a_0^2 = (0.374 \pm 0.006)$ fm [8]. With the decreasing condensate this difference increases and can be up to 25% larger [9]. The precise measurements of the $\pi\pi$-scattering lengths thus submit the understanding of chiral symmetry breaking of QCD to a crucial test.

The method of the lifetime measurement is based on the production of $\pi^+\pi^-$ atoms in a thin target and subsequent detection of highly correlated $\pi^+\pi^-$ pairs leaving the target as a result of the breakup of a part of the $\pi^+\pi^-$ atoms which did not decay within the target [10]. Clearly, the breakup probability is a unique function of the target geometry and material, the Lorentz factor and the ground-state lifetime of the $\pi^+\pi^-$ atom. The analysis shows that, to achieve the accuracy of 10% in the lifetime, the breakup probability, in more or less optimal conditions, should be measured to 4% [1].

There are two methods [2] — extrapolation and subtraction ones — which can be used to measure the breakup probability $P_{\rm br}$ (or a combination of the breakup probabilities in different targets) defined as the ratio of the number $N_A^{\rm br}$ of breakup atoms to the number N_A of the atoms produced in the target:

$$P_{\rm br} = \frac{N_A^{\rm br}}{N_A}. \tag{1}$$

The extrapolation method requires the calculation of the number of produced $\pi^+\pi^-$ atoms N_A based on the theory of the final-state interaction (FSI) in discrete and continuous spectrum [10–12]. This calculation, as well as the determination of $N_A^{\rm br}$, is not required in the subtraction method which exploits the data taken on at least three different targets made out of the same material but consisting of a different number of layers of the same total thickness. However, this method

needs a factor of 7 larger statistics [1] and cannot yield the required precision within the approved time-scale of the DIRAC experiment.

The FSI effect on $\pi^+\pi^-$ production is sensitive to the space-time extent of the pion-production region mainly through the distance r^* between the π^+- and π^--production points in their center-of-mass (c.m.) system. In [10], only the Coulomb FSI was considered and the r^* dependence was treated in an approximate way, dividing the pion emitters into short-lived (SL) and long-lived (LL) ones. It was assumed that $r^* = 0$ for pion pairs arising solely from the SL emitters and characterized by the distances r^* much smaller than the Bohr radius $|a|$ of the $\pi^+\pi^-$ system ($a = -387.5$ fm), otherwise $r^* = \infty$.

The finite-size correction to such calculated number of nonatomic $\pi^+\pi^-$ pairs in the region of very small relative momenta in the pair c.m. system, $Q \ll 1/r^*$, is determined by the three dimensionless combinations r^*/a, f_0/r^*, and f_0/a of r^*, a and the s-wave $\pi^+\pi^-$-scattering length: $f_0 = (1/3)(2a_0^0 + a_0^2) \approx 0.2$ fm. Typically $\langle r^* \rangle^{\text{SL}} \sim 10$ fm so that the correction is dominated by the strong interaction effect and can amount up to $\sim 10\%$.

Fortunately, due to a small binding energy $\epsilon_b \sim (m_\pi a^2)^{-1}$, the finite-size correction to the production probability in discrete spectrum at $r^* \ll |a|$ is nearly the same as that in continuous spectrum at zero energy. Since the calculated number N_A of produced atoms is approximately determined by the measured number of nonatomic $\pi^+\pi^-$ pairs and by the ratio of weighted means of the finite-size correction factors corresponding to the production in discrete and continuous spectrum, the finite-size correction would cancel out in N_A, up to $O((r^*/a)^2)$ and $O(f_0/a)$, provided we could measure the number of nonatomic pairs in the region of very small $Q \ll 1/r^*$ [13, 14].

At small values of Q and r^*, the relative correction to the number of nonatomic pairs is positive (due to the effect of the strong FSI $\sim 2f_0/r^*$) and changes sign at $r^* \sim 10$ fm (due to negative finite-size effect of the Coulomb FSI $\sim 2r^*/a$). It appears that for $r^* < 20$ fm the correction shows a quasi-linear behaviour in Q up to ~ 50 MeV/c, with almost a universal negative slope. For larger distances r^*, the slope becomes positive and has a nontrivial Q dependence. If the pions were produced at small distances r^* of several fm, one could safely neglect the nonuniversal correction $O((r^*/a)^2)$ and use the quasi-linear Q dependence of the correction factor to interpolate to $Q = 0$. However, there is a non-negligible tail of the distances $r^* > 10$ fm due to particle rescatterings and resonances (particularly, $r^* \sim 30$ fm in the case when one of the two pions comes from the ω-meson decay). In the DIRAC experiment, the finite-size correction can lead to a percent underestimation of N_A and to several percent overestimation of N_A^{br}. As a result, the corresponding overestimation of the extracted lifetime can be comparable with the 10% statistical error and should be taken into account.

We discuss how to diminish the systematic error due to the finite-size effect on the lifetime measurement of hadronic atoms, using the correlation data on identical charged pions (containing the information about the distances r^* between the pion production points in the same experiment) together with the complete phase-space simulations within transport models.

The formalism accounting for the finite space-time separation of particle emitters is also in the basis of the correlation measurements of the space-time characteristics of particle production — the so-called *particle interferometry* or *correlation femtoscopy* (see reviews [15–21]). In fact, the femtoscopic correlations due to the Coulomb FSI between the emitted electron or positron and the residual nucleus in beta decay are known for more than 70 years; the sensitivity of the differential decay rate to the nucleus charge and radius is taken into account in terms of the Fermi function which can be considered as an analogue of the correlation function in multiparticle production (see [22] for a discussion of the similarity and difference of femtoscopic correlations in beta decay and multiparticle production). The femtoscopic correlations due to the quantum statistics (QS) of produced identical particles were observed almost 50 years ago as an enhanced production of pairs of identical pions with small opening angles (GGLP effect). The basics of the modern correlation femtoscopy were settled by Kopylov and Podgoretsky in early seventieth of the last century; they also pointed out a striking analogy between the femtoscopic momentum correlations of identical particles and the spectroscopic space-time correlations of photons (HBT effect), the latter allowing one to measure the spectral width of the light source, as well as the angular radii of distant (stellar) objects (see [22] and references therein). Besides the space-time characteristics of particle production, the femtoscopic correlations yield also a valuable information on low-energy strong interaction between specific particles which can hardly be achieved by other means (see [20] and Subsubsec. 3.3.5).

The paper is organized now as follows. In Secs. 1 and 3, we give the basics of the theory of two-particle correlations due to the FSI and QS effects. Particularly, the formalism and assumptions behind the correlation femtoscopy are discussed in Sec. 3. Sections 4 and 5 deal with the one- and two-channel wave functions in the continuous and discrete spectrum. In Secs. 2 and 6, we apply the developed formalism to estimate the finite-size effect on the pionium lifetime measurement in the DIRAC experiment at CERN. The results are summarized in Conclusions. In Appendices A and B we consider the effect of nonequal times and derive the analytical expression for the normalization effect of the short-range interaction on the wave function of a hadronic atom, modifying the usual $n^{-3/2}$ dependence of the pure Coulomb wave function on the main quantum number n. The reader interested mainly in practical application of the formalism to the lifetime measurement of hadronic atoms can start reading from Secs. 2 and 6 and consult the rest of the paper to clarify the eventual questions.

1. FORMALISM

Production of two particles at small relative momenta is strongly influenced by their mutual FSI and, for identical particles, also by QS. One can separate the FSI effect from the production amplitude provided a sufficiently long two-particle interaction time in the final state as compared with the characteristic time of the production process. This condition requires the magnitude of the relative three-momentum $\mathbf{q}^* = \mathbf{p}_1^* - \mathbf{p}_2^* \equiv 2\mathbf{k}^* \equiv \mathbf{Q}$ in the two-particle c.m. system much smaller than several hundreds of MeV/c — the momentum transfer typical for particle production. For a two-particle bound state the momentum k^* in this condition has to be substituted by $(2\mu\epsilon_b)^{1/2}$, where ϵ_b is the binding energy, and $\mu = m_1 m_2/(m_1 + m_2)$ is the reduced mass.

Consider first the differential cross section for the production of a pair of nonidentical particles 1 and 2 with the four-momenta $p_i = \{\omega_i, \mathbf{p}_i\}$ and the Lorentz factors $\gamma_i = \omega_i/m_i$. It can be expressed through the invariant production amplitudes $T(p_1, p_2; \alpha)$ in the form

$$(2\pi)^6 \gamma_1 \gamma_2 \frac{d^6\sigma}{d^3\mathbf{p}_1\, d^3\mathbf{p}_2} = \sum_\alpha |T(p_1, p_2; \alpha)|^2, \tag{2}$$

where the sum is done over $\alpha = \{S, M, \alpha'\}$, i.e., the total spin S of the pair and its projection M (which is equivalent to the sum over helicities of the two particles) and the quantum numbers α' of other produced particles, including integration over their momenta with the energy-momentum conservation taken into account.

We are interested in the pairs $(1, 2)$ of the particles produced with a small relative velocity in a process with an ordinary phase space density of final-state particles so that a main contribution to the double inclusive cross section comes from the configurations $(1, 2, \ldots, i, \ldots)$ with large relative velocities of the particles 1 and 2 with respect to other produced particles $(i = 3, 4, \ldots, n)$. Due to a sharp fall of FSI with the increasing relative velocity, we can then neglect the effect of FSI in all pairs $(1, i)$ and $(2, i)$ except $(1, 2)$ and, in accordance with the upper diagram in Fig. 1, write the production amplitude as (see however [23] and Subsubsec. 3.3.3 for the account of the residual Coulomb field)

$$T(p_1, p_2; \alpha) = T_0(p_1, p_2; \alpha) + \Delta T(p_1, p_2; \alpha). \tag{3}$$

Here $T_0(p_1, p_2; \alpha)$ is the production amplitude in the case of no FSI, and $\Delta T(p_1, p_2; \alpha)$ represents the contribution of the FSI between particles 1 and 2, described by the formula

$$\Delta T(p_1, p_2; \alpha) = \frac{i\sqrt{P^2}}{2\pi^3} \int d^4\kappa \frac{T_0(\kappa, P - \kappa; \alpha) f^{S*}(p_1, p_2; \kappa, P - \kappa)}{(\kappa^2 - {m_1}^2 - i0)[(P - \kappa)^2 - {m_2}^2 - i0]}, \tag{4}$$

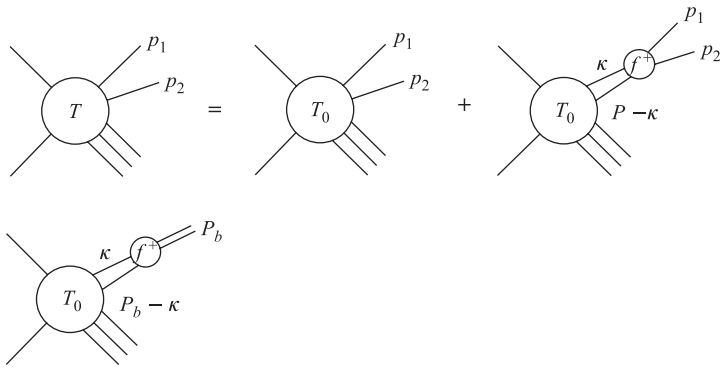

Fig. 1. The diagrams describing production of particles 1 and 2 in continuous and discrete spectrum

where $P \equiv 2p = p_1 + p_2$, $T_0(\kappa, P-\kappa; \alpha)$ is the production amplitude analytically continued off mass-shell; $f^S(p_1, p_2; \kappa, P-\kappa)$ is the scattering amplitude of particles 1 and 2 also analytically continued to the unphysical region. In the case of small k^*, we are interested in, the central forces dominate, so the scattering amplitude f^S is diagonal with respect to the total spin S and does not depend on its projections. Since most of the systems of our interest ($\pi^+\pi^-$, $K^\pm\pi^\mp$, $\pi^- p$, K^+K^-, $K^- p$, except for $\bar{p}p$) are described by a single value of S, we will often skip it to simplify the notation.

Let us express the amplitude T_0 in a form of the Fourier integral

$$T_0(p_1, p_2; \alpha) = \int d^4x_1\, d^4x_2\, \mathrm{e}^{-ip_1x_1 - ip_2x_2} \mathcal{T}(x_1, x_2; \alpha) = \\ = \int d^4x\, \mathrm{e}^{-i\tilde{q}x/2} \tau_P(x; \alpha), \quad (5)$$

where the last expression arises after the integration over the pair c.m. four-coordinate $X = [(p_1P)x_1 + (p_2P)x_2]/P^2$ ($d^4x_1 d^4x_2 = d^4X d^4x$) based on the separation of the phase factors due to the free c.m. and relative motions: $\mathrm{e}^{-ip_1x_1 - ip_2x_2} = \mathrm{e}^{-iPX}\, \mathrm{e}^{-i\tilde{q}x/2}$. Here the relative four-coordinate $x \equiv \{t, \mathbf{r}\} = x_1 - x_2$ and the generalized relative four-momentum $\widetilde{q} = q - P(qP)/P^2$, $q = p_1 - p_2$; note that $qP = {m_1}^2 - {m_2}^2$. Apparently, the function $\mathcal{T}(x_1, x_2; \alpha)$ represents the production amplitude of particles 1 and 2 at the space-time points x_1 and x_2, respectively. It should be stressed that the representation (5) concerns virtual particles as well. Inserting now in (4) the representation (5) with the

substitutions $p_1 \to \kappa$, $p_2 \to P - \kappa$, we get

$$T(p_1, p_2; \alpha) = \int d^4x_1\, d^4x_2 \Psi^{S(-)}_{p_1,p_2}(x_1, x_2)\mathcal{T}(x_1, x_2; \alpha) = \\ = \int d^4x \psi^{S(-)}_{\widetilde{q}}(x)\tau_P(x; \alpha), \quad (6)$$

where

$$\Psi^{S(-)}_{p_1,p_2}(x_1, x_2) = \left[\Psi^{S(+)}_{p_1,p_2}(x_1, x_2)\right]^* = \left[\mathrm{e}^{iPX}\psi^{S(+)}_{\widetilde{q}}(x)\right]^* \quad (7)$$

coincides with the Bethe–Salpeter amplitude in continuous spectrum [24]. The second equality in (6), similar to the one in (5), merely arises after the integration over the pair c.m. coordinate X as a consequence of the factorization of the free c.m. motion in the phase factor e^{-iPX}. Thus, on the assumption of the quasi-free propagation of the low-mass two-particle system, the momentum dependence of the two-particle amplitude is determined by the convolution of the reduced production amplitude

$$\tau_P(x; \alpha) = \int d^4X\, \mathrm{e}^{-iPX}\mathcal{T}(x_1, x_2; \alpha) \quad (8)$$

and the reduced Bethe–Salpeter amplitude $\psi^{S(-)}_{\widetilde{q}}(x)$, the latter depending only on the relative four-coordinate x and the generalized relative four-momentum $\widetilde{q}$. Using (3)–(6), we can write

$$\psi^{S(+)}_{\widetilde{q}}(x) = \mathrm{e}^{i\tilde{q}x/2} + \Delta\psi^{S(+)}_{\widetilde{q}}(x), \quad (9)$$

where the correction to the plane wave is

$$\Delta\psi^{S(+)}_{\widetilde{q}}(x) = \frac{\sqrt{P^2}}{2\pi^3 i}\,\mathrm{e}^{-iPx(1+Pq/P^2)/2}\times \\ \times \int d^4\kappa \frac{\mathrm{e}^{i\kappa x} f^S(p_1, p_2; \kappa, P - \kappa)}{(\kappa^2 - {m_1}^2 + i0)[(P - \kappa)^2 - {m_2}^2 + i0]}. \quad (10)$$

In the two-particle c.m. system, where $\mathbf{P} = 0$, $\tilde{q} = \{0, 2\mathbf{k}^*\}$, $x = \{t^*, \mathbf{r}^*\}$, the amplitude $\psi^{S(+)}_{\widetilde{q}}(x)$ at $t^* \equiv t^*_1 - t^*_2 = 0$ coincides (up to the sign of vector $\mathbf{k}^*$) with a stationary solution $\psi^S_{-\mathbf{k}^*}(\mathbf{r}^*)$ of the scattering problem having at large $r^* = |\mathbf{r}^*|$ the asymptotic form of a superposition of the plane and outgoing spherical waves [25].

We see that one and the same production amplitude $\mathcal{T}(x_1, x_2; \alpha)$ or $\tau_P(x; \alpha)$, corresponding to the space-time representation, enters into relations (5) and (6). The effect of FSI manifests itself in the fact that the role of the functional basis,

which the asymptotic two-particle state is projected on, is transferred from the plane waves to Bethe–Salpeter amplitudes $\Psi^{S(-)}_{p_1,p_2}(x_1,x_2)$ or $\psi^{S(-)}_{\widetilde{q}}(x)$.

Equation (6) is valid also for identical particles 1 and 2 provided the substitution of the nonsymmetrized Bethe–Salpeter amplitudes $\Psi^{S(-)}_{p_1,p_2}(x_1,x_2)$ by their properly symmetrized combinations satisfying the requirements of QS:

$$\Psi^{S(-)}_{p_1,p_2}(x_1,x_2) \to \frac{1}{\sqrt{2}}\left[\Psi^{S(-)}_{p_1,p_2}(x_1,x_2) + (-1)^S \Psi^{S(-)}_{p_2,p_1}(x_1,x_2)\right]. \qquad (11)$$

In this case $m_1 = m_2$, $\widetilde{q} = q$ and $X = (x_1 + x_2)/2$. Similar to the case of nonidentical particles, the assumption of the ordinary phase space density of the final-state particles allows one to account for the FSI and QS effects only in a given pair of identical particles produced with a small relative velocity.

After substituting the representation (5) into (2), the double inclusive cross section takes on the form

$$\begin{aligned}(2\pi)^6\gamma_1\gamma_2\frac{d^6\sigma}{d^3\mathbf{p}_1\,d^3\mathbf{p}_2} &= \\ =\sum_S\int d^4x_1\,d^4x_2\,d^4x_1'\,d^4x_2'\rho_{PS}(x_1,x_2;x_1',x_2')\Psi^{S(-)}_{p_1,p_2}(x_1,x_2)\Psi^{S(-)*}_{p_1,p_2}(x_1',x_2') &= \\ = \sum_S\int d^4x\,d^4x'\rho_{PS}(x;x')\psi^{S(-)}_{\widetilde{q}}(x)\psi^{S(-)*}_{\widetilde{q}}(x'), \qquad (12)\end{aligned}$$

where the functions

$$\begin{aligned}\rho_{PS}(x_1,x_2;x_1',x_2') &= \sum_{M,\alpha'}\mathcal{T}(x_1,x_2;S,M,\alpha')\mathcal{T}^*(x_1',x_2';S,M,\alpha'), \\ \rho_{PS}(x;x') = \sum_{M,\alpha'}\tau_P(x;S,M,\alpha')\tau_P^*(x';S,M,\alpha') &\equiv \int d^4X\,d^4X'\times \qquad (13) \\ \times\mathrm{e}^{-iP(X-X')}\rho_{PS}&\left(X+\frac{p_2P}{P^2}x, X-\frac{p_1P}{P^2}x; X'+\frac{p_2P}{P^2}x', X'-\frac{p_1P}{P^2}x'\right)\end{aligned}$$

represent elements of the unnormalized two-particle space-time density matrices; the density matrix $\rho_{PS}(x_1,x_2;x_1',x_2')$ depends on the pair four-momentum P due to the account of the energy-momentum conservation in the sum $\sum\limits_{\alpha'}$. On the assumption of an instantaneous emission in the two-particle c.m. system ($t_1^* = t_2^*$), the second expression in (12) reduces to the ansatz used in [10, 14].

Switching off the FSI and QS effects, for example, by mixing particles from different events with similar global characteristics, one can define the reference

differential cross section

$$(2\pi)^6\gamma_1\gamma_2\frac{d^6\sigma_0}{d^3\mathbf{p}_1 d^3\mathbf{p}_2} = \\ = \sum_S \int d^4x_1\, d^4x_2\, d^4x_1'\, d^4x_2' \rho_{PS}(x_1,x_2;x_1',x_2')\, \mathrm{e}^{-ip_1(x_1-x_1')-ip_2(x_2-x_2')} = \\ = \sum_S \int d^4x\, d^4x' \rho_{PS}(x;x')\, \mathrm{e}^{-i\widetilde{q}(x-x')/2} \quad (14)$$

and rewrite (12) as

$$\frac{d^6\sigma}{d^3\mathbf{p}_1 d^3\mathbf{p}_2} = \\ = \frac{d^6\sigma_0}{d^3\mathbf{p}_1 d^3\mathbf{p}_2} \sum_S \mathcal{G}_S(p_1,p_2) \left\langle \Psi^{S(-)}_{p_1,p_2}(x_1,x_2) \Psi^{S(-)*}_{p_1,p_2}(x_1',x_2') \right\rangle'_{p_1p_2S} = \\ = \frac{d^6\sigma_0}{d^3\mathbf{p}_1 d^3\mathbf{p}_2} \sum_S \mathcal{G}_S(p_1,p_2) \left\langle \psi^{S(-)}_{\widetilde{q}}(x) \psi^{S(-)*}_{\widetilde{q}}(x') \right\rangle'_{\widetilde{q}PS}, \quad (15)$$

where we have introduced the quasi-averages of the bilinear products of the Bethe–Salpeter amplitudes:

$$\left\langle \Psi^{S(-)}_{p_1,p_2}(x_1,x_2) \Psi^{S(-)*}_{p_1,p_2}(x_1',x_2') \right\rangle'_{p_1p_2S} = \\ = \frac{\int d^4x_1\, d^4x_2\, d^4x_1'\, d^4x_2' \rho_{PS}(x_1,x_2;x_1',x_2') \Psi^{S(-)}_{p_1,p_2}(x_1,x_2) \Psi^{S(-)*}_{p_1,p_2}(x_1',x_2')}{\int d^4x_1\, d^4x_2\, d^4x_1'\, d^4x_2' \rho_{PS}(x_1,x_2;x_1',x_2')\, \mathrm{e}^{-ip_1(x_1-x_1')-ip_2(x_2-x_2')}} = \\ = \left\langle \psi^{S(-)}_{\widetilde{q}}(x) \psi^{S(-)*}_{\widetilde{q}}(x') \right\rangle'_{\widetilde{q}PS} = \frac{\int d^4x\, d^4x' \rho_{PS}(x;x') \psi^{S(-)}_{\widetilde{q}}(x) \psi^{S(-)*}_{\widetilde{q}}(x')}{\int d^4x\, d^4x' \rho_{PS}(x;x')\, \mathrm{e}^{-i\widetilde{q}(x-x')/2}} \quad (16)$$

and the statistical factors $\mathcal{G}_S$ — the population probabilities of the pair spin-S states in the absence of the correlation effect:

$$\mathcal{G}_S(p_1,p_2) = \\ = \frac{\int d^4x_1\, d^4x_2\, d^4x_1'\, d^4x_2' \rho_{PS}(x_1,x_2;x_1',x_2')\, \mathrm{e}^{-ip_1(x_1-x_1')-ip_2(x_2-x_2')}}{\sum\limits_S \int d^4x_1\, d^4x_2\, d^4x_1'\, d^4x_2' \rho_{PS}(x_1,x_2;x_1',x_2')\, \mathrm{e}^{-ip_1(x_1-x_1')-ip_2(x_2-x_2')}} = \\ = \frac{\int d^4x\, d^4x' \rho_{PS}(x;x')\, \mathrm{e}^{-i\widetilde{q}(x-x')/2}}{\sum\limits_S \int d^4x\, d^4x' \rho_{PS}(x;x')\, \mathrm{e}^{-i\widetilde{q}(x-x')/2}}. \quad (17)$$

Note that for unpolarized particles with spins j_1 and j_2 one has

$$\mathcal{G}_S = (2S+1)[(2j_1+1)(2j_2+1)]^{-1}, \qquad \sum_S \mathcal{G}_S = 1. \tag{18}$$

Generally, the spin factors are sensitive to particle polarization. For example, if two spin-1/2 particles were emitted independently with the polarizations $\mathbf{P}_1$ and $\mathbf{P}_2$, then $\mathcal{G}_0 = (1 - \mathbf{P}_1 \cdot \mathbf{P}_2)/4$ and $\mathcal{G}_1 = (3 + \mathbf{P}_1 \cdot \mathbf{P}_2)/4$.

The same procedure can be also applied to describe the production of weakly bound two-particle systems, like deuterons or hadronic atoms ($\pi^+\pi^-$ atoms, in particular). Due to a low binding energy, as compared with the energy transfers at the initial stage of the collision, there is practically no direct production of such bound systems. Their dominant production mechanism is thus due to the particle interaction in the final state. The invariant production amplitude $T_b(P_b; S, M, \alpha')$ of a spin-S bound system $b = \{1+2\}$ is then described by the lower diagram in Fig. 1 corresponding to the second term in the upper diagram with the free two-particle final state substituted by the bound one. Therefore, similar to (6), this amplitude is related to the Fourier transforms $\mathcal{T}$ or τ_{P_b} of the off-mass-shell two-particle amplitude T_0:

$$T_b(P_b; S, M, \alpha') = \int d^4x_1\, d^4x_2 \Psi^{S(-)}_{b,P_b}(x_1, x_2)\mathcal{T}(x_1, x_2; S, M, \alpha') = \\ = \int d^4x \psi^{S(-)}_b(x)\tau_{P_b}(x; S, M, \alpha') \tag{19}$$

and the corresponding differential cross section — to the same two-particle space-time density matrices ρ_{PS} or ρ_{PS} as enter into (12), up to the substitution $P \to P_b$:

$$(2\pi)^3\gamma_b \frac{d^3\sigma^S_b}{d^3\mathbf{P}_b} = \\ = \int d^4x_1\, d^4x_2\, d^4x'_1\, d^4x'_2 \rho_{P_bS}(x_1, x_2; x'_1, x'_2)\Psi^{S(-)}_{b,P_b}(x_1, x_2)\Psi^{S(-)*}_{b,P_b}(x'_1, x'_2) = \\ = \int d^4x\, d^4x' \rho_{P_bS}(x; x')\psi^{S(-)}_b(x)\psi^{S(-)*}_b(x'). \tag{20}$$

Here $\Psi^{S(-)}_{b,P_b}(x_1, x_2) = [\Psi^{S(+)}_{b,P_b}(x_1, x_2)]^* = [\mathrm{e}^{iP_bX}\psi^{S(+)}_b(x)]^*$ is the Bethe–Salpeter amplitude for the bound system. At equal emission times of the two particles in their c.m. system, the amplitude $\psi^{S(+)}_b(x)$, describing their relative motion, coincides with the usual nonrelativistic wave function in discrete spectrum $\psi^S_b(\mathbf{r}^*)$. Similar to (15), one can also rewrite the production cross section of the bound system through the reference cross section in (14) taken at

$\mathbf{p}_1 \doteq \mathbf{P}_b m_1/(m_1+m_2)$, $\mathbf{p}_2 \doteq \mathbf{P}_b m_2/(m_1+m_2)$ and $\gamma_1 \doteq \gamma_2 \doteq \gamma_b$ (i.e., $\widetilde{q} \doteq 0$, $P \doteq P_b$):

$$\frac{d^3\sigma_b^S}{d^3\mathbf{P}_b} = (2\pi)^3\gamma_b \frac{d^6\sigma_0}{d^3\mathbf{p}_1\, d^3\mathbf{p}_2}\mathcal{G}_S(p_1,p_2)\left\langle \Psi_{b,P_b}^{S(-)}(x_1,x_2)\Psi_{b,P_b}^{S(-)*}(x_1',x_2')\right\rangle'_{p_1p_2S} =$$
$$= (2\pi)^3\gamma_b \frac{d^6\sigma_0}{d^3\mathbf{p}_1\, d^3\mathbf{p}_2}\mathcal{G}_S(p_1,p_2)\left\langle \psi_b^{S(-)}(x)\psi_b^{S(-)*}(x')\right\rangle'_{0PS}. \quad (21)$$

We see that the production of a weakly bound system $\{1{+}2\}$ is closely related with the production of particles 1 and 2 in continuous spectrum at small kinetic energies in their c.m. system. This relation was first formulated [26] in connection with the production of nonrelativistic deuterons and then generalized [27] to the relativistic case and the inclusive production. Similar relation was obtained, in the limit of an instantaneous emission from a point-like region, also for the case of the production of pure Coulomb hadronic atoms [10]. A complete treatment of the production of weakly bound systems, accounting for the finite-size effect, can be found in [11].

2. APPROXIMATE DESCRIPTION OF THE $\pi^+\pi^-$ PRODUCTION

Following [10], let us first neglect the $\pi^+\pi^-$ strong FSI and assume only two types of pion emitters: SL emitters (e.g., ρ or Δ resonances) characterized by small sizes or decay lengths on a fm level, and LL emitters (e.g., η, K_s or Λ) with very large or macroscopic decay lengths. Since the relative space-time distance between the emission points x enters in the pure Coulomb $\pi^+\pi^-$ amplitudes $\psi_q^{(-)\mathrm{coul}}(x)$ and $\psi_b^{(-)\mathrm{coul}}(x)$ scaled by the Bohr radius $a = -387.5$ fm, one can put in (12) and (20) $\psi_q^{(-)}(x) \approx \mathrm{e}^{-i\tilde{q}x/2}\psi_q^{(-)\mathrm{coul}}(0) = \mathrm{e}^{i\mathbf{k}^*\mathbf{r}^*}[\psi_{-\mathbf{k}^*}^{\mathrm{coul}}(0)]^*$ and $\psi_b^{(-)}(x) \approx \psi_b^{(-)\mathrm{coul}}(0) = [\psi_b^{\mathrm{coul}}(0)]^*$ for the fraction λ of the pairs with both pions from SL emitters ($r^* \ll |a|$), and $\psi_q^{(-)\mathrm{coul}}(x) \approx \exp\left[i\mathbf{k}^*\mathbf{r}^* - i(k^*a)^{-1}\ln\left(\mathbf{k}^*\mathbf{r}^* + k^*r^*\right)\right]$ (a plane wave amplitude with the phase modified by Coulomb interaction) and $\psi_b^{(-)\mathrm{coul}}(x) \approx \psi_b^{(-)\mathrm{coul}}(\infty) = 0$ for the remaining fraction $(1-\lambda)$ of the pairs with at least one pion from a LL emitter ($r^* \gg |a|$). As a result, (12) and (20) reduce to:

$$\frac{d^6\sigma}{d^3\mathbf{p}_1\, d^3\mathbf{p}_2} \approx \frac{d^6\sigma_0}{d^3\mathbf{p}_1\, d^3\mathbf{p}_2}\left[\lambda\left|\psi_{-\mathbf{k}^*}^{\mathrm{coul}}(0)\right|^2 + (1-\lambda)\right], \quad (22)$$

$$\frac{d^3\sigma_b}{d^3\mathbf{P}_b} \approx (2\pi)^3\gamma_b \frac{d^3\sigma_0}{d^3\mathbf{p}_1\, d^3\mathbf{p}_2}\lambda\left|\psi_b^{\mathrm{coul}}(0)\right|^2, \quad (23)$$

where σ_0 represents the production cross section of the noninteracting pions and the expression for the production of bound $\pi^+\pi^-$ system implies $\mathbf{p}_1 \doteq \mathbf{p}_2 \doteq$

$\mathbf{P}_b/2$ and $\gamma_1 \doteq \gamma_2 \doteq \gamma_b$. The squares of the nonrelativistic Coulomb wave functions at zero separation are well known:

$$\left|\psi^{\rm coul}_{-\mathbf{k}^*}(0)\right|^2 \equiv A_c(\eta) = 2\pi\eta[\exp(2\pi\eta) - 1]^{-1}, \qquad \eta = (k^* a)^{-1}, \tag{24}$$

$$\left|\psi^{\rm coul}_b(0)\right|^2 = \delta_{l0}\left(\pi|a|^3 n^3\right)^{-1}, \qquad b = \{nl\}, \tag{25}$$

where the Bohr radius $a = (\mu e_1 e_2)^{-1}$ is negative for $\pi^+\pi^-$ system due to the opposite signs of π^+ and π^- charges ($e_1 = -e_2 = e$). The Coulomb penetration factor $A_c(\eta)$ (sometimes called Gamow factor) behaves at small $Q = 2k^* < Q_c$ as Q_c/Q and at large Q approaches unity as $1 + (1/2)Q_c/Q$, where $Q_c = 4\pi/|a| = 6.4$ MeV/c. As for the bound $\pi^+\pi^-$ states $b = \{nl\}$, only the s-wave states $\{n0\}$ are produced at zero separation and their fractions with given main quantum numbers n are uniquely fixed by the n^{-3} law in (25).

The numbers N_A and $N_A^{\rm br}$ of produced and breakup $\pi^+\pi^-$ atoms, required to calculate the breakup probability (1), can then be obtained in two steps [10]. First, one simulates the noncorrelated two-pion spectrum $d^6N_0/d^3\mathbf{p}_1\, d^3\mathbf{p}_2$ or, constructs it by mixing pions from different events, and determines the overall normalization parameter g and the fraction λ or $\Lambda = \lambda g$ by fitting the theoretical spectrum

$$\frac{d^6N}{d^3\mathbf{p}_1\, d^3\mathbf{p}_2} \approx g\frac{d^6N_0}{d^3\mathbf{p}_1\, d^3\mathbf{p}_2}\left[\lambda A_c(\eta) + (1-\lambda)\right] \equiv \frac{d^6N_0}{d^3\mathbf{p}_1\, d^3\mathbf{p}_2}\left[\Lambda A_c(\eta) + \Lambda'\right] \tag{26}$$

to the measured spectrum of the pion pairs; to get rid of the pairs from the breakup of the $\pi^+\pi^-$ atoms in the target, the fit should be done in the region $Q >\sim 3$ MeV/c. In the second step, one can use (23) and the fitted parameter $\Lambda = \lambda g$ to calculate the three-momentum distribution of the numbers of produced atoms in given states $b = \{n0\}$:

$$\frac{d^3N_b}{d^3\mathbf{P}_b} \approx (2\pi)^3\gamma_b\frac{d^3N_0}{d^3\mathbf{p}_1 d^3\mathbf{p}_2}\Lambda\left|\psi^{\rm coul}_{n0}(0)\right|^2, \tag{27}$$

where $\mathbf{p}_1 \doteq \mathbf{p}_2 \doteq \mathbf{P}_b/2$. Then, taking into account that $d^3\mathbf{p}_1 d^3\mathbf{p}_2 = = (1/8)d^3\mathbf{P}d^3\widetilde{\mathbf{q}} = (1/8)\gamma d^3\mathbf{P}d^3\mathbf{Q}$ and that at sufficiently small $Q < Q_0$ the noncorrelated two-pion spectrum is practically Q-independent (up to a correction $O(Q_0^2/m_\pi^2)$), one can calculate N_A from the number $N_0(Q < Q_0)$ of simulated or mixed noncorrelated pion pairs with $Q < Q_0$:

$$N_A = \sum_b \int d^3\mathbf{P}_b \frac{d^3N_b}{d^3\mathbf{P}_b} \doteq \frac{3\Lambda}{4\pi^2}N_0(Q < Q_0)\left(\frac{4\pi}{|a|Q_0}\right)^3\sum_n n^{-3}. \tag{28}$$

One can also calculate N_A from the number of correlated nonatomic pairs,

$$N^{\rm cna}_{\pi^+\pi^-}(Q < Q_0) \doteq \frac{3\Lambda}{Q_0^3}N_0(Q < Q_0)\int_0^{Q_0} dQ\, Q^2 A_c(\eta), \tag{29}$$

using the so-called k factor [4]:

$$k(Q<Q_0)=\frac{N_A}{N^{\rm cna}_{\pi^+\pi^-}}(Q<Q_0)\doteq\frac{(4\pi)^3}{4\pi^2|a|^3}\frac{\sum\limits_n n^{-3}}{\int\limits_0^{Q_0} dQ\,Q^2A_c(\eta)}, \tag{30}$$

e.g., $k=0.615$, 0.263, and 0.140 for $Q_0=2$, 3, and 4 MeV/c, respectively. As for the number of breakup atoms $N_A^{\rm br}$, it is simply obtained by subtracting the fitted numbers of correlated (cna) and noncorrelated (nc) nonatomic pion pairs (see (26)) from the measured number of pion pairs:

$$N_A^{\rm br}\doteq N_{\pi^+\pi^-}(Q<Q_{\rm cut})-N^{\rm cna}_{\pi^+\pi^-}(Q<Q_{\rm cut})-N^{\rm nc}_{\pi^+\pi^-}(Q<Q_{\rm cut}), \tag{31}$$

$$N^{\rm nc}_{\pi^+\pi^-}(Q<Q_{\rm cut})=\Lambda' N_0(Q<Q_{\rm cut}). \tag{32}$$

The value of $Q_{\rm cut}$ should be chosen sufficiently large so that the interval $(0,Q_{\rm cut})$ contains the signal from practically all atomic pairs. The possible choice is $Q_{\rm cut}=Q_0=4$ MeV/c. One can also choose a smaller value, correcting for the loss of atomic pairs with the help of simulated efficiency factor $\epsilon_A^{\rm br}$ [4]. One can obtain $N_A^{\rm br}$ also in a more direct way using the data from multilayer targets [2].

Let us now consider the modification of (26) and (27) due to the strong FSI and finite space-time separation of the particle emitters. Formally one can write

$$\frac{d^6N}{d^3\mathbf{p}_1\,d^3\mathbf{p}_2}\doteq\frac{d^6N_0}{d^3\mathbf{p}_1\,d^3\mathbf{p}_2}\left\{\Lambda\left[1+\delta(\mathbf{k}^*)\right]A_c(\eta)+\Lambda'\right\}, \tag{33}$$

$$\frac{d^3N_b}{d^3\mathbf{P}_b}\doteq(2\pi)^3\gamma_b\frac{d^3N_0}{d^3\mathbf{p}_1d^3\mathbf{p}_2}\Lambda(1+\delta_n)\left|\psi^{\rm coul}_{n0}(0)\right|^2, \tag{34}$$

$$N_A\doteq\frac{3\Lambda}{4\pi^2}N_0(Q<Q_0)\left(\frac{4\pi}{|a|Q_0}\right)^3\sum_n n^{-3}(1+\delta_n), \tag{35}$$

$$N^{\rm cna}_{\pi^+\pi^-}(Q<Q_0)\doteq\frac{3\Lambda}{Q_0^3}N_0(Q<Q_0)\int\limits_0^{Q_0}dQ\,Q^2A_c(\eta)[1+\delta(k^*)], \tag{36}$$

$$k(Q<Q_0)\doteq\frac{(4\pi)^3}{4\pi^2|a|^3}\frac{\sum\limits_n n^{-3}(1+\delta_n)}{\int\limits_0^{Q_0}dQ\,Q^2A_c(\eta)[1+\delta(k^*)]}, \tag{37}$$

where the correction factors are determined by the averaging of the bilinear products of the reduced Bethe–Salpeter amplitudes over the distribution of the

relative space-time separations of the SL emitters:

$$1+\delta(\mathbf{k}^*) \doteq \left\langle \psi^{(-)}_{\widetilde{q}}(x)\psi^{(-)*}_{\widetilde{q}}(x')\right\rangle'^{\rm SL}_{\widetilde{q}P} [A_c(\eta)]^{-1}, \tag{38}$$

$$1+\delta_n \doteq \left\langle \psi^{(-)}_{n0}(x)\psi^{(-)*}_{n0}(x')\right\rangle'^{\rm SL}_{0P} \left|\psi^{\rm coul}_{n0}(0)\right|^{-2}. \tag{39}$$

The averaging is defined in (16) with the reduced space-time density matrix substituted by its part, $\rho^{\rm SL}_P$, related only with the SL emitters. Equations (38) and (39) account only for the elastic transition $\alpha \to \alpha$ and ignore a small contribution of the inelastic one $\beta \to \alpha$, where $\alpha = \{\pi^+\pi^-\}$, $\beta = \{\pi^0\pi^0\}$; see Sec. 5 and (161), (162) for the complete treatment.

In fact, it can be argued [13, 14] that

$$\delta_n \approx \delta(0), \tag{40}$$

provided the characteristic spatial separation of the pion SL emitters in the two-pion c.m. system is much less than the two-pion Bohr radius $|a|$. This result immediately follows from the well-known Migdal's argument [26]. Namely, since the particles in continuous spectrum at zero kinetic energy and in discrete spectrum at very small binding energy $\kappa^2/(2\mu) \to 0$ are described by practically the same wave equations, the r^* dependence of the corresponding wave functions at a given orbital angular momentum should be the same for the distances $r^* \ll \kappa^{-1}$ (i.e., $r^* \ll n|a|$ in the case of a hadronic atom with the main quantum number n).

One may see that the approximate equality (40), together with the assumption of a weak k^* dependence of the correction $\delta(\mathbf{k}^*)$, justify the use of the approximate equations (26)–(30). In this approximation, the finite-size correction merely reduces to the rescaling $\Lambda \to \Lambda[1+\delta(0)]$.

We show in Secs. 4 and 5 that (40) is subject to a normalization correction $O(f_0/a) \sim 0.3\%/n$ and other small corrections $4\pi O(k^*_\beta (f_0^{\beta\alpha})^2/a)$ and $O(a^{-2})$, where $k^*_\beta = 35.5$ MeV/c is the momentum in the channel $\beta = \{\pi^0\pi^0\}$ at the threshold transition to the channel $\alpha = \{\pi^+\pi^-\}$, $f_0^{\beta\alpha} = \sqrt{2}(a_0^2 - a_0^0)/3 \approx -0.2$ fm is the transition amplitude. Taking the normalization correction explicitly into account (see (154), (143), and (147)):

$$1+\delta_n = (1+\delta'_n)\left\{1+\phi(n)\frac{2f_0}{n|a|}\left[1+O\left(\left(k^*_\beta f_0^{\beta\alpha}\right)^2\right)\right] - 4\pi^2 O\left(\left(\frac{f_0}{a}\right)^2\right)\right\}, \tag{41}$$

where $\phi(n) \approx 3$ is defined in (109), one can rewrite the approximate equality in (40) as

$$\delta'_n = \delta(0) + 4\pi O\left(\frac{k^*_\beta (f_0^{\beta\alpha})^2}{a}\right) + O\left(\left\langle \frac{r^{*2}}{a^2}\right\rangle^{\rm SL}\right). \tag{42}$$

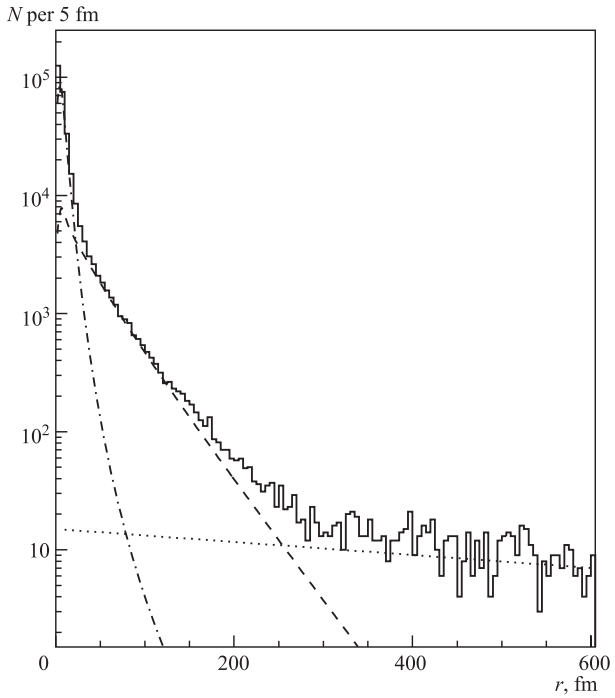

Fig. 2. The distribution of the relative distance r^* between the pion production points in the pair c.m. system simulated with the UrQMD transport code [28] for pNi interactions at 24 GeV and the relative momenta in the pair c.m. system $Q = 2k^* < 50$ MeV/c in the conditions of the DIRAC experiment at CERN [29]. The curves are the results of the fits to short-distance, ω and η' contributions described in the text

The neglect of the corrections δ_n and $\delta(\mathbf{k}^*)$, i.e., the use of the approximate equations (26)–(30) instead of (33)–(37), leads to the systematic shift of the breakup probability:

$$\frac{\Delta P_{\rm br}}{P_{\rm br}} \doteq -\frac{\Delta N_A}{N_A} + \frac{\Delta N_A^{\rm br}}{N_A^{\rm br}}. \tag{43}$$

To estimate this shift, one can approximate the correlation function

$$\mathcal{R}(Q) \equiv \frac{dN/dQ}{dN_0/dQ} = A_c(\eta)[1 + \delta(k^*)], \tag{44}$$

where $\delta(k^*) = \langle\delta(\mathbf{k}^*)\rangle$ is the finite-size correction averaged over the pion three-momenta at a fixed $k^* = |\mathbf{k}^*| = Q/2$, by

$$\widetilde{\mathcal{R}}(Q) = \widetilde{\Lambda} A_c(\eta) + \widetilde{\Lambda}' \tag{45}$$

and use the fitted parameters $\widetilde{\Lambda}$, $\widetilde{\Lambda}'$ to calculate $\Delta N_A/N_A$ and $\Delta N_A^{\rm br}/N_A^{\rm br}$:

$$-\frac{\Delta N_A}{N_A} = \frac{\sum\limits_n n^{-3}(1+\delta_n-\widetilde{\Lambda})}{\sum\limits_n n^{-3}(1+\delta_n)}, \tag{46}$$

$$\frac{\Delta N_A^{\rm br}}{N_A^{\rm br}} = \frac{N^{\rm cna}_{\pi^+\pi^-}(Q<Q_{\rm cut})}{N_A^{\rm br}(Q<Q_{\rm cut})} \frac{\int\limits_0^{Q_{\rm cut}} dQ\, Q^2[\mathcal{R}(Q)-\widetilde{\mathcal{R}}(Q)]}{\int\limits_0^{Q_{\rm cut}} dQ\, Q^2\mathcal{R}(Q)}. \tag{47}$$

In the DIRAC experiment, $N^{\rm cna}_{\pi^+\pi^-}/N_A^{\rm br} \doteq 16$ at $Q_{\rm cut} = 4$ MeV/c [4] and, for $Q_{\rm cut} < Q_c$, when $QA_c(\eta) \approx {\rm const}$, it decreases approximately quadratically with decreasing $Q_{\rm cut}$ provided the signal region contains most of the atomic pion pairs, i.e., down to $Q_{\rm cut} \approx 2$ MeV/c.

In the following, we perform an analytical and numerical study of the corrections δ_n and $\delta(k^*)$ and their effect on the breakup probability $P_{\rm br}$. Here we only mention that the condition $r^* \ll n|a|$ can be violated for pion pairs containing pions from the decays of some resonances such as ω and η' with the decay lengths of about 30 and 900 fm, respectively. The corresponding exponential tails are clearly seen in Fig. 2, where the r^*-distribution simulated with the UrQMD transport code [28] is shown for pion pairs produced in pNi interactions at 24 GeV in the conditions of the DIRAC experiment at CERN [29].

3. CORRELATION FEMTOSCOPY — BASIC ASSUMPTIONS

3.1. Noninteracting Nonidentical Particles: Space-Time Coherence. To clarify the meaning of the two-particle space-time density matrix $\rho_S(x_1,x_2;x_1',x_2')$, let us first neglect the FSI effect and substitute the Bethe–Salpeter amplitudes by the plane waves. Changing in (12) the integration variables x_i, x_i' by the new ones:

$$\bar{x}_i = \frac{1}{2}(x_i + x_i'), \qquad \epsilon_i = x_i - x_i', \tag{48}$$

we can rewrite the production cross section of two nonidentical particles as

$$(2\pi)^6\gamma_1\gamma_2\frac{d^6\sigma_0}{d^3\mathbf{p}_1\, d^3\mathbf{p}_2} = \\ = \sum_S \int d^4\bar{x}_1\, d^4\bar{x}_2\, G_S(\bar{x}_1,p_1;\bar{x}_2,p_2) = \sum_S \int d^4\bar{x} g_{PS}(\bar{x},\widetilde{q}), \tag{49}$$

where $\bar{x} = \bar{x}_1 - \bar{x}_2$ and the real functions

$$\begin{aligned} &G_S(\bar{x}_1, p_1; \bar{x}_1, p_2) = \\ &\quad = \int d^4\epsilon_1\, d^4\epsilon_2\, \mathrm{e}^{-ip_1\epsilon_1 - ip_2\epsilon_2} \rho_{PS}\Big(\bar{x}_1 + \frac{\epsilon_1}{2}, \bar{x}_2 + \frac{\epsilon_2}{2}; \bar{x}_1 - \frac{\epsilon_1}{2}, \bar{x}_2 - \frac{\epsilon_2}{2}\Big)\,, \\ &g_{PS}(\bar{x}; \widetilde{q}) = \int d^4\bar{X} G_S\Big(\bar{X} + \frac{p_2 P}{P^2}\bar{x}, p_1; \bar{X} - \frac{p_1 P}{P^2}\bar{x}, p_2\Big) = \\ &\qquad\qquad = \int d^4\epsilon\, \mathrm{e}^{-i\widetilde{q}\epsilon/2} \rho_{PS}\Big(\bar{x} + \frac{\epsilon}{2}, \bar{x} - \frac{\epsilon}{2}\Big)\,. \end{aligned} \tag{50}$$

The function G_S, usually called emission function, being a partial Fourier transform of the space-time density matrix, is closely related to the Wigner density, the latter collecting all contributions due to free streaming of the emitted particles to given space-time points through an integral over the emission function (see (49) in [30]).

It is clear from (49) and (50) that more narrow is the width of the diagonal of the space-time density matrix (the width of the ϵ_i distribution), more wide is the distribution of particle four-momenta. In particular, the diagonal space-time density matrix (i.e., zero width of the ϵ_i distribution) would yield the uniform four-momentum distribution, in correspondence with the infinite uncertainty in the four-momenta of the particles localized at certain space-time points.

Consider as an example the particle emission by independent one-particle emitters of various types A according to the one-particle production amplitudes (see also [31])

$$\begin{aligned} \mathcal{T}_A^{(1)}(x_1; x_A) &\sim v_A(x_A) \exp\Big[-\frac{(\mathbf{x}_1 - \mathbf{x}_A)^2}{2{r_A}^2} - \frac{(x_{01} - x_{0A})^2}{2{\tau_A}^2}\Big]\,, \\ v_A(x_A) &\sim \exp\Big(-\frac{{\mathbf{x}_A}^2}{4{r_0}^2} - \frac{{x_{0A}}^2}{4{\tau_0}^2}\Big)\,. \end{aligned} \tag{51}$$

These amplitudes correspond to the emitters at rest with a Gaussian distribution of the emission points $x_1 = \{t_1, \mathbf{r}_1\}$ around the emitter centers $x_A = \{t_A, \mathbf{r}_A\}$, also distributed according to a Gaussian law. In four-momentum representation,

$$\begin{aligned} T_A^{(1)}(p_1; x_A) &\sim v_A(x_A) u_A(p_1) \exp\left(-ip_1 x_A\right), \\ u_A(p_1) &\sim \exp\big(-{r_A}^2 {\mathbf{p}_1}^2/2 - {\tau_A}^2 {p_{01}}^2/2\big)\,. \end{aligned} \tag{52}$$

Assuming further that the emitters are sufficiently heavy, we can describe them classically. The four-coordinates of the emitter centers x_A can then be considered as a part of the quantum numbers α', the sum in (13) thus containing

the integration over x_A. Performing this integration, we get for the elements of the one-particle space-time density matrix related to the emitter A:

$$\rho_A^{(1)}(x_1, x_1') = \int d^4x_A \mathcal{T}_A^{(1)}(x_1; x_A)\mathcal{T}_A^{(1)*}(x_1'; x_A) \sim$$
$$\sim \exp\left(-\frac{{\boldsymbol{\epsilon}_1}^2}{4{r_A}^2} - \frac{{\epsilon_{01}}^2}{4{\tau_A}^2}\right) \exp\left(-\frac{{\bar{\mathbf{x}}_1}^2}{2{r_0}^2 + {r_A}^2} - \frac{{\bar{x}_{01}}^2}{2{\tau_0}^2 + {\tau_A}^2}\right) \quad (53)$$

and for the corresponding emission function:

$$G_A^{(1)}(\bar{x}_1, p_1) = \int d^4\epsilon_1 \, \mathrm{e}^{-ip_1\epsilon_1} \rho_A^{(1)}\left(\bar{x}_1 + \frac{\epsilon_1}{2}, \bar{x}_1 - \frac{\epsilon_1}{2}\right) \sim$$
$$\sim |u_A(p_1)|^2 \exp\left(-\frac{{\bar{\mathbf{x}}_1}^2}{2{r_0}^2 + {r_A}^2} - \frac{{\bar{x}_{01}}^2}{2{\tau_0}^2 + {\tau_A}^2}\right). \quad (54)$$

The contribution of the emitter A to the single-particle production cross section is

$$(2\pi)^3\gamma_1 \frac{d^3\sigma_A}{d^3\mathbf{p}_1} = \int d^4\bar{x}_1 G_A^{(1)}(\bar{x}_1, p_1) = \int d^4x_A \left|T_A^{(1)}(p_1; x_A)\right|^2 \sim$$
$$\sim |u_A(p_1)|^2 \sim \exp\left(-{r_A}^2{\mathbf{p}_1}^2 - {\tau_A}^2{p_{01}}^2\right). \quad (55)$$

We may see that the emitter space-time dimensions r_A and τ_A determine both the space-time coherence of particle production (the nondiagonality of the space-time density matrix) and the distribution of particle four-momenta. In particular case of the emitters of a vanishing space-time extent: $r_A = \tau_A = 0$ (no coherence), any particle four-momenta are equally probable.

Note that for the emitter moving with a nonrelativistic velocity $\boldsymbol{\beta}_A$ and emitting a particle 1 with the mean three-momentum $\mathbf{p}_A = m_1\boldsymbol{\beta}_A$, the amplitude (51) and the density matrix (53), respectively, acquire phase factors $\mathrm{e}^{-i\mathbf{p}_A\mathbf{x}_1}$ and $\mathrm{e}^{-i\mathbf{p}_A\boldsymbol{\epsilon}_1}$ and the substitution $\mathbf{p}_1 \to \mathbf{p}_1 - \mathbf{p}_A$ has to be done in the amplitude $u_A(p_1)$. After averaging over the $\mathbf{p}_A$ distribution that decouples from the distribution of other emitter characteristics in a Gaussian form of a width Δ_0, we still arrive at (53)–(55), up to a substitution ${r_A}^2 \to {r_A}^2/[2(r_A\Delta_0)^2 + 1]$ in the ϵ- and momentum-dependent factors, corresponding to a widening of the momentum distribution due to the dispersion of the emitter velocities.

As for the actual values of the parameters r_A and τ_A, we can estimate them using the information about particle transverse momenta, p_t, which are much less influenced by the motion of the emitters than the longitudinal ones. Doing this for pions or kaons, we should however exclude the low-p_t region which is dominantly populated by the decays of low-lying resonances. We can also use the p_t-distributions of these resonances. In both cases the ${p_t}^2$ slopes in the interactions of elementary hadrons are of $\sim$3 (GeV/c)$^{-2}$ (see, e.g., [32]), yielding

on average ${r_A}^2, {\tau_A}^2 \sim 0.1$ fm^2. Somewhat larger values can be expected in heavy ion collisions where a substantial part of the emitters can be associated with the centers of the last rescatterings characterized by sufficiently large momentum transfer. It is important that the estimated values of ${r_A}^2, {\tau_A}^2$ appear to be much smaller than the effective values of the parameters ${r_0}^2$, ${\tau_0}^2$ obtained in femtoscopic measurements. The latter being of about 1 fm^2 for pions produced at $p_t \sim \langle p_t \rangle$ in hadron–hadron interactions and up to several tens fm^2 in the collisions involving heavy nuclei.

3.2. Noninteracting Identical Particles: QS Correlations. *3.2.1. Correlation Function.* Consider the production of noninteracting identical particles. It should be noted that this consideration is not of academic interest only. Thus for identical pions or kaons, the effect of the strong FSI is usually small and the effect of the Coulomb FSI can be in first approximation simply corrected for (see [33] and references therein). The corrected correlation effect is then determined by the QS symmetrization only, i.e., the Bethe–Salpeter amplitudes have to be substituted by properly symmetrized combinations of the plane waves (see (11)). As a result of the interference of these waves, there appears the additional term, not present in (49):

$$(2\pi)^6 \gamma_1 \gamma_2 \frac{d^6\sigma}{d^3\mathbf{p}_1\, d^3\mathbf{p}_2} - $$
$$= \sum_S \int d^4\bar{x}_1\, d^4\bar{x}_2 \left[G_S(\bar{x}_1, p_1; \bar{x}_2, p_2) + G_S(\bar{x}_1, p; \bar{x}_2, p)(-1)^S \cos(q\bar{x}) \right] =$$
$$= \sum_S \int d^4\bar{x} \left[g_{PS}(\bar{x}, q) + g_{PS}(\bar{x}, 0)(-1)^S \cos(q\bar{x}) \right]. \quad (56)$$

Note that the off-mass-shell four-momentum $p = (p_1 + p_2)/2$ enters as an argument of the emission function G_S in the interference term.

It is convenient to define the correlation function $\mathcal{R}(p_1, p_2)$ as the ratio of the double inclusive cross section $d^6\sigma$ to the reference one $d^6\sigma_0$ which would be observed in the case of absent QS and FSI effects:

$$\mathcal{R}(p_1, p_2) = \frac{d^6\sigma(p_1, p_2)}{d^6\sigma_0(p_1, p_2)}. \quad (57)$$

In the high-energy collisions involving nuclei, we can neglect the kinematic constraints, as well as rather weak dynamical correlations and construct the reference distribution using the particles from different events with similar topology. In case of a negligible FSI, there is no correlation for nonidentical particles: $\mathcal{R}(p_1, p_2) = 1$, while for identical particles the correlation arises due to the

interference effect:

$$\mathcal{R}(p_1,p_2)=1+\frac{\sum\limits_S\int d^4\bar{x}_1\,d^4\bar{x}_2 G_S(\bar{x}_1,p;\bar{x}_2,p)(-1)^S\cos(q\bar{x})}{\sum\limits_S\int d^4\bar{x}_1\,d^4\bar{x}_2 G_S(\bar{x}_1,p_1;\bar{x}_2,p_2)}\equiv$$

$$\equiv 1+\sum_S\mathcal{G}_S(-1)^S\langle\cos(q\bar{x})\rangle''_{p_1p_2S}=1+\frac{\sum\limits_S\int d^4\bar{x}g_{PS}(\bar{x},0)(-1)^S\cos(q\bar{x})}{\sum\limits_S\int d^4\bar{x}g_{PS}(\bar{x},q)}\equiv$$

$$\equiv 1+\sum_S\mathcal{G}_S(-1)^S\langle\cos(q\bar{x})\rangle''_{qPS}\,, \quad (58)$$

where the quasi-averages satisfy the equalities

$$\langle\cos(q\bar{x})\rangle''_{p_1p_2S}=\left\langle \mathrm{e}^{ip_1(x_1-x_2')+ip_2(x_2-x_1')}\right\rangle'_{p_1p_2S}=$$

$$=\langle\cos(q\bar{x})\rangle''_{qPS}=\left\langle \mathrm{e}^{iq(x+x')/2}\right\rangle'_{qPS}; \quad (59)$$

the factors $\mathcal{G}_S$ represent the population probabilities of the pair spin-S states out of the region of the correlation effect. They are defined in (17) and can be expressed through the emission functions as

$$\mathcal{G}_S(p_1,p_2)=\frac{\int d^4x_1\,d^4x_2 G_S(x_1,p_1;x_2,p_2)}{\sum\limits_S\int d^4x_1\,d^4x_2 G_S(x_1,p_1;x_2,p_2)}=\frac{\int d^4x g_{PS}(x,q)}{\sum\limits_S\int d^4x g_{PS}(x,q)},$$
$$\sum_S\mathcal{G}_S=1. \quad (60)$$

They can be also considered as the initial (QS switched off) statistical factors. For initially unpolarized spin-j particles: $\sum\limits_S\mathcal{G}_S(-1)^S=(-1)^{2j}/(2j+1)$.

Assuming, for example, that for a (generally momentum-dependent) fraction λ of the pairs the particles are emitted by independent SL one-particle emitters described by the Gaussian amplitudes (51) or (52), while for the remaining fraction $(1-\lambda)$, related to LL emitters (η, K^0_s, Λ, ...), the relative distances r^* between the emission points in the pair c.m. system are extremely large, the correlation function

$$\mathcal{R}(p_1,p_2)=1+\lambda\sum_S\mathcal{G}_S(-1)^S\frac{\mathrm{Re}\sum\limits_{A,B}u_A(p_1)u_B(p_2)u^*_A(p_2)u^*_B(p_1)\,\mathrm{e}^{-iq(x_A-x_B)}}{\sum\limits_{A,B}|u_A(p_1)u_B(p_2)|^2}, \quad (61)$$

where the sum $\sum_{A,B}$ is done over all characteristics of the emitters. In the case of only one type of the SL emitters that are at rest and differ only by the four-coordinates x_A of their centers, the amplitudes u_A reduce to a single universal amplitude u and the sum merely reduces to the averaging over x_A, i.e.,

$$\mathcal{R}(p_1,p_2) = 1 + \lambda \sum_S \mathcal{G}_S (-1)^S \langle \cos\left(q(x_A - x_B)\right)\rangle = \\ = 1 + \lambda \sum_S \mathcal{G}_S (-1)^S \exp\left(-{r_0}^2 \mathbf{q}^2 - {\tau_0}^2 q_0^2\right). \quad (62)$$

We see that a characteristic feature of the correlation function of identical particles is the presence of an interference maximum or minimum at small $|\mathbf{q}|$, changing to a horizontal plateau at sufficiently large $|\mathbf{q}|$, large compared with the inverse characteristic space-time distance between the particle emission points.

3.2.2. Smoothness Assumption. In the simple model of only one type of the emitters contributing to the observable interference effect and in the absence of the relative emitter motion, the width of the low-$|\mathbf{q}|$ structure is solely determined by the characteristic space-time distance between the one-particle emitters and does not depend on the parameters r_A and τ_A, characterizing the space-time extent of the emitters themselves, see (62). It means that the enlargement of the production region related to the latter (${r_0}^2 \to {r_0}^2 + (1/2){r_A}^2$, ${\tau_0}^2 \to {\tau_0}^2 + (1/2){\tau_A}^2$) is compensated in the correlation function due to the different momentum arguments of the emission functions in the numerator and denominator of (58). This is clearly seen when calculating the correlation function directly from (2), substituting the production amplitude $T(p_1,p_2;\alpha)$ by the symmetrized product of the Kopylov–Podgoretsky one-particle amplitudes in momentum representation, see (61) and (62). Of course, the independence of the interference effect on the space-time extent of the emitters in this model (assuming that the emitters decay according to a single universal amplitude u and differ by the four-coordinates of their centers only) is justified only in the case of sufficiently small overlap of the emitters to guarantee the assumption of their independence.

Generally, even in the case of independent emitters, the particles are emitted by moving emitters of different types and the correlation function depends also on their space-time extent r_A, τ_A. Particularly, for a Gaussian distribution of the mean emission three-momentum $\mathbf{p}_A$ of a width Δ_0, (62) is modified by the substitution [31] ${r_0}^2 \to {r_0}^2 + {r_A}^2/[2 + (r_A\Delta_0)^{-2}]$. Usually, the effect of a finite space-time extent of the one-particle emitters is negligible:

$$\frac{{r_A}^2}{2} \ll {r_0}^2, \qquad \frac{{\tau_A}^2}{2} \ll {\tau_0}^2. \quad (63)$$

Note that these conditions guarantee sufficiently smooth four-momentum dependence of the emission function $G_S(\bar{x}_1,p_1;\bar{x}_2,p_2)$, such that we can neglect its

dependence on the four-momentum difference q in the region of the interference effect characterized by the inverse space-time distance between the particle production points. On this, the so-called *smoothness* assumption, (58) reduces to

$$\mathcal{R}(p_1, p_2) \doteq 1 + \sum_S (-1)^S \mathcal{G}_S \left\langle \cos(qx) \right\rangle_{qPS}, \tag{64}$$

where $\mathcal{G}_S$ are the normalized spin factors defined in (17) and (60), and

$$\left\langle \cos(qx) \right\rangle_{qPS} = \frac{\int d^4x_1\, d^4x_2 G_S(x_1, p_1; x_2, p_2) \cos(qx)}{\int d^4x_1\, d^4x_2 G_S(x_1, p_1; x_2, p_2)} = \\ = \frac{\int d^4x g_{PS}(x, q) \cos(qx)}{\int d^4x g_{PS}(x, q)}. \tag{65}$$

Equation (64) is valid up to a correction representing a fraction of ${r_A}^2/{r_0}^2$, ${\tau_A}^2/{\tau_0}^2$. This correction composes a few percent for high-energy hadron–hadron collisions and a fraction of percent for the collisions involving heavy nuclei. Note that (64) is often used to calculate the correlation functions of noninteracting identical particles with the help of various classical transport codes (like RQMD, VENUS or UrQMD) [28] — the emission points are identified with the points of the last collisions or the resonance decays.

At sufficiently small Q, one can calculate the one-dimensional correlation function $\mathcal{R}(Q)$ using a more simple and faster procedure than the averaging according to (64). For this, one can exploit the fact that the angular distribution of the vector $\mathbf{Q}$ becomes isotropic at $Q \to 0$ and calculate $\langle \cos(qx) \rangle \equiv \langle \cos(\mathbf{Q}\mathbf{r}^*) \rangle$ by averaging over the uniform distribution of the cosine of the angle between the vectors $\mathbf{Q}$ and $\mathbf{r}^*$ and, over the one-dimensional r^* distribution determined at $Q \to 0$. We have checked the accuracy of this procedure using the UrQMD simulation of the pNi interactions at 24 GeV in the conditions of the DIRAC experiment [29] and determined the r^* distributions in various Q intervals. It appears that the $\pi^-\pi^-$ correlation functions calculated from the r^* distributions corresponding to the intervals 50–100, 100–150 and 150–200 MeV/c agree with that corresponding to the r^* distribution in the lowest Q interval of 0–50 MeV/c within 0.2–0.9%, $\sim 3\%$ and $\sim 7\%$, respectively. It should be noted that the increasing difference of the correlation functions with the increasing lower boundary of the above Q intervals is not related with the violation of the *smoothness* assumption but rather with the approximate treatment of the angular dependence of the vector $\mathbf{Q}$ and with the Q dependence of the fractions of pairs containing pions from resonance decays.

3.2.3. Femtoscopy with Identical Particles. One can see from (62) that, due to the on-shell constraint $q_0 = \mathbf{v}\mathbf{q} \equiv vq_L$, the correlation function at $v\tau_0 > r_0$ substantially depends on the direction of the vector $\mathbf{q}$ even in the case of spherically

symmetric spatial form of the production region. Thus, the transverse ($\mathbf{q} \perp \mathbf{v}$) and longitudinal ($\mathbf{q} \parallel \mathbf{v}$) correlation radii are $r_T = r_0$ and $r_L = (r_0^2 + v^2\tau_0^2)^{1/2}$, respectively.

The on-shell constraint makes the q dependence of the correlation function essentially three-dimensional (particularly, in pair c.m. system, $qx = -2\mathbf{k}^*\mathbf{r}^*$) and thus makes impossible the unique Fourier reconstruction of the space-time characteristics of the emission process. However, within realistic models, the directional and velocity dependence of the correlation function can be used to determine both the duration of the emission and the form of the emission region [15], as well as to reveal the details of the production dynamics (such as collective flows; see, e.g., [34,35] and reviews [18–21]). For this, the correlation functions can be analyzed in terms of the out (x), side (y), and longitudinal (z) components of the relative momentum vector $\mathbf{q} = \{q_x, q_y, q_z\}$ [36,37]; the out and side denote the transverse components of the vector $\mathbf{q}$, the out direction is parallel to the transverse component of the pair three-momentum. The corresponding correlation widths are usually parameterized in terms of the Gaussian correlation (interferometry) radii r_i, e.g., for spin-0 bosons

$$\mathcal{R}(p_1, p_2) = 1 + \lambda \exp\left(-r_x^2 q_x^2 - r_y^2 q_y^2 - r_z^2 q_z^2 - 2r_{xz}^2 q_x q_z\right), \tag{66}$$

and the radii dependence on pair rapidity and transverse momentum is studied. The correlation strength parameter λ can differ from unity due to the contribution of LL emitters, particle misidentification and coherence effects. Equation (66) assumes azimuthal symmetry of the production process. Generally, e.g., in case of the correlation analysis with respect to the reaction plane, all three cross terms $q_i q_j$ contribute.

It is well known that particle correlations at high energies usually measure only a small part of the space-time emission volume, being only slightly sensitive to its increase related to the fast longitudinal motion of particle emitters. In fact, due to limited emitter decay momenta p_{dec} of few hundred MeV/c, the correlated particles with nearby velocities are emitted by almost comoving emitters and so — at nearby space-time points. In other words, the maximal contribution of the relative motion to the correlation radii in the two-particle c.m. system is limited by the moderate emitter decay length $\tau p_{\mathrm{dec}}/m$. The dynamical examples are resonances, colour strings or hydrodynamic expansion. To substantially eliminate the effect of the longitudinal motion, the correlations can be analyzed in terms of the invariant variable $Q = 2k^* \equiv (-\widetilde{q}^2)^{1/2}$ and the components of the three-momentum difference in the pair c.m. system ($\mathbf{q}^* \equiv \mathbf{Q} = 2\mathbf{k}^*$) or in the longitudinally comoving system (LCMS) [38]. In LCMS, each pair is emitted transverse to the reaction axis so that the generalized relative three-momentum $\widetilde{\mathbf{q}}$ coincides with $\mathbf{q}^*$, except for the *out*-component $\widetilde{q}_x = \gamma_t q_x^*$, where γ_t is the LCMS Lorentz factor of the pair. Particularly, in the

case of one-dimensional boost-invariant expansion, the longitudinal correlation radius in LCMS reads [35]

$$r_z = (T/m_t)^{1/2}\tau, \tag{67}$$

where T is the freeze-out temperature; τ is the proper freeze-out time and m_t is the transverse particle mass. In this model, the side radius measures the transverse radius of the system while the square of the out radius gets an additional contribution $(p_t/m_t)^2\Delta\tau^2$ due to the finite emission duration $\Delta\tau$. The additional transverse expansion leads to a slight modification of the p_t dependence of the longitudinal radius and — to a noticeable decrease of the side radius and the spatial part of the out radius with p_t. Thus in the case of a linear nonrelativistic transverse flow velocity profile $\beta_{\rm F} = \beta_0 r_t/R$ of the expanding fireball with the freeze-out transverse radius R, the side radius

$$r_y \approx \frac{R}{(1 + m_t\beta_0^2/T)^{1/2}}. \tag{68}$$

The decrease of the two-pion correlation radii with increasing transverse mass (expansion) and decreasing centrality (geometry) has been demonstrated, e.g., in Au + Au collisions at $\sqrt{s}_{NN} = 200$ GeV [39].

Since the freeze-out temperature and the transverse flow determine also the shapes of the m_t spectra, the simultaneous analysis of correlations and single-particle spectra for various particle species allows one to disentangle all the freeze-out characteristics (see, e.g., [18]). Thus in heavy-ion collisions, the correlation data show rather weak energy dependence and point to the kinetic freeze-out temperature somewhat below the pion mass, a strong transverse flow (with the mean transverse flow velocity of about half the velocity of light), a short evolution time of 8–10 fm/c and a very short emission duration of about 2–3 fm/c (see, e.g., a recent review [21]).

3.3. Interacting Particles: FSI Correlations. *3.3.1. Production of Interacting Particles.* It is clear that the *smoothness* assumption allows one to express the production cross section through the emission function $G_S(x_1, p_1; x_2, p_2)$ also in the case of interacting particles. Thus, separating the two-particle c.m. motion in the phase factor $\exp[iP(X - X')] \equiv \exp[i(p_1 - \widetilde{q}/2)\epsilon_1 + i(p_2 + \widetilde{q}/2)\epsilon_2]$ and using the *smoothness* assumption to neglect here $\widetilde{q}$ compared with $p_{1,2}$ * and substitute, in the amplitudes $\psi^{S(+)}_{\widetilde{q}}(x)$, the relative coordinates $x = \bar{x} + (\epsilon_1 - \epsilon_2)/2$ and $x' = \bar{x} - (\epsilon_1 - \epsilon_2)/2$ by their mean value $\bar{x}$, we can rewrite (12) in a simple

*The account of $\widetilde{q}$ in the phase factor would lead to the substitution of the particle four-momenta in the emission function by their mean (off-mass-shell) values: $p_i \to Pm_i/(m_1 + m_2)$.

approximate form:

$$(2\pi)^6\gamma_1\gamma_2\frac{d^6\sigma}{d^3\mathbf{p}_1\,d^3\mathbf{p}_2} \doteq \sum_S \int d^4x_1\,d^4x_2 G_S(x_1,p_1;x_2,p_2)\left|\psi^{S(+)}_{\widetilde{q}}(x)\right|^2 = \\ = \sum_S \int d^4x g_{PS}(x,\widetilde{q})\left|\psi^{S(+)}_{\widetilde{q}}(x)\right|^2 \equiv \\ \equiv (2\pi)^6\gamma_1\gamma_2\frac{d^6\sigma_0}{d^3\mathbf{p}_1\,d^3\mathbf{p}_2}\sum_S \mathcal{G}_S\left\langle\left|\psi^{S(+)}_{\widetilde{q}}(x)\right|^2\right\rangle_{\widetilde{q}PS}, \quad (69)$$

where $d^6\sigma_0$ is the production cross section of noninteracting particles introduced in (49). The averaging $\langle\ldots\rangle_{\widetilde{q}PS}$ and the initial spin factors $\mathcal{G}_S$ are defined in (65) and (60). The correlation function defined as the ratio $d^6\sigma/d^6\sigma_0$ then takes on the form:

$$\mathcal{R}(p_1,p_2) \doteq \sum_S \mathcal{G}_S\left\langle\left|\psi^{S(+)}_{\widetilde{q}}(x)\right|^2\right\rangle_{\widetilde{q}PS}. \quad (70)$$

Recall that for identical particles, the Bethe–Salpeter amplitudes $\psi^{S(+)}_{\widetilde{q}}(x)$ should be symmetrized according to (11).

Note that for nonidentical particles, one also arrives at (69) and (70) using the approximate ansatz $\Psi^{S(+)}_{p_1,p_2}(x_1,x_2) \doteq \mathrm{e}^{i(p_1\epsilon_1+p_2\epsilon_2)}\Psi^{S(+)}_{p_1,p_2}(\bar{x}_1,\bar{x}_2)$ which becomes exact in the absence of FSI. For identical particles, this ansatz, applied to the nonsymmetrized amplitudes $\widetilde{\Psi}^{S(+)}$, leads to the correlation function (see also (58) and (60) in [30])

$$\mathcal{R}(p_1,p_2) \doteq \sum_S \mathcal{G}_S\left[\left\langle\left|\widetilde{\psi}^{S(+)}_q(x)\right|^2\right\rangle_{qPS} + \right. \\ \left. + (-1)^S\mathrm{Re}\left\langle\widetilde{\psi}^{S(+)}_q(x)\widetilde{\psi}^{S(+)*}_{-q}(x)\right\rangle''_{qPS}\right], \quad (71)$$

where $\widetilde{\psi}$ is the reduced nonsymmetrized Bethe–Salpeter amplitude ($\widetilde{\psi}^{S(+)}_q(x) = \mathrm{e}^{iqx/2}$ for noninteracting particles). Clearly, the *smoothness* assumption allows one to put $\langle\ldots\rangle''_{qPS} \doteq \langle\ldots\rangle_{qPS}$ and thus recover symmetrized equation (70).

Similar to the case of noninteracting particles, the relative correction to the *smoothness* approximations in (69)–(71) is determined by the ratios ${r_A}^2/{r_0}^2$, ${\tau_A}^2/{\tau_0}^2$ — the measures of the nondiagonality of the space-time density matrix. For identical particles, the correction arises mainly from the simplified treatment of the symmetrization effect and, according to Subsubsec. 3.2.2, it is expected on a few per mil level for the processes involving heavy nuclei. For nonidentical particles, the corrections to the finite-size FSI contributions are of the same

order while, those to the complete correlation functions are usually substantially smaller, being scaled by the relative finite-size contributions of the strong and Coulomb FSI. In case of $|f^S| \ll r^* \ll |a|$, we are interested in, the corresponding strong and Coulomb FSI contributions are of $2f^S/r^*$ and $2r^*/a$, respectively (see Sec. 4).

Proceeding in a similar way with the production cross section of a bound two-particle system, we arrive, on the same conditions as in the case of continuous spectrum, at the approximate form:

$$(2\pi)^3\gamma_b\frac{d^3\sigma_b^S}{d^3\mathbf{P}_b} \doteq \int d^4x_1\, d^4x_2 G_S(x_1,p_1;x_2,p_2)\left|\psi_b^{S(+)}(x)\right|^2 = \\ = \int d^4x g_{PS}(x,0)\left|\psi_b^{S(+)}(x)\right|^2 \equiv \\ \equiv (2\pi)^6\gamma_1\gamma_2\frac{d^6\sigma_0}{d^3\mathbf{p}_1\, d^3\mathbf{p}_2}\mathcal{G}_S\left\langle\left|\psi_b^{S(+)}(x)\right|^2\right\rangle_{0PS}, \quad (72)$$

where $\mathbf{p}_i = \mathbf{P}_b m_i/(m_1+m_2)$, $\mathbf{P} = \mathbf{P}_b$ and $P_0 \doteq P_{b0}$.

3.3.2. Equal-Time Approximation. For noninteracting particles, the nonsymmetrized Bethe–Salpeter amplitude $\psi_{\tilde{q}}^{(+)}(x) = \mathrm{e}^{-i\mathbf{k}^*\mathbf{r}^*}$ is independent of the relative emission time t^* in the pair c.m. system. On the contrary, the amplitude of two interacting particles contains an explicit dependence on t^* — the interaction effect vanishes at $|t^*| \to \infty$. However, it can be shown [12] (see Appendix A) that the effect of nonequal times can be neglected on condition

$$|t^*| \ll m(t^*)r^{*2}, \quad (73)$$

where $m(t^* > 0) = m_2$ and $m(t^* < 0) = m_1$. On this condition, one can use the approximation of equal emission times of the two particles in their c.m. system ($t^* = 0$) and substitute the Bethe–Salpeter amplitude by the usual nonrelativistic two-particle wave function. The applicability condition (73) of the *equal-time* approximation is usually satisfied for heavy particles like kaons or nucleons. But even for pions, this approximation merely leads to a slight overestimation (typically less than a few percent) of the strong FSI contribution to the production cross section [12]. To demonstrate this, one can use the simple static Gaussian model of independent one-particle emitters described by the amplitude (51). The applicability condition (73) of the *equal-time* approximation can then be written as [12]

$$\tau_0 \ll \mu\gamma r_0({r_0}^2 + v^2{\tau_0}^2)^{1/2}. \quad (74)$$

Recall, however, that in high-energy collisions, the static model is relevant for a limited rapidity region only. It means that the pair velocity v in the rest frame of the contributing emitters is essentially determined by the distribution of particle

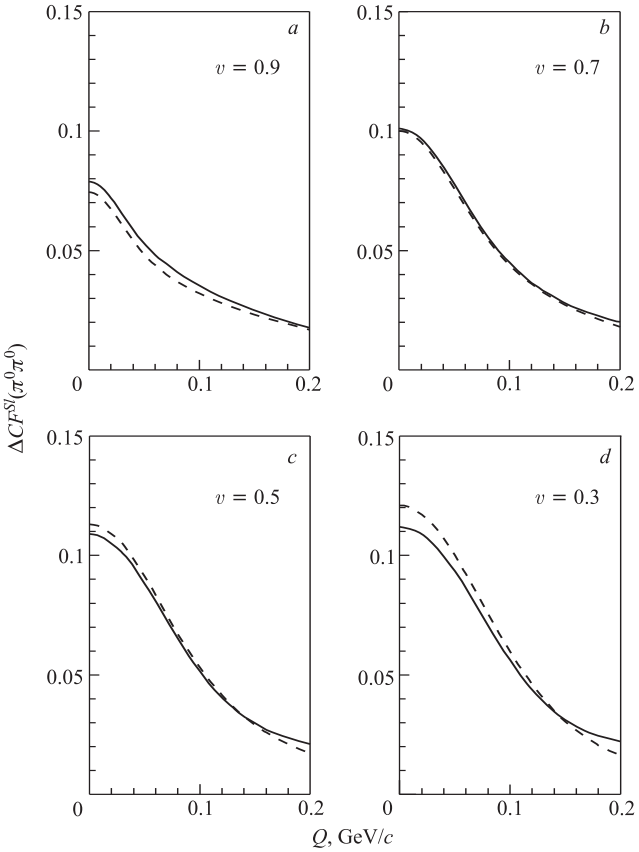

Fig. 3. The FSI contribution to the $\pi^0\pi^0$ correlation function calculated for different values of the pair velocity v in a model of independent one-particle emitters distributed according to a Gaussian law with the spatial and time width parameters $r_0 = 2$ fm and $\tau_0 = 2$ fm/c. The exact results (solid curves) are compared with those obtained in the *equal-time* approximation (dashed curves)

transverse momenta. For pion pairs at $Q \to 0$ one then has $\langle v \rangle \approx 0.8$. For $\tau_0 <\sim r_0$, condition (74) requires sufficiently small Compton wave lengths of the particles in the emitter rest frame: $1/\omega_i \ll r_0$, while for large characteristic emission times, $\tau_0 \gg r_0/v$, it requires small de Broglie wave lengths: $1/p_i \ll r_0$. Clearly, this condition is not satisfied for very slow particles emitted by the emitters of a long lifetime. The increasing importance of the nonequal time effect with the decreasing pair velocity and increasing lifetime of the emitters is demonstrated in Figs. 3 and 4 for the FSI contribution in the $\pi^0\pi^0$ correlation

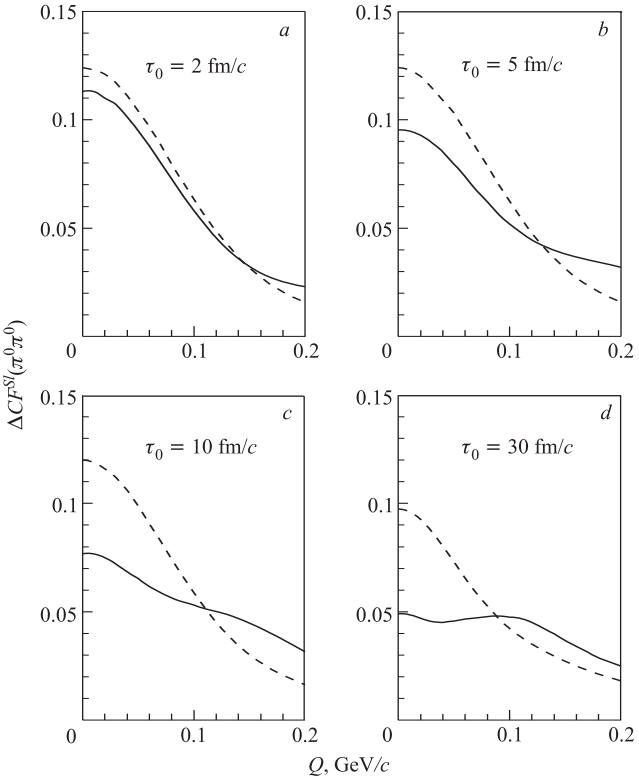

Fig. 4. The same as in Fig. 3 for the pair velocity $v = 0.1$, the spatial width parameter $r_0 = 2$ fm and different values of the time width parameter τ_0

function. For sufficiently large velocities $v > 0.5$ and radii $r_0 > 1$ fm, we are interested in, the effect is rather small, not exceeding 5% of the FSI contribution in the low-k^* region, corresponding to the effect of a few per mil in the correlation function.

As for the effect of nonequal times on the Coulomb FSI it does not influence the leading zero-distance ($r^* = 0$) part, and the effect of the subleading part (expected on a similar percent level as in the case of the strong FSI) can be neglected when scaled by its contribution $\sim 2r^*/a$. It concerns also the case of hadronic atoms since the subleading part is the same as in the continuous spectrum at $k^* = 0$.

Adopting the *smoothness* and *equal-time* approximations (with the accuracy of a few per mil), we can rewrite (69) and (72) for the production cross sections of particles 1 and 2 in continuous and discrete spectrum at low relative or binding

energies as follows:

$$\gamma_1\gamma_2\frac{d^6\sigma}{d^3\mathbf{p}_1 d^3\mathbf{p}_2} \doteq \gamma_1\gamma_2\frac{d^6\sigma_0}{d^3\mathbf{p}_1 d^3\mathbf{p}_2}\sum_S \mathcal{G}_S \left\langle \left|\psi^S_{-\mathbf{k}^*}(\mathbf{r}^*)\right|^2\right\rangle_{\tilde{q}PS}, \tag{75}$$

$$\gamma_b\frac{d^3\sigma^S_b}{d^3\mathbf{P}_b} \doteq (2\pi)^3\gamma_1\gamma_2\frac{d^6\sigma_0}{d^3\mathbf{p}_1\, d^3\mathbf{p}_2}\mathcal{G}_S \left\langle \left|\psi^S_b(r^*)\right|^2\right\rangle_{0PS}, \tag{76}$$

where $b = \{n0\}$ and $\mathbf{p}_i = \mathbf{P}_b m_i/(m_1+m_2)$ in (76); for equal-mass particles $\mathbf{p}_1 = \mathbf{p}_2 = \mathbf{P}_b/2$ and $\gamma_1 = \gamma_2 = \gamma_b$. Particularly, for $\pi^+\pi^-$ production, one can then rewrite the correction factors in (38) and (39) as

$$1+\delta(\mathbf{k}^*) \doteq \left\langle \left|\psi_{-\mathbf{k}^*}(\mathbf{r}^*)\right|^2\right\rangle^{\text{SL}}_{\tilde{q}P}[A_c(\eta)]^{-1}, \tag{77}$$

$$1+\delta_n \doteq \left\langle \left|\psi_{n0}(r^*)\right|^2\right\rangle^{\text{SL}}_{0P}\left|\psi^{\text{coul}}_{n0}(0)\right|^{-2}. \tag{78}$$

We will show that the r^* dependence of the wave functions $\psi^S_{-\mathbf{k}^*}$ and ψ^S_b for two oppositely charged particles in continuous and discrete spectrum is practically the same at separations r^*, in the pair c.m. system, much smaller than the Bohr radius $|a|$. Therefore, the corrections to (75) and (76) (arising due to the *smoothness* and *equal-time* approximations used in their respective derivation from (12) and (20)) practically cancel out in the ratio of the numbers of pairs produced in continuous and discrete spectrum provided $\langle r^*\rangle^{\text{SL}} \ll |a|$.

3.3.3. The Effect of Residual Charge. The formalism of Sec. 1 assumes a free motion of a given particle pair during the final stage of the collision. Here we will estimate the FSI effect of the residual charge which is known to substantially influence particle spectra and, to a lesser extent, also particle correlations in low-energy collisions involving nuclei [23]. Since, at high energies, this effect can be expected of minor importance, we will estimate only its upper limit.

Generally, instead of the two-particle Bethe–Salpeter amplitude $\Psi^{(+)S}_{p_1p_2}(x_1,x_2)$, the correlation function is determined by the amplitude $\Psi^{(+)S\{\alpha\}}_{p_1p_2}(x_1,x_2)$ representing the solution of a complicated multibody problem, taking into account interaction between the two particles and also their interaction with the residual system described by the quantum numbers $\{\alpha\}$. For our purpose, it is sufficient to approximate these quantum numbers by an effective (comoving with a given pair) point-like residual charge Ze and consider a thermal motion of the two particles with the temperature $T \sim m_\pi$ in the rest frame of this charge.

Let us start with the hypothetical case of particles that interact with the charge Ze but their mutual interaction is «switched off». In such a situation, we can treat the systems $(1,Z)$ and $(2,Z)$ independently. Then the interaction with the Coulomb center just leads to the substitution of the spatial parts of the plane waves $\mathrm{e}^{ip_ix_i}$ by the usual Coulomb wave functions: $\mathrm{e}^{-i\mathbf{p}_i\mathbf{r}_i} \to \mathrm{e}^{-i\mathbf{p}_i\mathbf{r}_i}\Phi^{z_iZ}_{\mathbf{p}_i}(\mathbf{r}_i)$,

where $\Phi^{z_i Z}_{\mathbf{p}_i}(\mathbf{r}_i) = \mathrm{e}^{i\delta_i}\sqrt{A_c(\eta_i)}F(-i\eta_i, 1, i\rho_i)$, $\rho_i = \mathbf{p}_i\mathbf{r}_i + \mathrm{p}_i r_i$, $\eta_i = (\mathrm{p}_i a_i)^{-1}$, $a_i = (\omega_i z_i Z e^2)^{-1}$ is the Bohr radius of the system (i, Z) (taking into account the sign of the interaction) generalized to the relativistic case by the substitution $m_i \to \omega_i$ of the particle masses by their energies; δ_i is the Coulomb s-wave phase shift; $A_c(\eta_i)$ is the Coulomb penetration factor and $F(\alpha, 1, z)$ is the confluent hypergeometrical function; see (24), (89), and (90). For the complete amplitude we have:

$$\widetilde{\Psi}^{(+)Z}_{p_1p_2}(x_1, x_2) = \mathrm{e}^{ip_1x_1+ip_2x_2}\Phi^{z_1Z}_{\mathbf{p}_1}(\mathbf{r}_1)\Phi^{z_2Z}_{\mathbf{p}_2}(\mathbf{r}_2) \equiv$$

$$\equiv \mathrm{e}^{iPX}\,\mathrm{e}^{-i\mathbf{k}^*\mathbf{r}^*}\Phi^{z_1Z}_{\mathbf{p}_1}(\mathbf{r}_1)\Phi^{z_2Z}_{\mathbf{p}_2}(\mathbf{r}_2). \quad (79)$$

Note that a small contribution of spin-dependent electro-magnetic forces is neglected here so that $\widetilde{\Psi}^{(+)SZ} \equiv \widetilde{\Psi}^{(+)Z}$ is independent of the total spin S of the particle pair.

Let us now «switch on» the interaction between particles 1 and 2. Since we consider the relative motion of the two particles at characteristic distances much slower compared with their motion with respect to the Coulomb center, it is natural to assume that in such a case the plane wave $\mathrm{e}^{-i\mathbf{k}^*\mathbf{r}^*}$ in (79) will be basically substituted by the Bethe–Salpeter amplitude $\psi^S_{\widetilde{q}}(x)$ describing the relative motion of isolated interacting particles. After this substitution we get the amplitude in the so-called adiabatic (factorization) approximation [23]:

$$\Psi^{(+)SZ}_{p_1p_2}(x_1, x_2) = \mathrm{e}^{iPX}\psi^S_{\widetilde{q}}(x)\Phi^{z_1Z}_{\mathbf{p}_1}(\mathbf{r}_1)\Phi^{z_2Z}_{\mathbf{p}_2}(\mathbf{r}_2). \quad (80)$$

Instead of the six-dimensional correlation function $\mathcal{R}(p_1, p_2)$ we calculate the one-dimensional one, $\mathcal{R}^Z(k^*)$, with the numerator and denominator integrated over the simulated particle spectra. In the *equal-time* approximation,

$$\mathcal{R}^Z(k^*) = \frac{\sum\limits_{i=1}^{N(k^*)}\sum\limits_S \rho_S|\psi^S_{-\mathbf{k}^*_i}(\mathbf{r}^*_i)\Phi^{z_1Z}_{\mathbf{p}_{1_i}}(\mathbf{r}_{1_i})\Phi^{z_2Z}_{\mathbf{p}_{2_i}}(\mathbf{r}_{2_i})|^2}{\sum\limits_{i=1}^{N(k^*)}|\Phi^{z_1Z}_{\mathbf{p}_{1_i}}(\mathbf{r}_{1_i})\Phi^{z_2Z}_{\mathbf{p}_{2_i}}(\mathbf{r}_{2_i})|^2}, \quad (81)$$

where $N(k^*)$ is the number of generated particle pairs in a given k^* bin. To separate the pure effect of the residual Coulomb field on particle correlations, we compare the correlation function $\mathcal{R}^Z(k^*)$ with the one, $\mathcal{R}^{«Z»}(k^*)$, taking into account for the latter the effect of the nucleus Coulomb field on one-particle spectra but not on particle correlations (i.e., simulating the argument $\mathbf{r}^*$ independently of the arguments $\mathbf{r}_1$ and $\mathbf{r}_2$). Note that due to the velocity dependence of the correlation function, $\mathcal{R}^{«Z»} = \mathcal{R}^{Z=0}$ only at a fixed pair velocity v. In Fig. 5, we present the ratios of the $\pi^+\pi^-$ correlation functions $\mathcal{R}^Z$ and $\mathcal{R}^{«Z»}$ assuming that

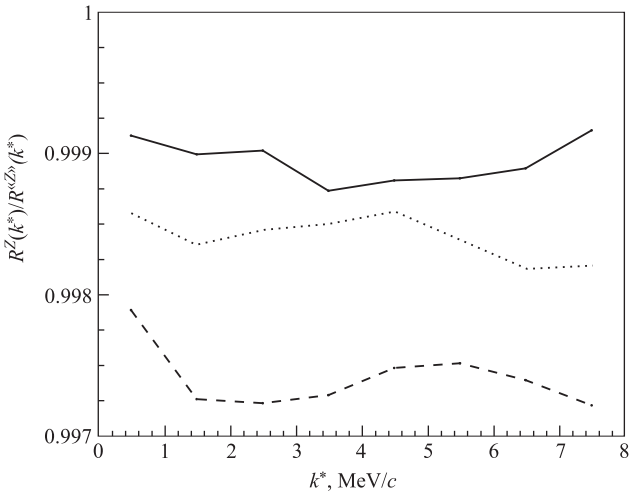

Fig. 5. The ratios of the $\pi^+\pi^-$ correlation functions $\mathcal{R}^Z$ and $\mathcal{R}^{\langle Z\rangle}$. For the latter, only one-particle spectra are influenced by the effective comoving charge Z. The pions are assumed to be emitted in the rest frame of a point-like charge Z according to the thermal law with a temperature of 140 MeV. The distribution of the space-time coordinates of the particle emitters is simulated as a product of Gauss functions with the equal spatial and time width parameters $r_0 = c\tau_0$. The full broken line corresponds to $Z = 30, r_0 = 2$ fm, the dashed and dotted ones — to $Z = 60, r_0 = 2$ and 3 fm, respectively

the pions are emitted in the rest frame of the residual charge Z according to the thermal law with a temperature of 140 MeV at the space-time points distributed according to a product of Gauss functions with the equal spatial and time width parameters $r_0 = c\tau_0$. One may see that even for the radius r_0 as low as 2 fm the effect of the residual comoving charge as large as $Z = 60$ is less than a few per mil. Taking into account that the effective radius r_0 is larger than 2 fm even for proton collisions with low-Z nuclei and that the effective residual charge is only a fraction of the target nucleus charge, one can conclude that the effect of the residual charge is on a negligible level of a fraction of per mil.

3.3.4. Femtoscopy with Nonidentical Particles. The FSI effect allows one to access the space-time characteristics of particle production also with the help of correlations of nonidentical particles. One should be however careful when analyzing these correlations in terms of simple models like those assuming the Gaussian space-time parameterization of the source. The simplified description of the r^* separations can lead to inconsistencies in the treatment of QS and FSI effects. While the QS and strong FSI effects are influenced by large r^* separations mainly through the correlation strength parameter λ, the shape of the Coulomb

FSI is sensitive to the distances as large as the pair Bohr radius (hundreds of fm for the pairs containing pions).

This problem can be at least partially overcome with the help of imaging techniques [40] or transport simulations. The former yield the $\mathbf{r}^*$ distribution inverting the measured correlation function using the integral equation (75) with the kernel given by the wave function squared. The latter account for the dynamical evolution of the emission process and provide the phase-space information required to calculate the QS and FSI effects on the correlation function.

Thus, the transport RQMD v.2.3 code was used in a preliminary analysis of the NA49 $\pi^+\pi^-$, π^+p and π^-p correlation data from central Pb + Pb 158A GeV collisions [20]. The model correlation functions $\mathcal{R}_{\mathrm{RQMD}}(Q; s_r)$ have been calculated using the FSI code based on the formalism developed in [12], weighting the simulated pairs by squares of the corresponding wave functions. The scale parameter s_r, multiplying the simulated space-time coordinates of the emitters, was introduced in the model correlation function to account for a possible mismatch of the r^* distribution. For this, a set of correlation functions $\mathcal{R}_{\mathrm{RQMD}}(Q; s_r^i)$ was calculated at three chosen values s_r^i of the scale parameter, and the quadratic interpolation was used to calculate $\mathcal{R}_{\mathrm{RQMD}}(Q; s_r)$ for arbitrary value of s_r:

$$\mathcal{R}_{\mathrm{RQMD}}(Q; s_r) = \sum_{i=1}^{3} \frac{(s_r - s_r^j)(s_r - s_r^k)}{(s_r^i - s_r^j)(s_r^i - s_r^k)} \mathcal{R}_{\mathrm{RQMD}}(Q; s_r^1), \tag{82}$$

where $\{i, j, k\}$ are permutations of the sequence $\{1, 2, 3\}$. The NA49 correlation functions were then fitted by

$$\mathcal{R}(Q) = N\left[\lambda \mathcal{R}_{\mathrm{RQMD}}(Q; s_r) + (1 - \lambda)\right] \tag{83}$$

with two additional parameters, the normalization N and the correlation strength λ. The fitted values of the λ parameter are in reasonable agreement with the expected contamination of $\sim 15\%$ from strange particle decays and particle misidentification. The fitted values of the scale parameter show that the RQMD transport model overestimates the r^* separations of the pion and proton emitters by 10–20% thus indicating an underestimation of the collective flow in this model.

The shape of the correlation function is less influenced by large r^* separations in the case of two-particle systems with the absent Coulomb FSI, e.g., in the case of $p\Lambda$ system. The data on $p\Lambda$ correlations in heavy-ion collisions show a significant enhancement at low relative momentum, consistent with the known singlet and triplet $p\Lambda$ s-wave scattering lengths. In fact, the fits using the analytical expression for the correlation function [12] yield the Gaussian correlation radii of 3–4 fm in agreement with the radii obtained from pp correlations in the same experiments. These radii are smaller than those obtained from two-pion and two-kaon correlation functions at the same transverse momenta [41] and are in

qualitative agreement with the approximate m_t scaling expected in the case of the collective expansion, see (67) and (68).

The correlation function of nonidentical particles, compared with the identical ones, contains a principally new piece of information on the relative space-time asymmetries in particle emission [42]. Since this information enters in the two-particle FSI amplitude through the terms odd in $\mathbf{k}^*\mathbf{r}^* \equiv \mathbf{p}_1^*(\mathbf{r}_1^* - \mathbf{r}_2^*)$, it can be accessed studying the correlation functions $\mathcal{R}_{+i}$ and $\mathcal{R}_{-i}$ with positive and negative projection k_i^* on a given direction $\hat{i}$ or — the ratio $\mathcal{R}_{+i}/\mathcal{R}_{-i}$. For example, $\hat{i}$ can be the direction of the pair velocity or any of the out (x), side (y), longitudinal (z) directions. In LCMS, we have $r_i^* = r_i$, except for $r_x^* \equiv \Delta x^* = \gamma_t(\Delta x - v_t \Delta t)$, where γ_t and v_t are the pair LCMS Lorentz factor and velocity. One may see that the asymmetry in the out (x) direction depends on both space and time asymmetries $\langle \Delta x \rangle^{\text{SL}}$ and $\langle \Delta t \rangle^{\text{SL}}$. In case of a dominant Coulomb FSI, the intercept of the correlation function ratio is directly related with the asymmetry $\langle r_i^* \rangle^{\text{SL}}$ scaled by the pair Bohr radius a:

$$\frac{\mathcal{R}_{+i}}{\mathcal{R}_{-i}} \approx 1 + \frac{2\langle r_i^* \rangle^{\text{SL}}}{a}. \tag{84}$$

It appears that the out correlation asymmetries between pions, kaons and protons observed in heavy-ion collisions at CERN and BNL are in agreement with practically charge independent meson production and, assuming $m_1 < m_2$, with a negative $\langle \Delta x \rangle^{\text{SL}} = \langle x_1 - x_2 \rangle^{\text{SL}}$ and/or positive $c\langle \Delta t \rangle^{\text{SL}} = c\langle t_1 - t_2 \rangle^{\text{SL}}$ on the level of several fm [20,43]. In fact, they are in quantitative agreement with the RQMD transport model as well as with the hydromotivated blast wave parametrization, both predicting the dominance of the spatial part of the asymmetries generated by large transverse flows.

In the thermal approach, the mean thermal velocity is smaller for heavier particle and thus washes out the positive spatial shift due to the flow to a lesser extent. As a result, $\langle x_\pi \rangle^{\text{SL}} < \langle x_K \rangle^{\text{SL}} < \langle x_p \rangle^{\text{SL}}$. The observation of the correlation asymmetries in agreement with the mass hierarchy of the shifts in the out direction may thus be considered as one of the most direct signals of a universal transversal collective flow [20]. This is in contrast with the effect of m_t scaling of the correlation radii which can be also explained by a large transverse temperature gradient like in the Buda–Lund model [44].

3.3.5. Correlation Measurement of Strong Interaction. One can also use the correlation measurements to improve knowledge of the strong interaction for various two-particle systems. In the collisions involving sufficiently heavy nuclei, the effective radius r_0 of the emission region can be considered much larger than the range of the strong interaction potential. The FSI contribution is then independent of the actual potential form [45]. At small $Q = 2k^*$ and a given total spin S, it is determined by the s-wave scattering amplitude $f^S(k^*)$ [12]. In

case of $|f^S| > r_0$, this contribution is of the order of $|f^S/r_0|^2$ and dominates over the effect of QS. In the opposite case, the sensitivity of the correlation function to the scattering amplitude is determined by the linear term f^S/r_0.

The possibility of the correlation measurement of the scattering amplitudes has been demonstrated [20] in a preliminary analysis of the NA49 $\pi^+\pi^-$ correlation data within the RQMD transport model. For this, besides the r^*-scale s_r, the strong interaction scale s_f has been introduced in the RQMD correlation function $\mathcal{R}(Q; s_r, s_f)$, rescaling the original s-wave $\pi^+\pi^-$ scattering amplitude taken from [5]: $f(k^*) \to s_f f(k^*)$; it approximately corresponds to the rescaling of the original scattering length $f_0 = 0.232$ fm. The fitted parameter $s_f = 0.63 \pm 0.08$ appears to be significantly lower than unity. To a similar but somewhat weaker rescaling (~ 0.8) point also the preliminary result of the DIRAC experiment on the pionium lifetime [4], the BNL and CERN data on K_{l4} [6] and $K^\pm \to \pi^\pm\pi^0\pi^0$ [7] decays, as well as the two-loop calculation in the chiral perturbation theory with a standard value of the quark condensate [8].

Comparing the fit results with the theoretical predictions, one should have in mind that the latter are subject to the electromagnetic corrections on the level of several percent and that the correlation measurement may underestimate $f(k^*)$ by a few percent due to the use of the equal-time approximation. A substantial systematic error can also arise from a simplified fit of the strong FSI amplitude. To avoid the latter, one can use the Roy equations and represent the $\pi^+\pi^-$ strong interaction amplitude at low energies as a unique function of the isoscalar and isotensor s-wave scattering lengths a_0^0 and a_0^2, see Appendix D in [46]. The two-parameter dependence of the scattering amplitude can be further reduced to a single-parameter one within the generalized chiral perturbation theory predicting a strong correlation between the two s-wave scattering lengths (see Eq. (13.2) in [8]). The systematic error due to the uncertainty in the fitted r^* distribution (e.g., in the scale parameter s_r) can be diminished in a simultaneous analysis of $\pi^+\pi^-$ and $\pi^\pm\pi^\pm$ correlation functions. The high statistics DIRAC data on two-pion correlations may thus allow one to determine the s-wave scattering lengths a_0^0 and a_0^2 better than to 10% and serve as complementary to the pionium lifetime measurement in the same experiment.

The correlation technique was also used to estimate the singlet $\Lambda\Lambda$ s-wave scattering length based on the fits of the $\Lambda\Lambda$ correlation data from Pb + Pb collisions at $158A$ GeV [20]. Though the fit results are not very restrictive, they likely exclude the possibility of a large singlet scattering length comparable to that of ~ 20 fm for the two-nucleon system. Similarly, the fit of the $p\bar{\Lambda}$ and $\bar{p}\Lambda$ correlation functions measured in Au + Au collisions at $\sqrt{s}_{NN} = 200$ GeV allowed one to determine the corresponding spin-averaged s-wave scattering length. The fitted imaginary part of the scattering length of ~ 1 fm is in agreement with the $\bar{p}p$ results (thus pointing to about the same $\bar{p}\Lambda$ and $\bar{p}p$ annihilation cross sections) while the real part appears to be more negative [47].

4. ONE-CHANNEL WAVE FUNCTIONS

4.1. Continuous Spectrum. *4.1.1. Short-Range FSI.* Let us start with the case when the two-particle FSI is due to the short-range forces only. In the considered region of small k^*, the short-range particle interaction is dominated by s waves. Since the radius of the s-wave interaction is usually small compared with the distance r^* between the production points of particles 1 and 2 in their c.m. system, the FSI effect is mainly determined by the asymptotic behaviour of the scattered wave outside the region of the strong interaction $r^* > d$:

$$\Delta\psi_{-\mathbf{k}^*}(\mathbf{r}^*) = f(k^*)\,\mathrm{e}^{ik^*r^*}/r^*. \tag{85}$$

The s-wave amplitude f depends on the magnitude of the vector $\mathbf{k}^*$ only. Assuming the absence of inelastic transitions, it satisfies the one-channel s-wave unitarity condition $\mathrm{Im}\, f = k^*|f|^2$ or, equivalently $\mathrm{Im}\, f^{-1} = -k^*$, and so can be represented as

$$f = \frac{\exp(2i\delta_0) - 1}{2ik^*} = \left(K^{-1} - ik^*\right)^{-1}, \tag{86}$$

where δ_0 is the s-wave phase shift and $K^{-1} = k^* \cot\delta_0$ is a real function of k^*. Usually (for potentials vanishing with the distance exponentially or faster) this function is real also for negative kinetic energies $k^{*2}/(2\mu)$, so that its expansion can contain only even powers of k^* [25]. Retaining near threshold only the first two terms in the expansion, one can express the function K^{-1} or K through the corresponding two parameters: scattering length f_0 and effective range d_0 or curvature b_0:

$$K^{-1} \doteq f_0^{-1} + \frac{1}{2}d_0k^{*2}, \qquad K \doteq f_0 + b_0k^{*2}, \qquad b_0 \doteq -\frac{1}{2}d_0{f_0}^2. \tag{87}$$

The expansion of K^{-1} is superior for two-nucleon systems (due to large scattering lengths, amounting to about 20 fm in the singlet case) while for other systems, the K expansion is often preferred. To extend the latter to a wider energy range, it is usually written in a relativistic form and additional parameters are added. For example [8]:

$$K = \frac{2}{\sqrt{s}}\frac{s_{\mathrm{th}} - s_0}{s - s_0}\sum_{j=0}^{3} A_j x^{2j}, \qquad x = \frac{2k^*}{\sqrt{s_{\mathrm{th}}}}, \tag{88}$$

where $s = (p_1{+}p_2)^2 = (\omega_1^*{+}\omega_2^*)^2$, $\omega_{1,2}^* = (m_{1,2}^2{+}k^{*2})^{1/2}$ and $s_{\mathrm{th}} = (m_1{+}m_2)^2$. The parameter s_0 takes into account the eventual resonance, specifying the value of the two-particle invariant mass squared where the phase $\delta_0(k^*)$ passes through 90°. The behaviour of the s-wave K function in a wide k^* interval is however of minor importance since we are interested in the near-threshold region and have

Table 1. **The pair Bohr radius including the sign of the interaction, $a = (\mu z_1 z_2 e^2)^{-1}$, and the characteristic width of the Coulomb correlation effect, $Q_c \equiv 2k_c^* = 4\pi/|a|$, corresponding to $|\eta|^{-1} = 2\pi$ (see (24) and the first panel in Fig. 6)**

Pair	$\pi^+\pi^\pm$	$\pi^+K^\pm$	$\pi^\pm p$	$K^+K^\pm$	$K^\pm p$	$pp^\pm$
a, fm	± 387.5	± 248.6	± 222.5	± 109.6	± 83.6	± 57.6
Q_c, MeV/c	6.4	10.0	11.1	22.6	29.7	43.0

already neglected the p-wave correction $O(k^{*2}a_1/r^*)$ in (85); here a_1 is a p-wave scattering length. For $\pi^+\pi^-$ system, $a_1 \approx 0.1$ fm^3, $f_0 \approx 0.2$ fm, $d_0 \approx -10$ fm and the relative p-wave contribution to the k^{*2} term due to the short-range FSI composes in the production cross section $\sim a_1/(a_1 - d_0{f_0}^2/2 - {f_0}^3/3) \sim 30\%$; the relative contribution of the k^{*2} term $\sim (a_1 - d_0{f_0}^2/2 - {f_0}^3/3)k^{*2}/f_0$ being less than 1% of the total short-range FSI contribution for $Q = 2k^* < 30$ MeV/c.

Note that the extension of the asymptotic wave function in the inner region leads to a relative shift in the production cross section of the order $|f|^2 \dfrac{d}{dk^{*2}} \mathrm{Re}(1/f)/(\langle r^* \rangle^{\text{SL}})^3$ [12, 48]. The leading part of this shift can be, in principle, corrected for (see Subsec. 5.3). However, being quadratic in the amplitude f, it is rather small for $\pi\pi$-, πK- or πp-systems — usually not exceeding several percent of the short-range FSI contribution.

4.1.2. Account of the Coulomb FSI. Similar to the case of neutral particles, we will approximate (with the same accuracy) the wave function of two charged particles near threshold by the asymptotic solution outside the region of the strong interaction $r^* > d$. It is well known that the long-range Coulomb interaction modifies both the plane and spherical waves [25]:

$$\psi_{-\mathbf{k}^*}(\mathbf{r}^*) = \mathrm{e}^{i\delta_c}\sqrt{A_c(\eta)}\left[\mathrm{e}^{-i\mathbf{k}^*\mathbf{r}^*}F(-i\eta, 1, i\xi) + f_c(k^*)\frac{\widetilde{G}(\rho,\eta)}{r^*}\right], \qquad (89)$$

where $\xi = \mathbf{k}^*\mathbf{r}^* + k^*r^* \equiv \rho(1+\cos\theta^*)$, $\rho = k^*r^*$, $\eta = (k^*a)^{-1}$, $a = (\mu z_1 z_2 e^2)^{-1}$ is the two-particle Bohr radius including the sign of the interaction (see Table 1), $\delta_c = \arg\Gamma(1+i\eta)$ is the Coulomb s-wave phase shift, $A_c(\eta)$ is the Coulomb penetration factor defined in (24),

$$F(\alpha, 1, z) = 1 + \alpha z/1!^2 + \alpha(\alpha+1)z^2/2!^2 + \ldots \qquad (90)$$

is the confluent hypergeometric function and $\widetilde{G} = \sqrt{A_c}(G_0 + iF_0)$ is a combination of the regular (F_0) and singular (G_0) s-wave Coulomb functions (see, e.g., [45]):

$$\widetilde{G}(\rho,\eta) = P(\rho,\eta) + 2\eta\rho\,[\ln\,|2\eta\rho| + 2C - 1 + \chi(\eta)]\,B(\rho,\eta). \qquad (91)$$

Here $C \doteq 0.5772$ is the Euler constant, the functions

$$\begin{aligned} B(\rho,\eta) &= \sum_{s=0}^{\infty} B_s, \qquad B_0 = 1, \qquad B_1 = \eta\rho, \ldots, \\ P(\rho,\eta) &= \sum_{s=0}^{\infty} P_s, \qquad P_0 = 1, \qquad P_1 = 0, \ldots \end{aligned} \tag{92}$$

are given by the following recurrence relations:

$$\begin{aligned} (n+1)(n+2)B_{n+1} &= 2\eta\rho B_n - \rho^2 B_{n-1}, \\ n(n+1)P_{n+1} &= 2\eta\rho P_n - \rho^2 P_{n-1} - (2n+1)2\eta\rho B_n, \end{aligned} \tag{93}$$

$B(\rho,\eta) \equiv F_0/(\rho\sqrt{A_c}) \to \sin(\rho)/\rho$ and $P(\rho,\eta) \to \cos(\rho)$ in the limit $\eta\rho \equiv r^*/a \to 0$. The function

$$\chi(\eta) = h(\eta) + \frac{iA_c(\eta)}{(2\eta)}, \tag{94}$$

where the function $h(\eta)$ is expressed through the digamma function $\psi(z) = \Gamma'(z)/\Gamma(z)$:

$$h(\eta) = \frac{\psi(i\eta) + \psi(-i\eta) - \ln(\eta^2)}{2}. \tag{95}$$

For $|\eta| < 0.3$, the function $h(\eta) \doteq 1.2\eta^2 - \ln|\eta| - C$, while at large $|\eta|$ this function can be represented by a truncated series in inverse powers of η^2: $h(\eta) = \eta^{-2}/12 + \eta^{-4}/120 + \ldots$ The amplitude

$$f_c(k^*) = \frac{f(k^*)}{A_c(\eta)}, \tag{96}$$

where $f(k^*)$ is the amplitude of the low-energy s-wave elastic scattering due to the short-range interaction renormalized by the long-range Coulomb forces. Assuming again the absence of inelastic transitions, the amplitude $f(k^*) = (\mathrm{e}^{2i\delta_0} - 1)/(2ik^*)$ and satisfies the one-channel s-wave unitarity condition. Similar to the case of neutral particles, one then has [25]:

$$f_c(k^*) = \left(K^{-1} - \frac{2\chi(\eta)}{a}\right)^{-1}, \tag{97}$$

where the function K can be parameterized according to (87) or (88).

Note that $\delta_c \to 0$, $A_c \to 1$ for $\eta \to 0$ ($k^* \gg |a|^{-1}$) and $\widetilde{G} \to \mathrm{e}^{i\rho}$, $F \to 1$ for $\eta\rho \equiv r^*/a \to 0$. So, the two-particle wave function in the absence of the long-range Coulomb forces is recovered provided r^*, f_0 and $1/k^*$ are much smaller than the Bohr radius $|a|$.

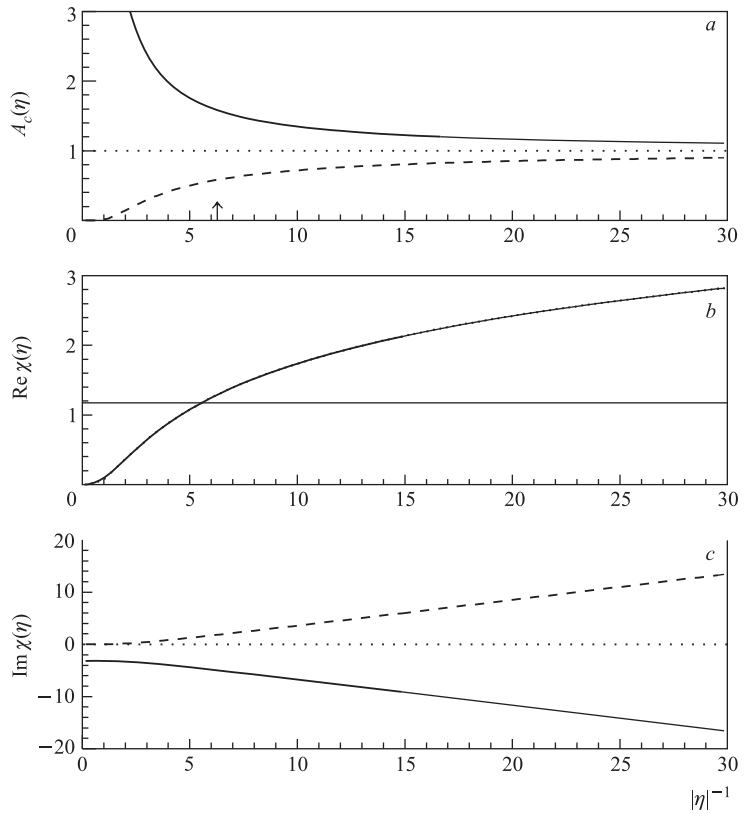

Fig. 6. The functions $A_c(\eta)$, $\mathrm{Re}\,\chi(\eta) \equiv h(\eta)$ and $\mathrm{Im}\,\chi(\eta) = A_c(\eta)/(2\eta)$ defined in (24), (94), and (95). The solid and dashed curves correspond to the attraction ($\eta < 0$) and repulsion ($\eta > 0$), respectively. For two-pion systems, the variable $|\eta|^{-1} \equiv |ak^*|$ approximately coincides with the relative three-momentum $Q = 2k^*$ in MeV/c: $|\eta|^{-1} \doteq 0.98Q/(\mathrm{MeV}/c)$. The arrow in panel a indicates the characteristic width $|\eta|^{-1} = 2\pi$ of the Coulomb effect

In Fig. 6, we plot $A_c(\eta)$ and $\chi(\eta)$ as functions of the variable $|\eta|^{-1} = |ak^*|$. For the system of two charged pions, this variable approximately corresponds to $Q = 2k^*$ in MeV/c. At $k^* \to 0$, the Coulomb penetration factor $A_c(\eta)$ respectively tends to 0 and ∞ for like and unlike particle charges. With the increasing k^*, this factor slowly approaches unity: $A_c(\eta) \approx 1 - \pi\eta$ for $k^* > 2\pi/|a|$. Note that the quadratic behaviour of $\mathrm{Re}\,\chi(\eta) \equiv h(\eta) \approx \eta^{-2}/12$ at $|\eta|^{-1} < 1$ is changed by a steep quasi-linear rise in the interval $1 < |\eta|^{-1} < 5$; the corresponding slope being about 0.26. As for $\mathrm{Im}\,\chi(\eta) \equiv A_c(\eta)/(2\eta)$, at

$k^* = 0$ it equals 0 and $-\pi$ for like and unlike charges, respectively, and, for $k^* > 2\pi/|a|$, it approaches the linear k^* dependence: $\mathrm{Im}\,\chi(\eta) \approx (\eta^{-1} - \pi)/2$.

4.1.3. The Small- and Large-r^* Limits. Since we are interested in the region of small relative distances r^* compared with the Bohr radius $|a|$ and small relative momenta $Q = 2k^*$ compared with $1/r^*$, it is useful to write the first terms in the expansion of the hypergeometric functions F and $\widetilde{G}$ in r^*/a and $\rho \equiv k^* r^*$. We have ($x = \cos\theta^*$):

$$F(-i\eta, 1, i\xi) = 1 + \frac{r^*}{a}(1+x)\times \\ \times \left[1 + \frac{i\rho}{4}(1+x) - \frac{\rho^2}{18}(1+x)^2 + O(\rho^3)\right] + O\left(\left(\frac{r^*}{a}\right)^2\right), \tag{98}$$

$$\widetilde{G}(\rho,\eta) = 1 - \frac{\rho^2}{2} + 2\frac{r^*}{a}\times \\ \times \left[\ln\left|2\frac{r^*}{a}\right| + 2C - 1 + \chi(\eta)\right]\left(1 - \frac{\rho^2}{6}\right) + O(\rho^4) + O\left(\left(\frac{r^*}{a}\right)^2\right).$$

For some systems of interest ($\pi\pi$, πK, πp), $|f_0|^2 < |f_0 d_0| <\sim {m_\pi}^{-2} \ll {r^*}^2$, one can neglect the Q dependence of the scattering amplitude and, after the averaging over the uniform x distribution, write the correlation function at a fixed separation r^* as

$$\mathcal{R}(k^*; r^*) \equiv \langle |\psi_{-\mathbf{k}^*}(\mathbf{r}^*)|^2 \rangle = \\ = A_c(\eta)\left\langle |F|^2 + 2\mathrm{Re}\left(\mathrm{e}^{i\mathbf{k}^*\mathbf{r}^*} F^* \widetilde{G}\frac{f_0}{r^*}\right) + O\left(\left(\frac{f_0}{r^*}\right)^2\right)\right\rangle = \\ = A_c(\eta)\left\{1 + 2\frac{r^*}{a} + 2\frac{f_0}{r^*} + 2\frac{f_0}{a}\left[1 + 2\left(\ln\left|\frac{2r^*}{a}\right| + 2C - 1 + h(\eta)\right)\right] - \right. \\ \left. -\rho^2\left(\frac{2}{9}\frac{r^*}{a} + \frac{4}{3}\frac{f_0}{r^*}\right) + O\left(\left(\frac{f_0}{r^*}\right)^2\right) + O\left(\left(\frac{r^*}{a}\right)^2\right) + O(\rho^4)\right\}. \tag{99}$$

Note that in the case of an anisotropic $\mathbf{r}^*$ distribution, Eq. (99) implies the integration over the direction of the vector $\mathbf{k}^* = \mathbf{Q}/2$, distributed isotropically for noncorrelated particles at $Q \to 0$. In the case of the cut $Q_T < Q_T^{\mathrm{cut}}$ on the component of the vector $\mathbf{Q}$ transverse to the direction of the pair three-velocity $\mathbf{v}$ and $Q > Q_T^{\mathrm{cut}}$, Eq. (99) should be modified by the substitution $2/9 \to g_{\mathrm{cut}} 2/9$,

$$g_{\mathrm{cut}} = 1 + \frac{1}{2}\left\langle \frac{1}{2}(3\cos^2\theta_{r^*} - 1)\right\rangle (c_{\min} + c_{\min}^2) \in (0.5, 2)\,, \tag{100}$$

where θ_{r^*} is the angle between the vectors $\mathbf{r}^*$ and $\mathbf{v}$, and $c_{\min} = [1 - (Q_T^{\mathrm{cut}}/Q)^2]^{1/2}$ is the minimal absolute value of the cosine of the angle

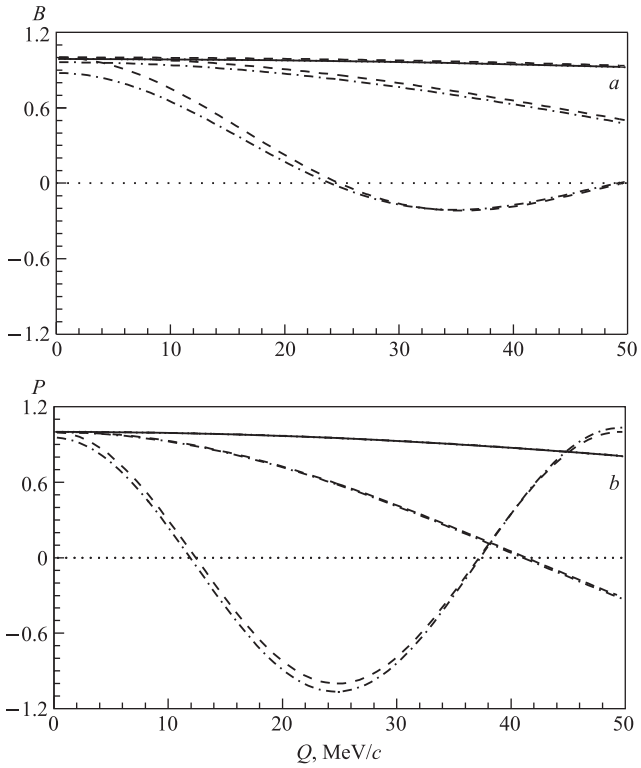

Fig. 7. The functions $B(\rho,\eta)$ (a) and $P(\rho,\eta)$ (b) defined in (92), (93) and calculated for the $\pi^+\pi^-$ system. The solid, dashed and dash-dotted curves correspond to $r^* = 5, 15$ and 50 fm, respectively. The dotted curves represent the functions $B(\rho,0) = \sin\rho/\rho$ and $P(\rho,0) = \cos\,\rho$ corresponding to the case of neutral particles

between the vectors $\mathbf{k}^*$ and $\mathbf{v}$. For pion pairs containing pions from resonance decays, one may expect $\langle r_L^2\rangle > \langle r_T^2\rangle$ [49] (i.e., $\langle\cos^2\theta_{r^*}\rangle > 1/3$) and so $g_{\rm cut} > 1$.

In Figs. 7, 8, and 9, we show the Q dependence of the functions $B(\rho,\eta)$, $P(\rho,\eta)$, $\widetilde{G}(\rho,\eta)$ and the reduced correlation function $\mathcal{R}/A_c$, as well as the corresponding main contributions due to the interference term and the modulus squared of the hypergeometric function for the $\pi^+\pi^-$ system at $r^* = 5, 15, 50$ fm. One may see that the almost universal quasi-linear decrease of $\mathcal{R}/A_c$ for $r^* <\sim 20$ fm is due to the interference term, and that it is changed, for higher r^* values, by a steep rise due to the $|F|^2$ term. It appears that the linear fit of $\mathcal{R}/A_c$ recovers the intercept better than to 2 per mil for $r^* <\sim 20$ fm and — better than to 2 percent even for $r^* = 50$ fm (see Table 2).

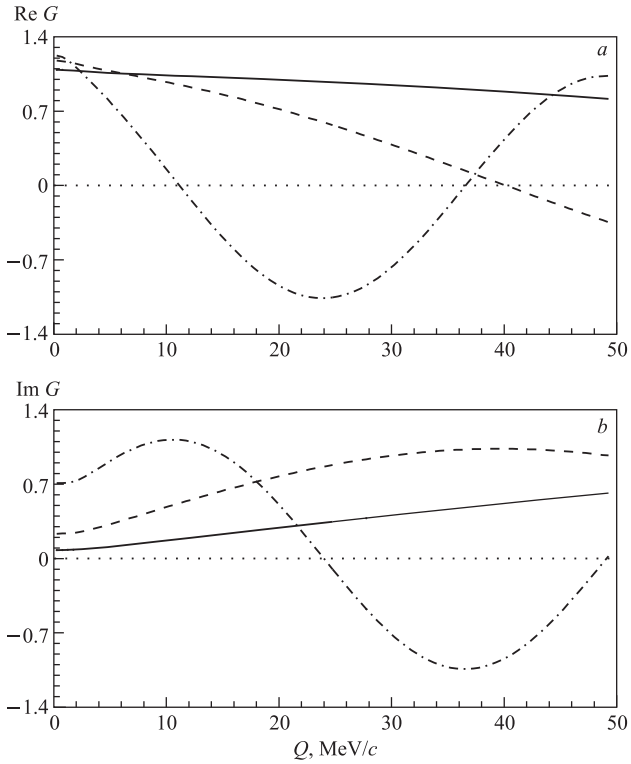

Fig. 8. The function $\widetilde{G}(\rho,\eta)$ defined in (91) and calculated for the $\pi^+\pi^-$ system. The solid, dashed and dash-dotted curves correspond to $r^* = 5$, 15 and 50 fm, respectively

To clarify the origin of the quasi-linear behaviour of the reduced correlation function $\mathcal{R}/A_c$, one can use (99) to estimate the slope at small Q:

$$\left(\frac{\mathcal{R}}{A_c}\right)' \equiv \frac{d}{dQ}\left(\frac{\mathcal{R}}{A_c}\right) \doteq \pm 2 f_0 \frac{dh}{d|\eta|^{-1}} - \left(\pm\frac{1}{9}\frac{r^*}{|a|} + \frac{2}{3}\frac{f_0}{r^*}\right) r^{*2} Q, \qquad (101)$$

where the sign $+$ $(-)$ corresponds to the Coulomb repulsion (attraction). Using the fact that $dh/d|\eta|^{-1} \approx 0.26$ for $1 < |\eta|^{-1} < 5$, one has $(\mathcal{R}/A_c)' \approx -(0.6 + bQ)$ (GeV/c)$^{-1}$ for the $\pi^+\pi^-$ system at $1 < Q < 5$ MeV/c and $f_0 = 0.232$ fm, where b is small ($b <\sim 0.03$ (MeV/c)$^{-1}$) and positive for $r^* <\sim 20$ fm and, for larger r^* values, b is negative and its magnitude rapidly increases with r^*. As a result, the slope of the reduced $\pi^+\pi^-$ correlation function is negative in this Q interval and nearly constant for small r^* values, while it becomes positive and rapidly increases with Q for r^* values

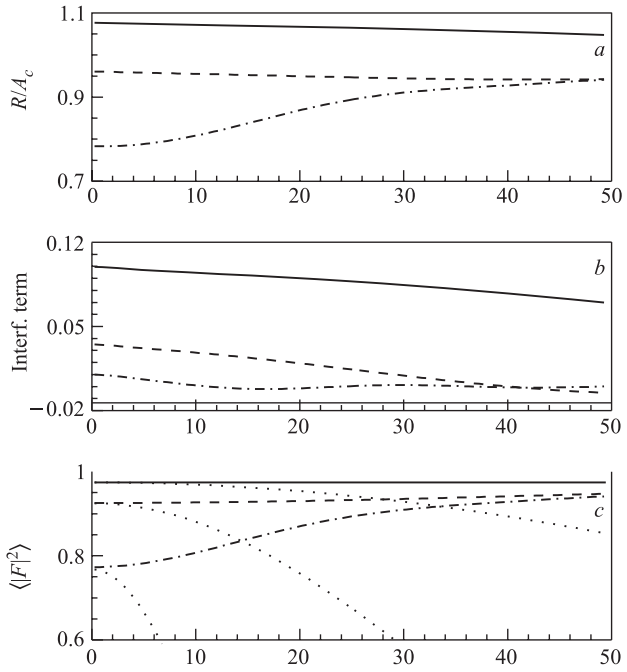

Fig. 9. The $\pi^+\pi^-$ correlation function at a fixed separation r^* divided by the Coulomb penetration factor: $\mathcal{R}/A_c = \langle|\mathrm{e}^{-i\mathbf{k}^*\mathbf{r}^*}F + f_c\widetilde{G}/r^*|^2\rangle$, and the corresponding main contributions due to the interference term and the modulus squared of the hypergeometric function (see (99)). The solid, dashed and dash-dotted curves correspond to $r^* = 5$, 15, and 50 fm, respectively. The calculation is done in the approximation of a constant scattering amplitude $f_c(k^*) = f_0 = 0.232$ fm, the averaging assumes the uniform distribution of the cosine of the angle between the vectors $\mathbf{r}^*$ and $\mathbf{k}^* = \mathbf{Q}/2$. The dotted curves in the lower panel represent the s-wave Coulomb contribution $B^2(\rho,\eta)$ to the quadratic term

of several tens of fm or larger. For $Q > 5$ MeV/c, the absolute value of the slope due to the h function decreases as $\sim 2.35|\eta|$. It appears that, for the $\pi^+\pi^-$ system at $r^* <\sim 20$ fm, this decrease is approximately compensated by the Q dependence of the functions B, P, and F (i.e., at $\rho \ll 1$, by the second term in (101)) so that $(\mathcal{R}/A_c)' \approx -0.5$ (GeV/c)$^{-1}$ up to $Q = 50$ MeV/c.

Note that the Q_T-cut substantially influences the Q dependence of the reduced correlation function only for sufficiently large values of $r^*/|a|$, leading to the substitution $r^*/|a| \to g_{\mathrm{cut}}r^*/|a|$ in (101) at $Q > Q_T$. Particularly, for $\pi^+\pi^-$ pairs containing an ω-decay pion, one may expect $g_{\mathrm{cut}} > 1$ and so a more steep rise of the reduced correlation function at $Q > Q_T$.

Table 2. **Results of the linear fits of the reduced $\pi^+\pi^-$ correlation function: $\mathcal{R}/A_c = c_0 + c_1 Q$ in different intervals $0 < Q < Q_{\max}$. The function $\mathcal{R}/A_c$ is calculated at $r^* = 5$, 15, and 50 fm in the approximation of a constant scattering amplitude $f_c(k^*) = f_0 = 0.232$ fm and assuming the uniform distribution of the cosine of the angle between the vectors $\mathbf{r}^*$ and $\mathbf{k}^* = \mathbf{Q}/2$. Also shown are the corresponding values of $\mathcal{R}/A_c$ at $Q = 0$ (the intercepts)**

r^*, fm	Intercept	$Q_{\max}$, MeV/c	10	20	30	40	50
5	1.077	c_0	1.077	1.077	1.077	1.077	1.078
		c_1, (GeV/c)$^{-1}$	–0.55	–0.47	–0.48	–0.52	–0.57
15	0.961	c_0	0.961	0.961	0.961	0.960	0.959
		c_1, (GeV/c)$^{-1}$	–0.59	–0.56	–0.55	–0.51	–0.42
50	0.783	c_0	0.778	0.768	0.766	0.773	0.783
		c_1, (GeV/c)$^{-1}$	2.55	4.61	4.99	4.38	3.69

To estimate the behaviour of the correlation function at large r^* or k^*, one can exploit the known asymptotic expressions for hypergeometric functions. Thus, at $\xi \gg 1 + \eta^2$,

$$\sqrt{A_c(\eta)}F(-i\eta, 1, i\xi) \to \left(1 - i\frac{\eta^2}{\xi}\right) \mathrm{e}^{i(-\delta_c + \eta \ln \xi)} + \frac{\eta}{\xi}\mathrm{e}^{i(\delta_c + \xi - \eta \ln \xi)} \qquad (102)$$

and, at $\rho \gg 1 + \eta^2$,

$$\widetilde{G}(\rho, \eta) \to \sqrt{A_c(\eta)}\, \mathrm{e}^{i(\delta_c + \rho - \eta \ln 2\rho)}, \qquad (103)$$

so that both the effects of the Coulomb and strong FSI vanish in the cross section as r^{*-2}. In fact, the asymptotic expression for the F function in (102) cannot be used in the case of nearly opposite directions of the vectors $\mathbf{k}^*$ and $\mathbf{r}^*$ ($\cos\theta^* \approx -1$) when the variable $\xi = \rho(1 + \cos\theta^*)$ is suppressed even at large $\rho = k^* r^*$. This leads, after averaging over the angles, to a slower vanishing of the Coulomb effect, as r^{*-1}, in agreement with the classical Jacobian factor $[1 - 2/(ar^*k^{*2})]^{1/2} \approx 1 - (ar^*k^{*2})^{-1}$.

4.2. Discrete Spectrum. *4.2.1. General s-Wave Solution.* Since the Schrödinger equation at a small negative energy $-\epsilon_b = -\kappa^2/(2\mu)$ practically coincides with that in continuous spectrum at zero energy, the r^* dependence of the corresponding wave functions at given orbital angular momentum l and $r^* \ll \kappa^{-1}$ is the same. This important conclusion was first stated by Migdal for the pn system [26]. In fact, both solutions (at positive and negative energies) can be written in the same form for any r^*, up to an energy-dependent normalization factor $\mathcal{N}$. Outside the region of the short-range interaction, $r^* > d$, we can write the s-wave

solution as a combination of the regular and singular Coulomb functions:

$$\psi_{l=0}(r^*) = \mathcal{N}(\eta)\left[\frac{F_0(\rho,\eta)}{\rho\sqrt{A_c(\eta)}} + f_c(k^*)\frac{\widetilde{G}(\rho,\eta))}{r^*}\right]. \tag{104}$$

At $d < r^* \ll |a|$ and $|\rho| \ll 1$ it takes on the form:

$$\psi_{l=0}(r^*) = \mathcal{N}\left\{\left(1+\frac{r^*}{a}\right) + O\left(\left(\frac{r^*}{a}\right)^2\right) + O(\rho^2) + \frac{f_c}{r^*}\times\right.$$
$$\left.\times\left[1 + 2\frac{r^*}{a}\left(\ln\left|2\frac{r^*}{a}\right| + 2C - 1 + \chi\right)\left(1+\frac{r^*}{a}\right) + O\left(\left(\frac{r^*}{a}\right)^2\right) + O(\rho^2)\right]\right\}. \tag{105}$$

For positive energies, $\mathcal{N} = \mathrm{e}^{i\delta_c}\sqrt{A_c(\eta)}$ and at $k^* \to 0$, $f_c = f_0/[1 - -2f_0\chi(\pm\infty)/a]$, $\chi(+\infty) = 0$ $(a > 0)$ or $\chi(-\infty) = -i\pi$ $(a < 0)$. In the case of opposite charges $(a < 0)$, (105) yields:

$$\psi_{k^*,l=0} = \mathrm{e}^{i\delta_c}\sqrt{A_c}\left\{\left(1-\frac{r^*}{|a|}\right)\left[1 - 2\frac{f_0}{|a|}\left(\ln\left|\frac{2r^*}{a}\right| + 2C - 1\right)\right] + \frac{f_0}{r^*} + \right.$$
$$\left. + \left(1+\frac{f_0}{r^*}\right)\left[2i\pi\frac{f_0}{|a|} + O\left(\left(\frac{r^*}{a}\right)^2\right) + O(\rho^2)\right]\right\}. \tag{106}$$

For the discrete levels at negative energies, the substitution $k^* \to i\kappa_n$ has to be done, particularly yielding [25, 48]:

$$\chi(\eta_n) = \frac{\pi}{2}\cot\left(\frac{\pi}{\kappa_n|a|}\right) + \frac{1}{2}\left[2\ln(\kappa_n|a|) + \psi\left(\frac{1}{\kappa_n|a|}\right) + \psi\left(-\frac{1}{\kappa_n|a|}\right)\right], \tag{107}$$

where $\eta_n = (i\kappa_n a)^{-1}$. A more compact form of (107) follows from the relation $\psi(-x) = \psi(x) + \pi\cot(\pi x) + x^{-1}$:

$$\chi(\eta_n) = \pi\cot(\pi x_n) - (2x_n)^{-1}[\phi(x_n) - 3], \qquad x_n = (\kappa_n|a|)^{-1}, \tag{108}$$
$$\phi(x) = 2 + 2x[\ln x - \psi(x)]. \tag{109}$$

4.2.2. Energy Levels. For a pure Coulombic atom ($a < 0$, $f_0 = 0$), only the solution F_0/ρ, regular at $r^* \to 0$, contributes and the requirement of its exponential damping at large distances fixes the energy levels. The corresponding κ values at a given principle quantum number n are equal to $\kappa_n^c = (n|a|)^{-1}$. The wave functions $\psi_{nl}^{\mathrm{coul}}(r^*)$ can then be expressed in terms of the Laguerre polynomials $L_{n+l-1}^{2l+1}(z)$. For $l = 0$,

$$\psi_{n0}^{\mathrm{coul}}(r^*) = \psi_{n0}^{\mathrm{coul}}(0)\exp\left(-\frac{r^*}{n|a|}\right)L_{n-1}^1\left(\frac{2r^*}{n|a|}\right)(n\cdot n!)^{-1}. \tag{110}$$

The square of the wave function $\psi_{n0}^{\mathrm{coul}}(0)$ at zero separation is given in (25) and the Laguerre polynomials are defined by the following recurrence relations:

$$\begin{aligned} L_{n-1}^{1}(z) &= (n\cdot n!)\sum_{s=0}^{n-1} l_{n-1}^{s}(z), \\ l_{n-1}^{0}(z) &= 1, \\ l_{n-1}^{s}(z) &= -\frac{z(n-s)}{s(s+1)} l_{n-1}^{s-1}(z). \end{aligned} \tag{111}$$

At $r^* \ll n|a|$,

$$\psi_{n0}^{\mathrm{coul}}(r^*) = \psi_{n0}^{\mathrm{coul}}(0)\left[1 - \frac{r^*}{|a|} + O\left(\left(\frac{r^*}{na}\right)^2\right)\right]. \tag{112}$$

The strong interaction slightly shifts the Coulombic energy levels thus making the regular part of the general solution (104) divergent at large distances. Therefore, the amplitude f_c has to have a pole at $k^* = i\kappa_n$, and so, according to (97),

$$\chi(\eta_n) = -\frac{|a|}{2K(i\kappa_n)} = -\frac{|a|}{2f_0}\left[1 + O\left(\frac{f_0 d_0}{(na)^2}\right)\right]. \tag{113}$$

Using (108) and (113), one can fix the energy levels $E_n = -{\kappa_n}^2/(2\mu)$ in discrete spectrum with the relative error of $O\big(a^{-3}\big)$:

$$\kappa_n = \kappa_n^{\mathrm{c}}\left\{1 + 2f_0\kappa_n^{\mathrm{c}}\left[1 + f_0\kappa_n^{\mathrm{c}}[\phi(n) - 1] - \frac{4\pi^2}{3}O\left(\frac{{f_0}^2}{a^2}\right) + O\left(\frac{f_0 d_0}{n^2 a^2}\right)\right]\right\}, \qquad \kappa_n^{\mathrm{c}} = (n|a|)^{-1}. \tag{114}$$

To show this, one can put $\kappa_n = \kappa_n^c(1+\epsilon)$, $x_n = |\kappa_n a|^{-1} = n/(1+\epsilon)$ and use the equality $\tan(\pi x_n) = -\tan(\pi x_n \epsilon) = -(\pi x_n \epsilon)[1 + (\pi^2 n^2/3)O(\epsilon^2)]$ and the inequality $|\phi(x_n) - \phi(n)| < O(\epsilon)$, the latter following from the fact that $\phi'(n)$ vanishes faster than n^{-1}. Equation (114) is in agreement with the result of [50] for the relative energy shift $\epsilon(n,0) \equiv (2+\epsilon)\epsilon \doteq \epsilon_0(n,0)[1 + \epsilon_0(n,0)p_1(n,0)]$, where $\epsilon_0(n,0) = 4f_0\kappa_n^c$ and $p_1(n,0) = \phi(n)/4$. The function $\phi(n)$ is defined in (109) with the digamma function for the integer values of the argument given by the recurrence relation:

$$\psi(n+1) = \psi(n) + 1/n, \qquad \psi(1) = -C \doteq -0.5772. \tag{115}$$

Note that $\phi(n) \approx 3$ is nearly constant: $\phi(1) = 2 + 2C \doteq 3.15443$, $\phi(2) \doteq 3.08145$, $\phi(3) \doteq 3.05497, \ldots$, $\phi(\infty) = 3$.

4.2.3. Normalization. Since $N(\eta_n) = 0$ (to compensate for the pole of the amplitude f_c at $k^* = i\kappa_n$), the s-wave solutions in discrete spectrum are now given (for $r^* > d$) by the second term in (104), exponentially vanishing at large distances:

$$\psi_{n0}(r^*) = \mathcal{N}'(n)K(i\kappa_n)\frac{\widetilde{G}(\rho_n,\eta_n)}{r^*} = \mathcal{N}'(n)f_0\frac{\widetilde{G}(\rho_n,\eta_n)}{r^*}\left[1 + O\left(\frac{f_0 d_0}{n^2a^2}\right)\right]. \tag{116}$$

The arguments ρ_n and η_n are taken at $k^* = i\kappa_n$ and the normalization factor

$$\mathcal{N}'(n) = \frac{\mathcal{N}(\eta_n)f_c(i\kappa_n)}{K(i\kappa_n)} \tag{117}$$

is set by the requirement

$$\int |\psi_{n0}(r^*)|^2 d^3\mathbf{r}^* = 1. \tag{118}$$

Note that the extension in the integral (118) of the asymptotic wave function (116) into the inner region $r^* < d$ leads to negligible relative errors $O(f_0 d^2/(na)^3)$, $O(f_0^2 d/(na)^3)$ in the normalization factor $\mathcal{N}'$. Using the expansion of the $\widetilde{G}$ function in the square brackets in (105) and the expression for $\chi(\eta_n)$ in (113), one can write for distances $d < r^* \ll |a|$:

$$\psi_{n0}(r^*) = \mathcal{N}'(n)\left\{\left(1 - \frac{r^*}{|a|}\right)\left[1 - 2\frac{f_0}{|a|}\left(\ln\left|\frac{2r^*}{a}\right| + 2C - 1\right)\right] + \frac{f_0}{r^*} + \right.$$
$$\left. + O\left(\frac{f_0 d_0}{n^2a^2}\right) + O\left(\frac{f_0 r^*}{a^2}\right)\right\}. \tag{119}$$

Comparing (119) with the low-r^* expansion (112) of the pure Coulombic wave function and also taking into account the exponential damping at large distances, one can approximate the wave function (116) at $r^* \ll |a^2/f_0|$ by the expression:

$$\psi_{n0}^{\mathrm{app}}(r^*) = \frac{\mathcal{N}'(n)}{\psi_{n0}^{\mathrm{coul}}(0)}\psi_{n0}^{\mathrm{coul}}(r^*)\left[1 - 2\frac{f_0}{|a|}\left(\ln\left|\frac{2r^*}{a}\right| + 2C - \frac{3}{2}\right) + \frac{f_0}{r^*}\right]. \tag{120}$$

From the results of calculations for the s-wave $\pi^+\pi^-$ atoms, presented in upper panel of Fig. 10, one can see that the squares of the approximate and exact expressions (120) and (116) practically coincide for the distances up to several tens fm and that the agreement is better than percent even at $r^* \sim |a|$.

It follows from (120) that the relative difference of the normalization factors $\mathcal{N}'(n)$ and $\psi_{n0}^{\mathrm{coul}}(0)$ scales as $O(f_0/a)$. In fact, this difference can be fixed when extending the theory to a multichannel case and requiring the equality of the

total width $\Gamma_n = -2\mathrm{Im}\, E_n$ and the sum of the partial widths (see (B.1) and (B.5) or (B.7), (B.8), and (B.4)). As a result:

$$\left|\frac{\mathcal{N}'(n)}{\psi_{n0}^{\mathrm{coul}}(0)}\right|^2 - 1 \doteq \phi(n)\frac{2f_0}{n|a|}. \tag{121}$$

We have checked (121), calculating $\mathcal{N}'$ from the integral (118) for various values of the scattering length f_0, the Bohr radius $|a|$ and the principle quantum number n.

4.3. Universality. Comparing (106) and (119), valid for the distances $d < r^* \ll |a|$, one confirms the important conclusion, already stated at the beginning of Subsec. 4.2, about the universality of the r^* behaviour of the moduli squared of the s-wave solutions in continuous ($k^* \to 0$) and discrete spectrum, up to corrections vanishing as inverse squares of the Bohr radius $|a|$. Assuming $f_0 <\sim d$, one has:

$$\Delta_{n0}^{k^*}(r^*) \equiv \left|\frac{\psi_{k^*0}(r^*)/\psi_{k^*0}^{\mathrm{coul}}(0)}{\psi_{n0}(r^*)/\mathcal{N}'(n)}\right|^2 - 1 = \\ = 4\pi^2 O\left(\frac{{f_0}^2}{a^2}\right) + O\left(\frac{f_0 d_0}{n^2 a^2}\right) + O\left(\frac{{r^*}^2}{a^2}\right) + O(\rho^2). \tag{122}$$

The universality holds with the same accuracy also if the s-wave solution in continuous spectrum is substituted by the complete wave function (recall that $\psi_{-\mathbf{k}^*}^{\mathrm{coul}}(0) = \psi_{k^*0}^{\mathrm{coul}}(0) \equiv A_c^{1/2}$), provided the averaging over the angle between the vectors $\mathbf{r}^*$ and $\mathbf{k}^*$:

$$\Delta_{n}^{k^*}(r^*) \equiv \left\langle\left|\frac{\psi_{-\mathbf{k}^*}(\mathbf{r}^*)/\psi_{-\mathbf{k}^*}^{\mathrm{coul}}(0)}{\psi_{n0}(r^*)/\mathcal{N}'(n)}\right|^2\right\rangle - 1 = \\ = 4\pi^2 O\left(\frac{{f_0}^2}{a^2}\right) + O\left(\frac{f_0 d_0}{n^2 a^2}\right) + O\left(\frac{{r^*}^2}{a^2}\right) + O(\rho^2). \tag{123}$$

This result follows from the fact that, at $k^* \to 0$ and typical distances $r^* \ll |a|$, the total wave function in continuous spectrum almost coincides with the s-wave amplitude $\psi_{k^*0}(r^*)$ (see Fig. 9, *c*):

$$\psi_{-\mathbf{k}^*}(\mathbf{r}^*) = \psi_{k^*0}(r^*) + \mathrm{e}^{i\delta_c}\sqrt{A_c}\frac{\mathbf{k}^*\mathbf{r}^*}{k^* a} + O\left(\frac{{r^*}^2}{a^2}\right) + O(\rho^2) \tag{124}$$

and, that the relatively significant correction term $O(r^*/a)$ in the square of the wave function $\psi_{-\mathbf{k}^*}(\mathbf{r}^*)$ vanishes after averaging over the direction of the relative three-momentum $\mathbf{Q} = 2\mathbf{k}^*$, or after suppressing the signs of the components Q_i of the vector $\mathbf{Q}$ (assuming a symmetric detector acceptance with respect to the reflection $Q_i \to -Q_i$). From Fig. 10, *c*, one can see that for the $\pi^+\pi^-$ system,

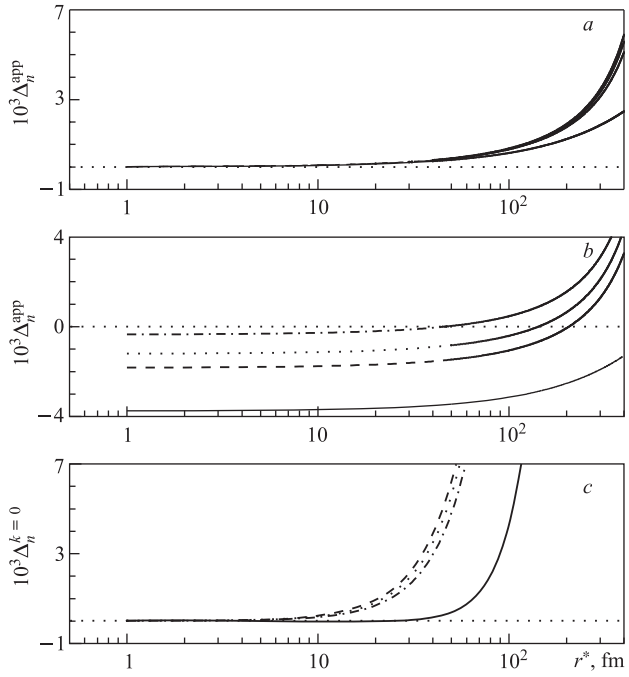

Fig. 10. Comparison of the approximate $\pi^+\pi^-$ atomic wave function $\psi_{n0}^{\rm app}(r^*)$ and the $\pi^+\pi^-$ wave function in continuous spectrum $\psi_{-\mathbf{k}^*}(\mathbf{r}^*)$ at $k^* \to 0$, respectively defined in (120) and (89) ($f_0 = 0.232$ fm), with the exact s-wave solution outside the range of the strong interaction $\psi_{n0}(r^*)$ given in (116): $\Delta_n^{\rm app}(r^*) = [\psi_{n0}^{\rm app}(r^*)/\psi_{n0}(r^*)]^2 - 1$ and $\Delta_n^{k^*=0}(r^*) = \langle|[\psi_{-\mathbf{k}^*}(\mathbf{r}^*)/\psi_{-\mathbf{k}^*}^{\rm coul}(0)]/[\psi_{n0}(r^*)/\mathcal{N}'(n)]|^2\rangle - 1$, $k^* \to 0$; the averaging in the latter expression is done over the uniform distribution of the cosine of the angle between the vectors $\mathbf{r}^*$ and $\mathbf{k}^* = \mathbf{Q}/2$. Figure b shows $\Delta_n^{\rm app}(r^*)$ assuming $\mathcal{N}'(n) = \psi_{n0}^{\rm coul}(0)$ in (120) in correspondence with the ansatz (125). The curves in the increasing order correspond to $n = 1, 2, 3, 10$

the universality holds to better than percent for $r^* <\sim 50$ fm. Note that Δ_{n0}^0 (not shown in Fig. 10) is negative and, contrary to Δ_n^0, it shows the strongest deviation from zero for $n = 1$, achieving a per mil level already at $r^* \approx 20$ fm.

Comparing (75) and (76), one can see that the number N_A of produced $\pi^+\pi^-$ atoms is determined by the number of nonatomic $\pi^+\pi^-$ pairs in the region of small k^*. So, N_A is actually proportional to the ratio $\langle|\psi_{n0}(r^*)|^2\rangle_{0P}/\langle|\psi_{-\mathbf{k}^*}(\mathbf{r}^*)|^2\rangle_{\tilde{q}P}$ in which the effects of the r^* dependence as well as the corrections due to nonequal emission times ($t^* \neq 0$) and *smoothness* assumption are to a large extent compensated for, being practically the same for the wave functions in continuous spectrum at $k^* \to 0$ and discrete spectrum at

$r^* \ll |a|$. In fact, according to (121)–(123), one can write the ratio of the finite-size correction factors at small relative momenta ($k^* \ll \langle 1/r^* \rangle^{\text{SL}}$) and moderate distances between the particle emitters ($\langle r^* \rangle^{\text{SL}} \ll |a|$) as

$$\frac{1+\delta_n}{1+\delta(k^*)} \equiv \frac{\langle |\psi_{n0}(r^*)/\psi_{n0}^{\text{coul}}(0)|^2 \rangle_{0P}^{\text{SL}}}{\langle |\psi_{-\mathbf{k}^*}(\mathbf{r}^*)/\psi_{k^*0}^{\text{coul}}(0)|^2 \rangle_{\tilde{q}P}^{\text{SL}}} \equiv \left| \frac{N'(n)}{\psi_{n0}^{\text{coul}}(0)} \right|^2 \frac{1+\delta'_n}{1+\delta(k^*)} =$$

$$= \left[1 + \phi(n) \frac{2f_0}{n|a|} \right] \left\{ 1 + O\left(\frac{\langle r^{*2} \rangle^{\text{SL}}}{a^2} \right) + O\left(k^{*2} \langle r^{*2} \rangle^{\text{SL}} \right) \right\} \quad (125)$$

thus leading to (42) up to a small correction due to the transition $\pi^0\pi^0 \to \pi^+\pi^-$ (see (154)). Recall that though the k^* dependence of the correction factor in braces is quadratic at very low values of k^*, in fact, in a wider k^* interval and for sufficiently small values $\langle r^* \rangle^{\text{SL}} <\sim 10$ fm, it shows a quasi-linear and almost universal behaviour (see Fig. 9 and [1]).

4.4. The n Dependence. Neglecting the production of the $\pi^+\pi^-$ atoms with the orbital angular momentum $l > 0$, suppressed by powers of the $\pi^+\pi^-$ Bohr radius $|a|$, the pionium production probability is given in (34) and depends on the main quantum number n as

$$w_n \propto (1+\delta_n)|\psi_{n0}^{\text{coul}}(0)|^2 \propto \frac{(1+\delta_n)}{n^3}. \quad (126)$$

The correction factor $(1+\delta_n)$ slightly modifies the n^{-3} law of a simple ansatz in (23). It follows from (125) that the n dependence of the short-distance part of the correction δ_n is dominated by the renormalization effect of the strong FSI on the two-pion atomic wave function and that the renormalized correction (see also (42))

$$\delta'_n \doteq \delta(0) + O\left(\left\langle \frac{r^{*2}}{a^2} \right\rangle^{\text{SL}} \right). \quad (127)$$

Figure 12, *c* confirms that the short-distance part of the correction δ'_n is practically independent of n and equal to $\delta(0)$. The renormalization correction $2\phi(n)f_0/(n|a|) \approx 6f_0/(n|a|)$ is the largest for low values of n. For example, for pionium at $n = 1$ it composes $\sim 0.3\%$ (see also Fig. 10, *b*). As for the ω and η' contributions to δ'_n, their n dependence is not negligible and the shifts from $\delta(0)$ compose up to ~ -0.004 and ~ -0.1, respectively.

In [51, 52], the effect of the strong interaction on the n dependence of the pionium wave function has been studied numerically, solving the corresponding Schrödinger equations. Thus, in [51], the ratio $R_n = \psi_{n0}/\psi_{n0}^{\text{coul}}$ and the difference $\Delta R_n = R_1 - R_n$ have been calculated for $n = 1-3$ using an exponential form of the short-range potential. According to (112), (119), and (121), one has, up to

corrections $O(f_0/a)$ and $O(r^{*2}/a^2)$:

$$R_n \equiv \frac{\psi_{n0}(r^*)}{\psi_{n0}^{\rm coul}(r^*)} \doteq 1 + \frac{f_0}{r^*},$$
$$\Delta R_n \equiv R_1 - R_n \doteq \frac{f_0}{|a|}\left\{\phi(1) - \frac{1}{n}\phi(n)\right\}\left(1 + \frac{f_0}{r^*}\right). \tag{128}$$

From Fig. 1 of [51], one can deduce a value of ~ 0.15 fm for the scattering length f_0 to achieve an agreement with the prediction of (128) for the ratio R_n at $d < r^* \ll |a|$. The differences ΔR_n, presented in Fig. 1 of [51] for $n = 2$ and 3, are however by a factor of 1.6 higher than the corresponding predictions of (128). For example, for $10^3 \Delta R_n$ at $r^* = 8$ fm, $n = 2$ and 3, one can read from this figure the values* 1.0 and 1.3, while (128) respectively predicts 0.6 and 0.8. This discrepancy may indicate that the calculation error, declared in [51] to be better than 10^{-4}, was underestimated by a factor of 5.

In [52], a more refined numerical study of the n dependence has been done accounting for the second channel ($\pi^0\pi^0$) and extended charges. The hadronic $\pi\pi$ potentials have been chosen to reproduce the phase shifts given by two-loop chiral perturbation theory. The quantity $d_n = n^{3/2}\psi_{n0}/\psi_{10} - 1$ has been calculated for $n = 1{-}4$. Similar to (128), one has for $d < r^* \ll |a|$

$$d_n \equiv n^{3/2}\frac{\psi_{n0}(r^*)}{\psi_{10}(r^*)} - 1 \doteq -\frac{f_0}{|a|}\left\{\phi(1) - \frac{1}{n}\phi(n)\right\}, \tag{129}$$

up to corrections $\mathcal{O}(f_0 r^*/a^2)$ and $O(r^{*2}/a^2)$. The results of numerical calculations presented in Fig. 2 of [52] are in qualitative agreement with (129), d_n being almost constant (except for the region of very small r^*) and showing the right n dependence: $d_n \sim -(1 - 1/n)$. Similar to [51], the numerical results for $|d_n|$ are however higher, now by a factor of 2.5, than the predictions of (129) calculated with $f_0 = 0.2$ fm which should correspond within $\sim 10\%$ to the choice of the potentials in [52]. Since the presence of the second channel leads to a negligible modification of (129) ($f_0 \to \mathrm{Re}\, A^{\alpha\alpha} \approx f_0$; see next chapter) and the correction due to the extended charges is also expected to be negligible ($\sim -1/6\,\langle r^2\rangle_\pi/a^2$), the discrepancy in the size of the correction d_n has to be attributed to the insufficient calculation accuracy, or to the incorrect matching of the scattering length.

*One should correct the figure by interchanging the curves. The author is grateful to O. Voskresenskaya for pointing out this misprint.

5. TWO-CHANNEL WAVE FUNCTIONS

5.1. Continuous Spectrum in Both Channels. It was implied until now that a long-time FSI takes place and can be separated in the Bethe–Salpeter amplitudes in the near-threshold final-state elastic transitions $1+2 \to 1+2$, only. In principle, however, it can be separated also in the inelastic transitions, $1+2 \to 3+4$, characterized by a slow relative motion in both entrance and exit channels. The necessary condition for such a separation is an approximate equality of the sums of particle masses in the intermediate (m_3+m_4) and final (m_1+m_2) states. Some examples are the transitions $\pi^+\pi^- \leftrightarrow \pi^0\pi^0$, $\pi^- K^+ \leftrightarrow \pi^0 K^0$, or $\pi^- p \leftrightarrow \pi^0 n$. For such processes only the second term in the upper diagram in Fig. 1 contributes, now with the particles $3,4$ in the intermediate state. In the *equal-time* approximation, the corresponding amplitudes reduce to the wave functions describing a two-channel scattering of the particles $1,2$ with the inverse direction of the relative three-momentum: $\mathbf{k}^* \to -\mathbf{k}^*$ (the scattering is viewed in the diagram from right to left so that the final-state particles $1,2$ are in the entrance scattering channel). We will denote the channels as $\alpha = \{1+2\}$ and $\beta = \{3+4\}$, and the corresponding wave functions describing the scattering $\alpha \to \alpha$ and $\alpha \to \beta$ — as ψ^α and ψ^β, respectively. Outside the range of the strong FSI, $r^* > d$, they can be written, for the α- and β-channel continuous spectrum, as [48]:

$$\psi^\alpha_{-\mathbf{k}^*}(\mathbf{r}^*) = \mathcal{N}(\eta_\alpha)\left[\mathrm{e}^{-i\mathbf{k}^*\mathbf{r}^*}F(-i\eta_\alpha,1,i\xi_\alpha) + f_c^{\alpha\alpha}(k^*)\frac{\widetilde{G}(\rho_\alpha,\eta_\alpha)}{r^*}\right], \tag{130}$$

$$\psi^\beta_{-\mathbf{k}^*}(\mathbf{r}^*) = \mathcal{N}(\eta_\alpha) f_c^{\beta\alpha}(k^*)\sqrt{\frac{\mu_\beta}{\mu_\alpha}}\frac{\widetilde{G}(\rho_\beta,\eta_\beta)}{r^*} \to \mathcal{N}(\eta_\alpha) f_c^{\beta\alpha}(k^*)\sqrt{\frac{\mu_\beta}{\mu_\alpha}}\frac{\exp(i\rho_\beta)}{r^*},$$

where $\mathcal{N}(\eta_\alpha) = \mathrm{e}^{i\delta_c(\eta_\alpha)}\sqrt{A_c(\eta_\alpha)}$, $\mathbf{k}^* \equiv \mathbf{k}^*_\alpha$ and

$$k^{*2}_\beta = \frac{[{m_4}^2 - {m_3}^2 + (\omega_1^* + \omega_2^*)^2]^2}{4(\omega_1^* + \omega_2^*)^2} - {m_4}^2 \doteq \frac{\mu_\beta}{\mu_\alpha}k^{*2}_\alpha + 2\mu_\beta(m_1+m_2-m_3-m_4). \tag{131}$$

The approximate equality in (131) corresponds to the nonrelativistic expressions for the energies: $\omega_j^* = m_j + k^{*2}_\alpha/(2m_j), j = 1,2$. We consider here the systems with the Coulomb interaction absent in the channel β, so $a_\beta = \infty$, $\eta_\beta = 0$, $A_c(\eta_\beta) = 1$, $\widetilde{G}(\rho_\beta,\eta_\beta) = \exp(i\rho_\beta)$, and $\chi(\eta_\beta)/a_\beta = ik^*_\beta$; the amplitude ψ^β in (130) then reduces to the expression indicated by the arrow. The β-channel momenta at the α-channel thresholds ($k^*_\alpha = 0$) for $\pi\pi$-, πK-, πN-, KK-, KN- and $\bar{N}N$-systems are given in Table 3. This table also demonstrates that even close to the α-channel threshold, the use of the nonrelativistic approximation can lead to noticeable shifts in k^*_β.

Table 3. **The β-channel momenta k^*_β calculated at the α-channel thresholds $k^*_\alpha = 0$. Also shown are the relative shifts $\Delta k^*_\beta/k^*_\beta$ arising from the nonrelativistic approximation in the second formula in (131)**

$\alpha \to \beta$	$\pi^+\pi^- \to$ $\to \pi^0\pi^0$	$\pi^- K^+ \to$ $\to \pi^0 K^0$	$\pi^- p \to$ $\to \pi^0 n$	$K^+K^- \to$ $\to K^0\bar{K}^0$	$K^- p \to$ $\to \bar{K}^0 n$	$\bar{p}p \to$ $\to \bar{n}n$
k^*_β, MeV/c	35.5	11.3	28.0	i 62.9	i 58.6	i 49.3
k^{*-1}_β, fm	5.6	17.5	7.0	$-i$ 3.1	$-i$ 3.4	$-i$ 4.0
$\Delta k^*_\beta/k^*_\beta$, %	–0.84	–0.07	–0.46	0.20	0.13	0.03

Similar to equation (96) in the single-channel case, the amplitudes

$$f_c^{\lambda\lambda'} = f^{\lambda\lambda'}[A_c(\eta_\lambda)A_c(\eta_{\lambda'})]^{-1/2}, \tag{132}$$

where $f^{\lambda\lambda'}$ are the amplitudes of the low-energy s-wave scattering due to the short-range interaction renormalized by the long-range Coulomb forces, $\lambda, \lambda' = \alpha, \beta$. The time-reversal invariance requires $f^{\lambda\lambda'} = f^{\lambda'\lambda}$. It is convenient to consider the amplitudes $f_c^{\lambda\lambda'}$ and $f^{\lambda\lambda'}$ as the elements of the symmetric matrices $\hat{f}_c$ and $\hat{f}$ related by the matrix equation

$$\hat{f}(k^*) = [A_c(\hat{\eta})]^{1/2}\hat{f}_c(k^*)[A_c(\hat{\eta})]^{1/2}. \tag{133}$$

The single-channel expression (97) for the amplitude f_c can then be rewritten in a matrix form:

$$\hat{f}_c(k^*) = \left(\hat{K}^{-1} - \frac{2\chi(\hat{\eta})}{\hat{a}}\right)^{-1}, \tag{134}$$

where $\hat{a}$, $\hat{\eta}$, $\chi(\hat{\eta})$, and $A_c(\hat{\eta})$ are diagonal matrices in the (α, β)-channel representation, for example, $[A_c(\hat{\eta})]_{\lambda\lambda'} = A_c(\eta_\lambda)\delta_{\lambda\lambda'}$. The symmetric matrix $\hat{K}$ has to be real for the energies above both thresholds due to the two-channel s-wave unitarity condition [25]

$$\mathrm{Im}\,\hat{f} = \hat{f}^+ \mathrm{Re}\,\hat{k}\;\hat{f}, \tag{135}$$

where the diagonal matrix $k_{\lambda\lambda'} = k^*_\lambda\delta_{\lambda\lambda'}$. Usually, the $\hat{K}$ matrix is real also for negative kinetic energies (provided sufficiently fast vanishing of the short-range potential with the distance), and so it can be expanded in even powers of $k^* \equiv k^*_\alpha$, similar to (87) or (88) with the parameters substituted by the corresponding matrices (e.g., $f_0 \to \hat{f}_0$).

Since, in the cases of practical interest, the particles (pions, kaons, nucleons) in the channels α and β are members of the corresponding isotopic multiplets, one can assume the parameter matrices diagonal in the representation of the total isospin [48]. The elements of the parameter or $\hat{K}$ ($\hat{K}^{-1}$) matrices in the

channel representation are then given by the corresponding isospin projections. Particularly, for $\alpha = \{\pi^+\pi^-\}$, $\beta = \{\pi^0\pi^0\}$, one has

$$\begin{aligned} f_0^{\alpha\alpha} &= \frac{2}{3} f_0^{(0)} + \frac{1}{3} f_0^{(2)}, \\ f_0^{\alpha\beta} &= f_0^{\beta\alpha} = -\frac{\sqrt{2}}{3}(f_0^{(0)} - f_0^{(2)}), \\ f_0^{\beta\beta} &= \frac{1}{3} f_0^{(0)} + \frac{2}{3} f_0^{(2)}. \end{aligned} \tag{136}$$

Analogous relations, with the substitutions $(0) \to (1/2)$ and $(2) \to (3/2)$, take place for the channels $\alpha = \{\pi^- p, \pi^- K^+, \pi^+ K^-\}$, $\beta = \{\pi^0 n, \pi^0 K^0, \pi^0 \bar{K}^0\}$. For the channels $\alpha = \{K^+K^-, K^- p, \bar{p}p\}$, $\beta = \{K^0\bar{K}^0, \bar{K}^0 n, \bar{n}n\}$, one has

$$f_0^{\alpha\alpha} = f_0^{\beta\beta} = \frac{1}{2}(f_0^{(0)} + f_0^{(1)}) \qquad f_0^{\alpha\beta} = f_0^{\beta\alpha} = -\frac{1}{2}(f_0^{(0)} - f_0^{(1)}), \tag{137}$$

where the parameters $f_0^{(0)}$ and $f_0^{(1)}$ have now positive imaginary parts due to the effective inclusion of the additional channels opened at the energies of the elastic thresholds ($k_\alpha^* = 0$) in the reactions $K\bar{K} \to \pi\pi, \pi\eta$, $\bar{K}N \to \pi' s\Lambda, \pi' s\Sigma$, $\bar{N}N \to$ mesons.

Note that the use of the isospin relations (136) and (137) implies that the violation of isotopic invariance is solely associated with the Coulomb factors $A_c(\eta_j)$ (strongly deviating from unity at $k_j^* < 2\pi/|a_j|$) and with the mass differences between the members of the same multiplets ($k_\alpha^* \neq k_\beta^*$). These relations, however, neglect the direct violation of isotopic invariance of the order of $O(f_0/a)$ due to the renormalization effect of the Coulomb interaction on the scattering lengths, usually leading to the shifts on the level of several percent. Within this uncertainty, one can also use (136) or (137) directly for the elements of the matrices $\hat{K}^{-1}$ or $\hat{K}$.

The difference between the channel momenta can be neglected sufficiently far from the threshold. Then, one can apply (136) or (137) to the amplitudes $\widetilde{f}_{jj'}$ in the absence of the Coulomb interaction and switch on this interaction in a similar way as in the single-channel case [53]:

$$\hat{f}(k^*) = [A_c(\hat{\eta})]^{1/2} \left\{ \hat{\widetilde{f}}^{-1}(k^*) + i\hat{k} - \frac{2\chi(\hat{\eta})}{\hat{a}} \right\}^{-1} [A_c(\hat{\eta})]^{1/2}. \tag{138}$$

One may note that (136), (137) correspond to the two-dimensional unitary transformation $\hat{f}_0 = \hat{U}^{-1}\hat{f}_0'\hat{U}$, $U_{11} = U_{22} = \cos\varphi$, $U_{12} = -U_{21} = \sin\varphi$. Since it applies also to the $\hat{d}_0$ matrix, one immediately arrives at the same transformation of the complete amplitude $\hat{f}$ in the case of the absent Coulomb interaction and $\hat{k} = k^*\hat{1}$.

5.2. Discrete Spectrum in the α Channel. One can repeat the same arguments as for the single-channel case, starting from the general solution in (104) with the substitution $f_c \to f_c^{\alpha\alpha}$. For a discrete energy level $E_n = -{\kappa_n}^2/(2\mu)$, the amplitude f_c has to have a pole or, equivalently, $\det \hat{f}_c^{-1}(i\kappa_n) = 0$. Following [50] and introducing the matrix

$$(\hat{A}^{-1})^{\lambda\lambda'} = (\hat{K}^{-1})^{\lambda\lambda'} - i\delta_{\lambda\lambda'}\delta_{\lambda\beta}k_\beta^*, \tag{139}$$

one can rewrite this requirement in the form of Eq. (113) modified by the substitution $K(i\kappa_n) \to A^{\alpha\alpha}(i\kappa_n)$ and thus, fix the discrete energy levels similar to (114):

$$\kappa_n = \kappa_n^{\mathrm{c}} \left\{1 + 2A^{\alpha\alpha}\kappa_n^{\mathrm{c}} \left[1 + A^{\alpha\alpha}\kappa_n^{\mathrm{c}}[\phi(n) - 1] + O(a^{-2})\right]\right\}, \tag{140}$$

$$A^{\alpha\alpha} = \frac{K^{\alpha\alpha} - ik_\beta^* \det \hat{K}}{1 - ik_\beta^* K^{\beta\beta}} = K^{\alpha\alpha} + \frac{ik_\beta^*(K^{\beta\alpha})^2}{1 - ik_\beta^* K^{\beta\beta}}, \tag{141}$$

where $a = a_\alpha$. Since $\hat{K}(i\kappa_n) = \hat{K}(0)[1 + \mathrm{Tr}\, O(\hat{f}_0\hat{d}_0(na)^{-2})]$ and $k_\beta^*(i\kappa_n) = k_\beta^*(0)[1 + O((nak_\beta^*)^{-2})]$, one can safely make the substitutions $\hat{K}(i\kappa_n) \to \hat{f}_0 \equiv \hat{K}(0)$ and $k_\beta^*(i\kappa_n) \to k_\beta^*(0)$ and write, with the relative errors $O(a^{-2})$ less than a fraction of per mil,

$$A^{\lambda\lambda'} = \frac{K^{\lambda\lambda'} - ik_\beta^* \det \hat{K}\delta_{\lambda\lambda'}\delta_{\lambda\alpha}}{1 - ik_\beta^* K^{\beta\beta}} \doteq \frac{f_0^{\lambda\lambda'} - ik_\beta^* \det \hat{f}_0\delta_{\lambda\lambda'}\delta_{\lambda\alpha}}{1 - ik_\beta^* f_0^{\beta\beta}}, \tag{142}$$

particularly,

$$\begin{aligned} \mathrm{Re}\, A^{\alpha\alpha} &= K^{\alpha\alpha} - K^{\beta\beta}\frac{(k_\beta^* K^{\beta\alpha})^2}{1 + (k_\beta^* K^{\beta\beta})^2} \doteq f_0^{\alpha\alpha} - f_0^{\beta\beta}\frac{(k_\beta^* f_0^{\beta\alpha})^2}{1 + (k_\beta^* f_0^{\beta\beta})^2}, \\ \mathrm{Im}\, A^{\alpha\alpha} &= \frac{k_\beta^*(K^{\beta\alpha})^2}{1 + (k_\beta^* K^{\beta\beta})^2} \doteq \frac{k_\beta^*(f_0^{\beta\alpha})^2}{1 + (k_\beta^* f_0^{\beta\beta})^2}. \end{aligned} \tag{143}$$

In (142) and (143), k_β^* simply denotes $k_\beta^*(0)$ or $k_\beta^*(i\kappa_n)$. It can be seen from Table 3 that k_β^{*-1} represents a scale which is intermediate between the Bohr radius $|a|$ and the elements of the matrix $\hat{f}_0$. As a result, the terms like $O(k_\beta^*(f_0^{\lambda\lambda'})^2/a)$ or $O((ak_\beta^*)^{-2})$ contribute less than a fraction of per mil and can be omitted. As for the terms $O((k_\beta^* f_0^{\lambda\lambda'})^2)$, their contribution is on a per mil level and is retained.

The s-wave solutions corresponding to the α-channel discrete spectrum are again given by the second term in (104) ($\mathcal{N}(\eta_n) = 0$) with the finite normalization $\mathcal{N}' = \mathcal{N}f_c^{\alpha\alpha}/A^{\alpha\alpha}$ introduced in the same way as in (117) modified by the

substitution $K \to A^{\alpha\alpha}$. As for the corresponding β-channel s-wave solutions $\psi^{\beta}_{n0}(r^*)$, they are given by the second of equations (130) with

$$\mathcal{N} f_c^{\beta\alpha} = \mathcal{N}' A^{\alpha\alpha} \frac{f_c^{\beta\alpha}}{f_c^{\alpha\alpha}} = \mathcal{N}' \frac{K^{\beta\alpha}}{1 - ik^*_\beta K^{\beta\beta}} \equiv \mathcal{N}' A^{\beta\alpha}, \tag{144}$$

the second equality following from (141) and the explicit inversion of the symmetric matrix $\hat{f}_c^{-1}$:

$$\begin{gathered} Df_c^{\alpha\alpha} = K^{\alpha\alpha} - ik^*_\beta \det \hat{K}, \qquad Df_c^{\beta\alpha} = K^{\beta\alpha}, \\ Df_c^{\beta\beta} = K^{\beta\beta} + \frac{2\chi}{|a|} \det \hat{K}, \qquad \det \hat{K} = K^{\alpha\alpha} K^{\beta\beta} - (K^{\beta\alpha})^2, \\ D = \det \hat{f}_c^{-1} \det \hat{K} = 1 - ik^*_\beta K^{\beta\beta} + \frac{2\chi}{|a|}(K^{\alpha\alpha} - ik^*_\beta \det \hat{K}), \end{gathered} \tag{145}$$

where χ denotes here $\chi(\eta_\alpha)$; recall that $\chi(\eta_\beta)/a_\beta = ik^*_\beta$ due to the absent Coulomb interaction in the channel β. Note that the product $Df_c^{\lambda\lambda'}$ is finite since the amplitude pole for a bound state is compensated by the corresponding zero of the factor $D \propto \det \hat{f}_c^{-1}$. For the continuous spectrum at the α-channel threshold, $\hat{K} = \hat{f}_0$ and $D = 1 - ik^*_\beta f_0^{\beta\beta} - (2i\pi/|a|)(f_0^{\alpha\alpha} - ik^*_\beta \det \hat{f}_0)$.

As a result,

$$\begin{aligned} \psi^{\alpha}_{n0}(r^*) &= \mathcal{N}'(n) A^{\alpha\alpha} \frac{\widetilde{G}}{r^*} = \mathcal{N}'(n) \frac{f_0^{\alpha\alpha} - ik^*_\beta \det \hat{f}_0}{1 - ik^*_\beta f_0^{\beta\beta}} \frac{\widetilde{G}}{r^*} \left[1 + \mathrm{Tr}\, O\left(\frac{\hat{f}_0 \hat{d}_0}{n^2 a^2}\right)\right], \\ \psi^{\beta}_{n0}(r^*) &= \mathcal{N}'(n) A^{\beta\alpha} \sqrt{\frac{\mu_\beta}{\mu_\alpha}} \frac{\mathrm{e}^{ik^*_\beta r^*}}{r^*} = \\ &= \frac{\mathcal{N}'(n) f_0^{\beta\alpha}}{1 - ik^*_\beta f_0^{\beta\beta}} \sqrt{\frac{\mu_\beta}{\mu_\alpha}} \frac{\mathrm{e}^{ik^*_\beta r^*}}{r^*} \left[1 + \mathrm{Tr}\, O\left(\frac{\hat{f}_0 \hat{d}_0}{n^2 a^2}\right)\right], \end{aligned} \tag{146}$$

where $\widetilde{G} = \widetilde{G}(\rho_n, \eta_n)$ with the arguments ρ_n and η_n taken at $k^*_\alpha = i\kappa_n$ (κ_n is expressed through $\hat{f}_0$ in (140) and (143)), and $\mathcal{N}'(n) = \psi^{\mathrm{coul}}_{n0}(0)[1 + O(f_0^{\alpha\alpha}/a)]$ is fixed by the normalization integral (118) for the wave function $\psi^{\alpha\alpha}_{n0}$. It can be calculated also analytically using (121) with the substitution $f_0 \to \mathrm{Re}\, A^{\alpha\alpha} \approx f_0^{\alpha\alpha}$ (see Appendix B):

$$\left| \frac{\mathcal{N}'(n)}{\psi^{\mathrm{coul}}_{n0}(0)} \right|^2 - 1 = \phi(n) \frac{2\mathrm{Re}\, A^{\alpha\alpha}}{n|a|} - 4\pi^2 O\left(\left(\frac{\mathrm{Re}\, A^{\alpha\alpha}}{a}\right)^2\right). \tag{147}$$

Using (145), one can express the amplitudes $f_c^{\lambda\lambda'}(k^*)$ at $k^*_\alpha = 0$ ($\chi = -i\pi$, $\hat{K} = \hat{f}_0$) through the elements of the A-matrix (related to the scattering lengths

$f_0^{\lambda\lambda'}$ in (142)) with the relative error $O(a^{-2})$ less than a fraction of per mil:

$$f_c^{\lambda\lambda'}(0) = A^{\lambda\lambda'}\left[1 + \frac{2i\pi}{|a|}A^{\alpha\alpha} + O(a^{-2})\right] - \frac{2i\pi}{|a|}\frac{\det \hat{f}_0}{1 - ik_\beta^* f_0^{\beta\beta}}\delta_{\lambda\lambda'}\delta_{\lambda\beta}. \quad (148)$$

5.3. Universality. Comparing (130) and (146), one may see that the universal r^* behaviour of the s-wave amplitudes ψ^λ in continuous ($k^* \to 0$) and discrete spectrum takes place with similar accuracy as in the single-channel case. Thus, using the expansions (106) and (119) for the amplitudes ψ^α, modified by the substitutions $f_0 \to f_c^{\alpha\alpha}(0)$ and $f_0 \to A^{\alpha\alpha}$, respectively, one has, for the measures of the universality violation defined as in (122),

$$\Delta_{n0}^{\alpha,k^*}(r^*) = 4\pi O\left(\frac{k_\beta^*(f_0^{\beta\alpha})^2}{a}\right) + 4\pi^2 O\left(\frac{(f_0^{\alpha\alpha})^2}{a^2}\right) + \\ + \operatorname{Tr} O\left(\frac{\hat{f}_0\hat{d}_0}{n^2a^2}\right) + O\left(\frac{r^{*2}}{a^2}\right) + O(\rho^2), \quad (149)$$

$$\Delta_{n0}^{\beta,k^*}(r^*) = \operatorname{Tr} O\left(\frac{\hat{f}_0\hat{d}_0}{n^2a^2}\right) + O\left(\frac{r^{*2}}{a^2}\right) + O(\rho^2).$$

The presence of the second channel manifests itself through a new scale k_β^* (see Table 3), basically leading to the additional correction of $4\pi O(k_\beta^*(f_0^{\beta\alpha})^2/a)$ which is still on the negligible level less than a fraction of per mil.

For the production cross sections, instead of (75) and (76), we now have:

$$\gamma_1\gamma_2\frac{d^6\sigma}{d^3\mathbf{p}_1 d^3\mathbf{p}_2} \doteq \gamma_1\gamma_2\frac{d^6\sigma_0^\alpha}{d^3\mathbf{p}_1\, d^3\mathbf{p}_2}\sum_S \mathcal{G}_{S,\alpha}\left\langle\left|\psi^{S,\alpha}_{-\mathbf{k}^*}(\mathbf{r}^*)\right|^2\right\rangle_{\widetilde{q}PS} + \\ + \gamma_3\gamma_4\frac{d^6\sigma_0^\beta}{d^3\mathbf{p}_3\, d^3\mathbf{p}_4}\sum_S \mathcal{G}_{S,\beta}\left\langle\left|\psi^{S,\beta}_{-\mathbf{k}^*}(\mathbf{r}^*)\right|^2\right\rangle_{\widetilde{q}PS}, \quad (150)$$

$$\gamma_b\frac{d^3\sigma_b^S}{d^3\mathbf{P}_b} \doteq (2\pi)^3\gamma_1\gamma_2\frac{d^6\sigma_0^\alpha}{d^3\mathbf{p}_1 d^3\mathbf{p}_2}\mathcal{G}_{S,\alpha}\left\langle\left|\psi_b^{S,\alpha}(r^*)\right|^2\right\rangle_{0PS} + \\ + (2\pi)^3\gamma_3\gamma_4\frac{d^6\sigma_0^\beta}{d^3\mathbf{p}_3 d^3\mathbf{p}_4}\mathcal{G}_{S,\beta}\left\langle\left|\psi_b^{S,\beta}(r^*)\right|^2\right\rangle_{0PS}, \quad (151)$$

where $\mathbf{p}_i = \mathbf{P}_b m_i/(m_1 + m_2)$ in (151) and $b = \{n0\}$. Since the particles $1, 3$ and $2, 4$ are usually the members of the same isospin multiplets, assuming isospin equilibration (justified for multiple hadron production at midrapidities), we can take $\gamma_1\gamma_2 d^6\sigma_0^\alpha \doteq \gamma_3\gamma_4 d^6\sigma_0^\beta$ as a common factor in (150) and (151) and also put $\mathcal{G}_{S,\alpha} \doteq \mathcal{G}_{S,\beta}$.

The two-channel effects in the production cross section, being quadratic in the amplitude $f_0^{\beta\alpha}$, usually represent less than several percent of the strong FSI contribution (a fraction of percent in the cross section). Thus, for a near-threshold two-pion system produced according to a Gaussian r^* distribution (159) with the characteristic radius $r_{\mathcal{G}} = 3$ fm and, taking the two-pion s-wave amplitudes from [8] ($f_0^{\alpha\alpha} = 0.186$ fm, $f_0^{\beta\alpha} = -0.176$ fm), the contributions of the FSI transitions $\pi^+\pi^- \leftrightarrow \pi^+\pi^-$ and $\pi^+\pi^- \leftrightarrow \pi^0\pi^0$ to the $\pi^+\pi^-$ production cross section respectively compose 7.72 and 0.16%; these contributions are somewhat higher, 9.66 and 0.20%, for the amplitudes from [5] ($f_0^{\alpha\alpha} = 0.232$ fm, $f_0^{\beta\alpha} = -0.192$ fm). At large $r_{\mathcal{G}}$, the elastic and inelastic contributions vanish as $f_0^{\alpha\alpha}/r_{\mathcal{G}}$ and $|f_0^{\beta\alpha}/r_{\mathcal{G}}|^2$, respectively. One should also account for the correction due to the deviation of the solutions in (130) and (146) from the exact ones in the inner region $r^* < d$. Though this correction vanishes as $r_{\mathcal{G}}^{-3}$, at $r_{\mathcal{G}} = 3$ fm, it is still comparable to the contribution of the inelastic two-pion transition, composing 0.25 and 0.20% for the amplitudes from [8] and [5], respectively.

Note that assuming $\gamma_1\gamma_2 d^6\sigma_0^\alpha \mathcal{G}_{S,\alpha} \doteq \gamma_3\gamma_4 d^6\sigma_0^\beta \mathcal{G}_{S,\beta}$, the correction to the correlation function at a given total spin S, total four-momentum P, and a small generalized relative four-momentum $\widetilde{q} = \{0, 2\mathbf{k}^*\} \to 0$ can be written as

$$\Delta\mathcal{R} \doteq \int d^3\mathbf{r}^* W_P(\mathbf{r}^*) \left\{ \left[\left|\psi^\alpha_{-\mathbf{k}^*}(\mathbf{r}^*)\right|^2 + \left|\psi^\beta_{-\mathbf{k}^*}(\mathbf{r}^*)\right|^2 \right] - \right.$$
$$\left. - \left[\left|\widetilde{\psi}^\alpha_{-\mathbf{k}^*}(\mathbf{r}^*)\right|^2 + \left|\widetilde{\psi}^\beta_{-\mathbf{k}^*}(\mathbf{r}^*)\right|^2 \right] \right\}, \quad (152)$$

where $W_P(\mathbf{r}^*) = \int dt^* g_P(t^*, \mathbf{r}^*; 0) / \int d^4x g_P(x; 0)$ is the normalized distribution of the vector $\mathbf{r}^*$ of the relative distances between the emission points in the pair c.m. system and $\widetilde{\psi}$ denotes the solutions in (130) extended to the inner region $r^* < d$. In the case of only two open channels α and β, the leading part of the correction scaled by $W_P(0)$ is expressed through bilinear products of the amplitudes $f^{\lambda\lambda'}$ in Eq. (44) of [48]. After a straightforward though lengthy algebra, it can be written in a more explicit form:

$$\Delta\mathcal{R} \approx -4\pi W_P(0) A_c(\eta_\alpha) \left[|f_c^{\alpha\alpha}|^2 \frac{d}{dk^{*2}} (\hat{K}^{-1})^{\alpha\alpha} + \right.$$
$$\left. + |f_c^{\beta\alpha}|^2 \frac{d}{dk^{*2}} (\hat{K}^{-1})^{\beta\beta} + 2\mathrm{Re}\,(f_c^{\alpha\alpha} f_c^{\beta\alpha *}) \frac{d}{dk^{*2}} (\hat{K}^{-1})^{\beta\alpha} \right]; \quad (153)$$

at $k^* = 0$, twice the derivatives of the inverse $\hat{K}$-matrix elements coincide with the effective radii $d_0^{\lambda\lambda'}$. Similarly, in the case of discrete spectrum, the leading correction to $\langle |\widetilde{\psi}^\alpha_{n0}(\mathbf{r}^*)|^2 + |\widetilde{\psi}^\beta_{n0}(\mathbf{r}^*)|^2 \rangle$ is also given by (153) with the substitutions $A_c(\eta_\alpha) \to N'(n)$ and $f_c^{\lambda\lambda'} \to A^{\lambda\lambda'}$. For the Gaussian r^* distribution, (153) is

valid up to subleading contributions $O(k^{*2}a_1/r_{\mathcal{G}})$ (see a discussion after (88)) and $O(f_0^{\alpha\alpha}d^4/r_{\mathcal{G}}^5)$.

It is important that the presence of the second channel does not practically modify the ratio (125) of the finite-size correction factors in discrete and continuous ($k^* \to 0$) spectrum at moderate distances $r^* \ll |a|$. The only modifications are the substitution $f_0 \to \mathrm{Re}\, A^{\alpha\alpha} \approx f_0^{\alpha\alpha}$ and the appearance of the negligible correction $4\pi O(k^*_\beta (f_0^{\beta\alpha})^2/|a|)$:

$$\frac{1+\delta_n}{1+\delta(k^*)} \equiv \frac{[\mathcal{G}_\alpha \langle|\psi^\alpha_{n0}(r^*)|^2\rangle^{\mathrm{SL}}_{0P} + \mathcal{G}_\beta \langle|\psi^\beta_{n0}(r^*)|^2\rangle^{\mathrm{SL}}_{0P}]|\psi^{\mathrm{coul}}_{n0}(0)|^{-2}}{[\mathcal{G}_\alpha \langle|\psi^\alpha_{-\mathbf{k}^*}(\mathbf{r}^*)|^2\rangle^{\mathrm{SL}}_{\widetilde{q}P} + \mathcal{G}_\beta \langle|\psi^\beta_{-\mathbf{k}^*}(\mathbf{r}^*)|^2\rangle^{\mathrm{SL}}_{\widetilde{q}P}]|\psi^{\mathrm{coul}}_{k^*0}(0)|^{-2}} \equiv$$

$$\equiv \left|\frac{N'(n)}{\psi^{\mathrm{coul}}_{n0}(0)}\right|^2 \frac{1+\delta'_n}{1+\delta(k^*)} = \left[1+\phi(n)\frac{2\mathrm{Re}\, A^{\alpha\alpha}}{n|a|}\right] \times$$

$$\times \left\{1 + O\left(\frac{\langle r^{*2}\rangle^{\mathrm{SL}}}{a^2}\right) + O(k^{*2}\langle r^{*2}\rangle^{\mathrm{SL}}) + 4\pi O\left(\frac{k^*_\beta (f_0^{\beta\alpha})^2}{|a|}\right)\right\}. \quad (154)$$

6. FINITE-SIZE EFFECT IN THE DIRAC EXPERIMENT

6.1. $\pi^+\pi^-$ System. We will use the results of the UrQMD transport code simulations of the pion production in pNi interactions at 24 GeV in the conditions of the DIRAC experiment at CERN [29]. Since we are interested in the region of very small relative momenta $Q = 2k^* < 20$ MeV/c, where the angular distribution of the vector $\mathbf{Q}$ is isotropic for noncorrelated pions and, for $Q < 10$ MeV/c, the detector acceptance is practically independent of the direction of the vector $\mathbf{Q}$, one can simplify the analysis integrating over this direction. The finite-size effect is then determined by the distribution of the relative distance r^* between the pion production points in the pair c.m. system, irrespective of the angular distribution of the vector $\mathbf{r}^*$. In fact, due to the applied cut $Q_T < Q_T^{\mathrm{cut}} = 4$ MeV/c [4], this is true for $Q < Q_T^{\mathrm{cut}}$ only, see the discussion after (99) and (101)). For larger Q values or, in the case of a two-dimensional (Q_T, Q_L) analysis, one needs two-dimensional (r^*_T, r^*_L)- or $(r^*, \cos\theta_{r^*})$-distributions. We will neglect this complication here.

The simulated r^* distribution is shown in Fig. 2. The tail of this distribution ($r^* > 50$ fm) is dominated by pion pairs containing a pion from the decays of ω and η' resonances, except for the pairs with both pions from one and the same decay. The respective decay lengths in the rest frame of the decay pion are about 30 and 900 fm; the decay length $l \approx \tau\langle p_{\mathrm{dec}}\rangle/m_\pi$ is determined by the resonance lifetime τ and the four-velocity p_{dec}/m_π of the decay pion. As a consequence of the exponential decay law, the form of the corresponding r^* distributions is nearly exponential, except for the region of small r^* dominated by the phase

space suppression factor $\propto r^{*2}$. The exponential form is also distorted due to the averaging over the continuous spectrum of the decay momenta and over the emission points of the second pion. For r^* less than 2000–3000 fm, the simulated η' contribution ($\sim 1\%$ of pion pairs at $Q < 50$ MeV/c) can be sufficiently well parametrized by an exponential-like formula interpolating between the phase space and exponential behaviour:

$$\sum_i \frac{dN(\pi_{\eta'}\pi_i)}{dr^*} \doteq n_{\eta'}\mathcal{F}(r^*; r_{\eta'}, l_{\eta'}), \tag{155}$$

$$\mathcal{F}(r^*; r_{\eta'}, l_{\eta'}) = \frac{x^2}{2.2}\left\{1 - \exp\left[-\frac{2.2}{x^2}\left(1 + 0.2x^2\frac{1 + 0.15x^2y}{1 + x^5/125}\right)\right]\right\}\mathrm{e}^{-y}, \tag{156}$$

$$x = \frac{r^*}{r_{\eta'}} \qquad y = \frac{r^*}{l_{\eta'}},$$

where $r_{\eta'} = 2$ fm, $l_{\eta'} = 790$ fm. At the same time, a good description of the ω contribution ($\sim 19\%$ of low-Q pion pairs) requires a superposition of two exponential-like expressions:

$$\sum_{i\neq\eta'} \frac{dN(\pi_\omega\pi_i)}{dr^*} \doteq n_{1\omega}\mathcal{F}(r^*; r_{1\omega}, l_{1\omega}) + n_{2\omega}\mathcal{F}(r^*; r_{2\omega}, l_{2\omega}). \tag{157}$$

The parameters $r_{1\omega} = 1.07$ fm, $l_{1\omega} = 43.0$ fm, $r_{2\omega} = 2.65$ fm, $l_{2\omega} = 25.5$ fm, $n_{1\omega}/n_{2\omega} = 0.991$ in the interval 2–200 fm and $r_{1\omega} = 1.00$ fm, $l_{1\omega} = 44.0$ fm, $r_{2\omega} = 2.55$ fm, $l_{2\omega} = 25.8$ fm, $n_{1\omega}/n_{2\omega} = 0.845$ in the interval 2–350 fm. We will use the former parameter set, but we have checked that the use of the latter one leads to a negligible change ($< 0.1\%$) of the breakup probability. The rest of the r^* distribution due to the pions produced directly in the collision, in the rescatterings or in the decays of resonances with the decay lengths shorter than l_ω is peaked at ~ 3 fm and its main part ($\sim 60\%$ of low-Q pion pairs) including the tail for $r^* = 10{-}100$ fm can be effectively described by a power-like expression:

$$\mathcal{M}(r^*; r_\mathcal{M}, \alpha, \beta) = r^{*2}\left[1 + \left(\frac{r^*}{r_\mathcal{M}}\right)^{2\alpha}\right]^{-2\beta}, \tag{158}$$

where $r_\mathcal{M} = 9.20$ fm, $\alpha = 0.656$, $\beta = 2.86$; note that the tail vanishes as $(r^*)^{-5.5}$, i.e., much faster than the Lorentzian ($\alpha = \beta = 1$). The remaining short-distance part of the r^* distribution ($\sim 20\%$ of low-Q pion pairs) is strongly shifted towards the origin because the UrQMD code assumes the point-like regions of the decays and rescatterings; particularly, $r^* = 0$ for $\sim 8\%$ of low-Q $\pi^+\pi^-$ pairs. Therefore, we will represent this part by a Gaussian distribution:

$$\mathcal{G}(r^*; r_\mathcal{G}) = r^{*2}\exp\left(-\frac{r^{*2}}{4r_\mathcal{G}^2}\right), \tag{159}$$

where the Gaussian radius $r_{\mathcal{G}} \approx 1{-}2$ fm. As a result,

$$\sum_{i,j\neq\omega,\eta'} \frac{dN(\pi_i\pi_j)}{dr^*} \doteq n_{\mathcal{M}}\mathcal{M}(r^*; r_{\mathcal{M}}, \alpha, \beta) + n_{\mathcal{G}}\mathcal{G}(r^*; r_{\mathcal{G}}). \tag{160}$$

We will also represent the short-distance part of the r^* distribution by the Gaussian contribution alone, i.e., put $n_{\mathcal{M}} = 0$ and $r_{\mathcal{G}} = 3$ and 2 fm in (160).

The correction factors $1 + \delta(k^*)$ and $1 + \delta_n$ corresponding to the r^* distributions $\eta', \omega, \mathcal{M}, \mathcal{G}$, required to calculate the $\pi^+\pi^-$-production cross section in the continuous and discrete spectrum, are shown in Fig. 11. The two sets of histograms denoted by the same lines (dotted, solid, dash-dotted, dashed and solid) correspond to the two-pion scattering amplitudes from [8] (lower) and [5] (upper). In increasing order, they correspond to the r^* distributions η', ω, $\mathcal{G}(r^*; 3\ \mathrm{fm})$, $\mathcal{M}(r^*; 9.20\ \mathrm{fm}, 0.656, 2.86)$ and $\mathcal{G}(r^*; 2\ \mathrm{fm})$. One may see that the correction factors corresponding to the η' contribution are practically independent of the two-pion scattering amplitudes, and noticeably deviate from the infinite-size correction factors $1 + \delta^{\infty}(k^*) = 1/A_c(\eta)$ (the curve) and $1 + \delta_n^{\infty} = 0$. We thus do not include the η' meson in the class of LL emitters, unlike the η meson with the decay length of $\sim 10^5$ fm.

The calculation of the correction factors was done according to the two-channel expressions given in the numerator and denominator of the first equality in (154):

$$1 + \delta(\mathbf{k}^*) \doteq \left\langle \left|\psi^{\alpha}_{-\mathbf{k}^*}(\mathbf{r}^*)\right|^2 + \left|\psi^{\beta}_{-\mathbf{k}^*}(\mathbf{r}^*)\right|^2 \right\rangle^{\mathrm{SL}}_{\bar{q}P} [A_c(\eta)]^{-1}, \tag{161}$$

$$1 + \delta_n \doteq \left\langle |\psi^{\alpha}_{n0}(r^*)|^2 + \left|\psi^{\beta}_{n0}(r^*)\right|^2 \right\rangle^{\mathrm{SL}}_{0P} \left|\psi^{\mathrm{coul}}_{n0}(0)\right|^{-2}, \tag{162}$$

where α and β respectively denote the channels $\pi^+\pi^-$ and $\pi^0\pi^0$. However, the account of the coupled $\pi^0\pi^0$ channel and of the leading correction due to the approximate treatment of the wave function inside the range of the strong interaction, does not practically influence the results corresponding to the η' and ω contributions and only slightly ($< 1\%$) shifts up the correction factors corresponding to the short-distance $\mathcal{M}$ and $\mathcal{G}$ ones. A shift of the correction factors can arise also from the uncertainty in the s-wave elastic $\pi^+\pi^-$-scattering length f_0. The shift due to $\sim 20\%$ difference of the two-pion scattering amplitudes from [8] ($f_0 = 0.186$ fm) and [5] ($f_0 = 0.232$ fm) is $\sim 2{-}3\%$ for the short-distance $\mathcal{M}$ and $\mathcal{G}$ contributions and $\sim 1\%$ for the ω one. The global shifts are however not important since they can be absorbed in the product $\lambda g = \Lambda$ in (33) and (34).

In accordance with the results in Table 2 and Fig. 9, one may see in Fig. 11 the nearly universal slope of the factors $1 + \delta(k^*)$ corresponding to the short-distance $\mathcal{M}$ and $\mathcal{G}$ contributions. In accordance with (101), the slope scales with

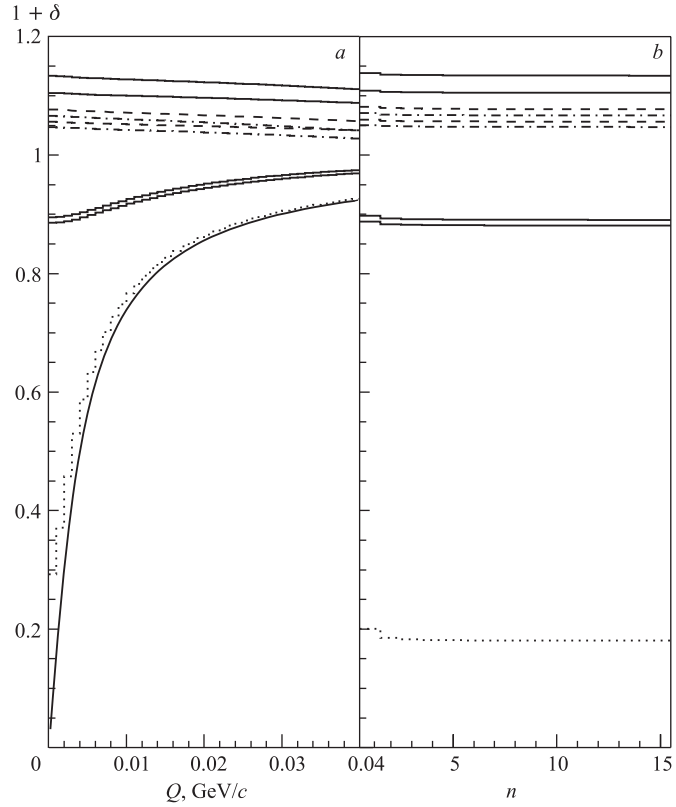

Fig. 11. The correction factors $1+\delta(k^*)$ (a) and $1+\delta_n$ (b) as functions of the relative momentum $Q=2k^*$ and the main atomic quantum number n, respectively. They are required to calculate the $\pi^+\pi^-$-production cross sections in the continuous and discrete spectrum according to (33) and (34). The two sets of histograms denoted by the same lines (dotted, solid, dash-dotted, dashed and solid) correspond to the two-pion scattering amplitudes from [8] (lower) and [5] (upper). In increasing order, they correspond to the r^* distributions η', ω, $\mathcal{G}(r^*;3\ \mathrm{fm})$, $\mathcal{M}(r^*;9.20\ \mathrm{fm}, 0.656, 2.86)$ and $\mathcal{G}(r^*;2\ \mathrm{fm})$ defined in (155)–(159). The calculation was done according to the two-channel expressions given in (161) and (162), taking into account the correction in (153). Note that the infinite-size correction factors $1+\delta^\infty(k^*)=1/A_c(\eta)$ (the curve) and $1+\delta_n^\infty=0$

f_0 and is $\sim 20\%$ steeper when using the two-pion amplitudes from [5] instead of those from [8]. This is clearly seen in Fig. 12, where we plot the same correction factors as in Fig. 11 in a larger scale and with the subtracted intercepts $1+\delta(0)$. At $Q>20$ MeV/c, there is also seen $\sim 5-10\%$ variation of the slope corresponding to different short-distance distributions.

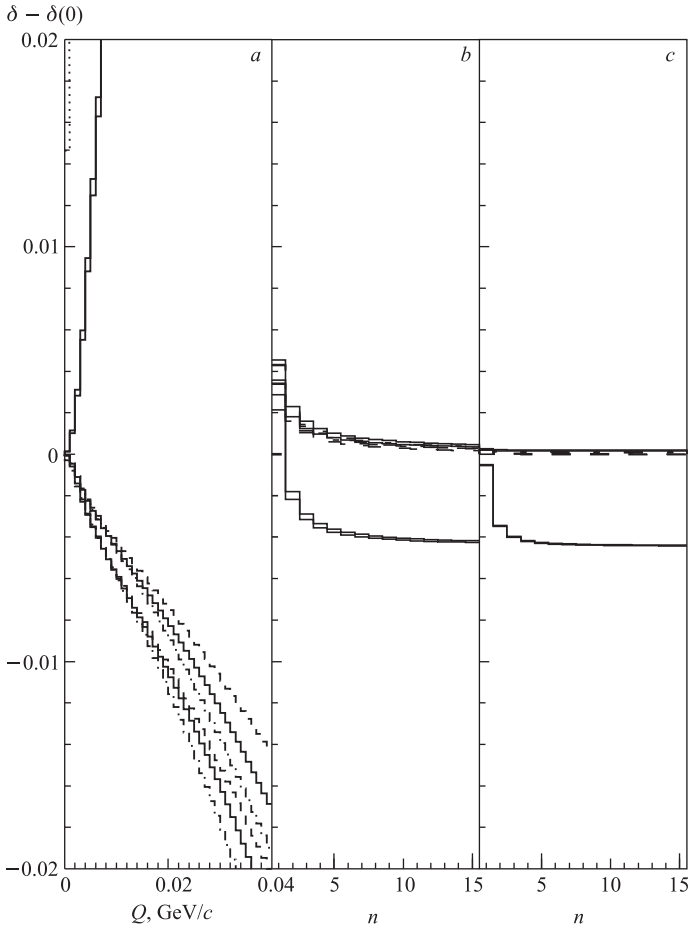

Fig. 12. The differences $\delta(k^*) - \delta(0)$ (a), $\delta_n - \delta(0)$ (b) and $\delta'_n - \delta(0)$ (c) calculated from the $\pi^+\pi^-$ correction factors given in Fig. 11. The latter difference is corrected for the effect of the strong interaction on the normalization of the pionium wave function according to (41). The differences corresponding to the η' contribution (dotted histograms) are not seen except for the first bin in plot a; in plots b and c they compose ~ -0.1

Figures 11 and 12 also demonstrate the violation of the universality relation $\delta_n \doteq \delta(0)$ up to $\sim 0.4\%$ for the short-distance and ω contributions and up to $\sim 9\%$ for the η' one. Figure 12, c shows that, in the case of the short-distance contribution, this violation is mainly related to the effect of the strong interaction on the normalization of the pionium wave function. Indeed, the difference $\delta'_n - \delta(0)$, corrected for this effect according to (41), practically vanishes.

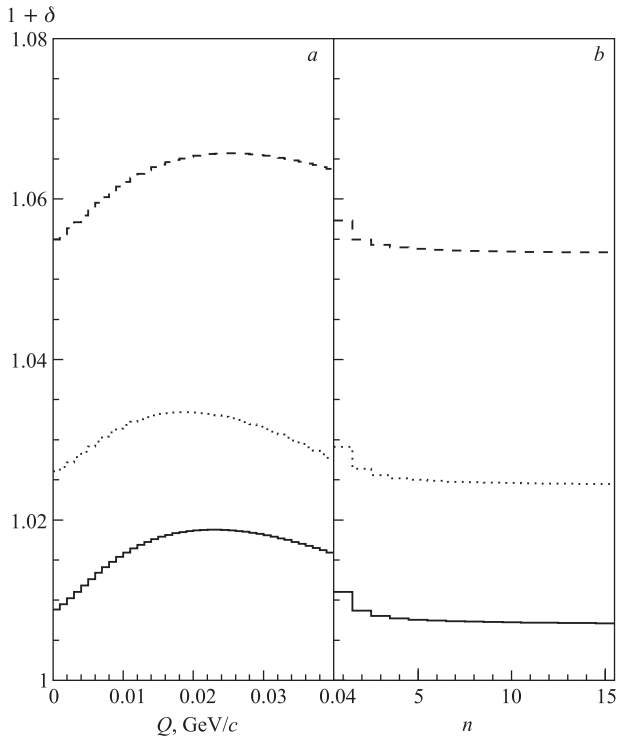

Fig. 13. The $\pi^+\pi^-$ correction factors $1 + \delta(k^*)$ (a) and $1 + \delta_n$ (b) calculated in the same way as in Fig. 11 assuming the mixtures of 1% η', 19% ω, and 80% $\mathcal{G}$ contributions with $r_{\mathcal{G}} = 3$ fm (lower and middle) and $r_{\mathcal{G}} = 2$ fm (upper). The lower and upper histograms correspond to the two-pion scattering amplitudes from [8], the middle one — to those from [5]

In Fig. 13 we plot the correction factors corresponding to the mixture of 1% η', 19% ω and 80% short-distance contributions, as expected from the UrQMD simulation of low-Q pairs of charged pions in conditions of the DIRAC experiment. We neglect here the dependence of the contributions on Q, as well as the dependence on the pion charges. In fact, within the analysis region of $Q < 15$ MeV/c, the simulated ω contribution increases with decreasing Q by ~ 0.01 and its average value for $\pi^+\pi^-$ pairs composes ~ 0.15 [29].

To show the effect of a possible uncertainty in the short-distance part, we describe it by the Gaussians with different characteristic radii $r_{\mathcal{G}} = 3$ and 2 fm. To account for the uncertainty in the two-pion scattering amplitudes, we have used those from [8] ($f_0 = 0.186$ fm) and from [5] ($f_0 = 0.232$ fm). One may see that the corresponding global variations of the correction factors compose ~ 5

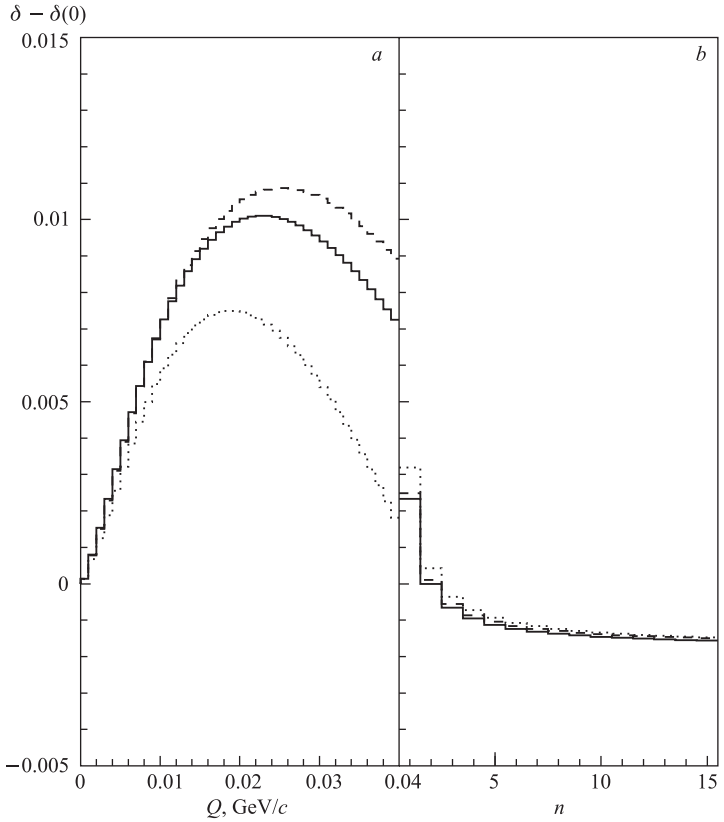

Fig. 14. The differences $\delta(k^*) - \delta(0)$ (a) and $\delta_n - \delta(0)$ (b) corresponding to the correction factors in Fig. 13

and $\sim 2\%$, respectively. In Fig. 14, we plot the same factors with the subtracted values of the intercept $1 + \delta(0)$. One may see that after the subtraction, the correction factors calculated for the same two-pion scattering amplitude but at different values of $r_{\mathcal{G}}$ practically coincide for any n in discrete spectrum and for $Q < 20$ MeV/c in continuous spectrum. Since the subtraction can be included in the overall normalization factor, one may conclude that the uncertainty in the short-distance part of the r^* distribution is of minor importance for the relative momenta $Q < 20$ MeV/c. As for the effect of $\sim 20\%$ increase of the s-wave elastic $\pi^+\pi^-$-scattering length, it leads to $\sim 20\%$ increase of $\delta_n - \delta_\infty$ and to $\sim 20\%$ decrease of $\delta(k^*) - \delta(0)$ at $Q = 12$ MeV/c.

To estimate the effect of the uncertainties in the ω and η' contributions, we plot in Fig. 15 the differences $\delta - \delta(0)$, varying these contributions by $\sim 30\%$.

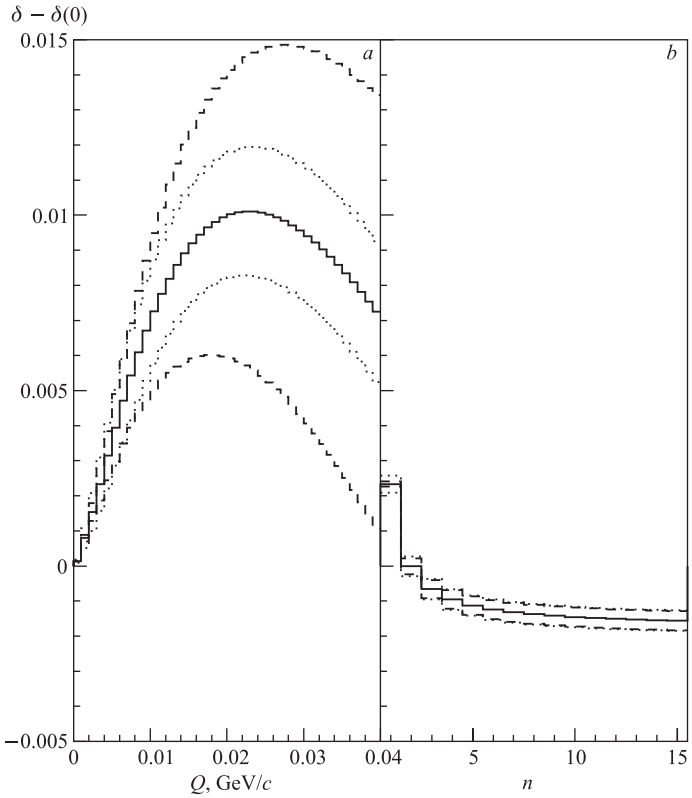

Fig. 15. The differences $\delta(k^*) - \delta(0)$ (a) and $\delta_n - \delta(0)$ (b). The solid histogram coincides with that in Fig. 14. The dashed ones correspond to the 0.19 ± 0.06 ω contributions and the dotted ones — to the 0.010 ± 0.003 η' contributions

One may see that the corresponding variations of the differences respectively compose ~ 30 and $\sim 20\%$ for $\delta(k^*) - \delta(0)$ at $Q = 12$ MeV/c and, they are quite small (< 0.0003) for $\delta_n - \delta(0)$. It should be noted that the η' contribution to the correction factor at $Q > Q_c$ is quite close to the infinite-size contribution $1/A_c$. The latter is included in the fit of the nonatomic $\pi^+\pi^-$ correlation function thus essentially reducing the corresponding uncertainty in the breakup probability. This is demonstrated in Table 4, where the contributions $-\Delta N_A/N_A$ and $\Delta N_A^{\rm br}/N_A^{\rm br}$ to the relative shifts $\Delta P_{\rm br}/P_{\rm br} = -\Delta N_A/N_A + \Delta N_A^{\rm br}/N_A^{\rm br}$ of the breakup probability due to the neglect of finite-size corrections, corresponding to different mixtures of the η', ω, and $\mathcal{G}$ contributions and different fit and signal intervals, are presented (see (43)–(47)). One may see that the 30% uncertainty in

Table 4. **The contributions $-\Delta N_A/N_A$ and $\Delta N_A^{\rm br}/N_A^{\rm br}$ to the relative shift $\Delta P_{\rm br}/P_{\rm br} = -\Delta N_A/N_A + \Delta N_A^{\rm br}/N_A^{\rm br}$ of the breakup probability (1) due to the neglect of finite-size corrections. The nonatomic $\pi^+\pi^-$ correlation functions, calculated according to (44) for different mixtures of the η', ω, and $\mathcal{G}(r_{\mathcal{G}})$ contributions, were fitted by (45) (fits $i = 1{-}7$), and $\Delta N_A/N_A$ and $\Delta N_A^{\rm br}/N_A^{\rm br}$ were calculated according to (46) and (47). In approximate correspondence with [4], a uniform population of noncorrelated pion pairs in Q was assumed in the considered fit intervals (Q_1, Q_2), and the ratios $N^{\rm cna}_{\pi^+\pi^-}/N_A^{\rm br}$ in the signal intervals $(0, Q_{\rm cut})$ were set equal to 16, 9, and 4 for $Q_{\rm cut}$ = 4, 3, and 2 MeV/c, respectively**

FIT i	1	2	3	4	5	6	7	Fit region Q_1, Q_2, MeV/c	Signal cut $Q_{\rm cut}$, MeV/c
$r_{\mathcal{G}}$, fm	3	3	3	3	3	3	2		
ω, %	19	25	13	19	19	19	19		
η', %	1.0	1.0	1.0	1.3	0.7	1.0	1.0		
Phase shifts	[8]	[8]	[8]	[8]	[8]	[5]	[8]		
$-\Delta N_A/N_A$, %	1.09	1.61	0.58	1.11	1.06	0.89	1.14	4, 20	—
$\Delta N_A^{\rm br}/N_A^{\rm br}$, %	4.06	6.77	1.30	4.22	3.86	2.69	4.48		4
	3.34	5.46	1.18	3.47	3.18	2.26	3.63		3
	2.08	3.37	0.80	2.17	1.98	1.44	2.24		2
$-\Delta N_A/N_A$, %	1.02	1.43	0.61	1.04	0.99	0.90	1.03	4, 15	—
$\Delta N_A^{\rm br}/N_A^{\rm br}$, %	3.62	5.57	1.50	3.70	3.42	2.66	3.82		4
	3.00	4.59	1.32	3.09	2.85	2.25	3.14		3
	1.89	2.88	0.88	1.96	1.80	1.44	1.96		2
$-\Delta N_A/N_A$, %	0.83	1.11	0.55	0.85	0.81	0.78	0.83	4, 10	—
$\Delta N_A^{\rm br}/N_A^{\rm br}$, %	2.43	3.62	1.16	2.53	2.35	1.92	2.51		4
	2.12	3.14	1.06	2.21	2.04	1.70	2.17		3
	1.39	2.05	0.72	1.46	1.33	1.12	1.41		2

the η' contribution leads to negligible variations in the relative shifts $\Delta N_A/N_A$ ($< 0.03\%$) and $\Delta N_A^{\rm br}/N_A^{\rm br}$ ($< 0.2\%$).

As for the uncertainty of the short-distance part of the r^* distribution, introduced by 30% decrease of the Gaussian radius from 3 to 2 fm, it also leads to negligible changes of the relative shifts $\Delta N_A/N_A$ ($< 0.05\%$) and $\Delta N_A^{\rm br}/N_A^{\rm br}$ ($< 0.4\%$) that rapidly decrease with decreasing upper boundaries of the fit and signal intervals.

One can also neglect the present $\sim 5\%$ uncertainty in the $\pi^+\pi^-$-scattering length f_0. Thus even the variation of f_0 by 20% leads to rather small variations of the relative shifts $\Delta N_A/N_A$ and $\Delta N_A^{\rm br}/N_A^{\rm br}$; e.g., for $Q_{\rm cut} = 4$ MeV/c and the fit interval $(4, 15)$ MeV/c they compose only 0.12 and 0.96%, respectively.

The dominant uncertainty in the finite-size correction to the breakup probability arises from the uncertainty in the ω contribution. One may see from Fig. 16 that the correction $\Delta P_{\rm br}$ almost linearly increases with the fraction f_ω of $\pi^+\pi^-$ pairs

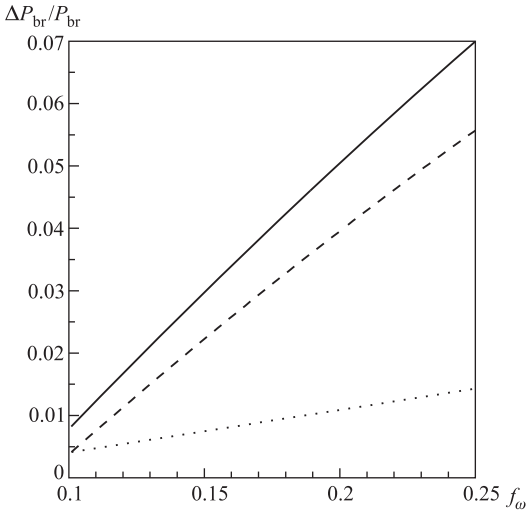

Fig. 16. Relative shift of the breakup probability $\Delta P_{\rm br}/P_{\rm br} = -\Delta N_A/N_A + \Delta N_A^{\rm br}/N_A^{\rm br}$ (solid curve) due to the neglect of the finite-size effect as a function of the fraction f_ω of $\pi^+\pi^-$ pairs containing a pion from ω decay and the other pion from any short-lived source, except for pion pairs from one and the same ω decay. The fit and signal intervals are $(4, 15)$ and $(0, 4)$ MeV/c, respectively (see Table 4). Also shown are contributions of the relative shifts $-\Delta N_A/N_A$ (dotted curve) and $\Delta N_A^{\rm br}/N_A^{\rm br}$ (dashed curve) in the calculated numbers of produced atoms and breakup atoms, respectively

containing a pion from ω decay and the other pion from any short-lived source, except for pion pairs from one and the same ω decay; $\Delta P_{\rm br}/P_{\rm br} \approx -0.032 + 0.41 f_\omega$ for $Q_{\rm cut} = 4$ MeV/c and the fit interval $(4, 15)$ MeV/c. Thus, taking $f_\omega = 0.19$, a 30% (± 0.06) variation in f_ω leads to $\sim 50\%$ (± 0.024) variation in $\Delta P_{\rm br}/P_{\rm br}$.

The correction rapidly decreases with decreasing upper boundaries of the fit and signal intervals. A decrease of the boundaries is however limited due to the increase of statistical errors. Also, the decrease of $Q_{\rm cut}$ below 3 MeV/c introduces a systematic shift of $\sim 5\%$ in the breakup probability due to possibly insufficiently accurate description of the shape of the Q spectrum of the atomic breakup $\pi^+\pi^-$ pairs [4]. The optimal choice seems to be $Q_{\rm cut} = 4$ MeV/c and the fit interval $(4, 15)$ MeV/c.

Taking $f_\omega = 0.15$, the overestimation of the breakup probability in these fit and signal intervals composes 3% and corresponds to $\sim 7.5\%$ overestimation of the pionium lifetime. Correcting for this overestimation and assuming rather conservative 30% uncertainty in the ω contribution, the uncertainty in the breakup probability composes 2%, corresponding to $\sim 5\%$ uncertainty in the extracted pionium lifetime.

One may expect an increase of the finite-size correction and its uncertainty when taking into account the increased slope of $\delta(k^*)$ at $Q > Q_T^{\rm cut} = 4$ MeV/c. On the other hand, one may expect a reduction of the correction when extending the fit region down to $Q = 0$ and performing a more constrained 2-dimensional fit of the (Q_T, Q_L) distribution taking into account also the shape of the spectrum of atomic pion pairs.

6.2. $\pi^-\pi^-$ and $\pi^+\pi^+$ Systems. As a by-product, the DIRAC experiment provides data on the correlation functions of identical charged pions which contains the information on the space-time characteristics of pion production and can be used to check the results of the UrQMD simulations. Thus, $\sim 5 \cdot 10^5$ $\pi^-\pi^-$ pairs have been collected in pNi interactions in 2001, representing $\sim 40\%$ of the available statistics [29]. The Q distribution of these pairs is peaked at ~ 60 MeV/c and drops essentially outside the interval $(20, 120)$ MeV/c due to a decrease of the phase space and detector acceptance at small and large Q, respectively.

Contrary to the case of the $\pi^+\pi^-$ system, the correlation effect in the system of identical pions extends and is measured up to the relative momenta $Q \sim 200$ MeV/c, so neither the distribution of the vector $\mathbf{Q}$ nor the detector acceptance can be considered independent of the direction of this vector. Since further the angular distribution of the vector $\mathbf{r}^*$ is not isotropic (particularly, the characteristic width of the out component of the $\mathbf{r}^*$ distribution increases with the transverse momentum while those of the side and longitudinal ones decrease), the required space-time information does not reduce to the distribution of the relative distance r^* between the pion production points in the pair c.m. system; generally, the 3-dimensional distribution of the vector $\mathbf{r}^*$ is required. Here we, however, neglect this complication and calculate the 1-dimensional correlation function of two identical charged pions in the same way as for the previously considered case of the near-threshold $\pi^+\pi^-$ system, i.e., assuming the uniform distribution of the cosine of the angle between the vectors $\mathbf{Q}$ and $\mathbf{r}^*$ for the noncorrelated pions.

The calculated $\pi^-\pi^-$ correlation functions $\mathcal{R}^{--}_{\eta'}$, $\mathcal{R}^{--}_{\omega}$, $\mathcal{R}^{--}_{\mathcal{M}}$, and $\mathcal{R}^{--}_{\mathcal{G}}$ corresponding to the r^* distributions η', ω, $\mathcal{M}(r^*; 9.20 \text{ fm}, 0.656, 2.86)$, and $\mathcal{G}(r^*; r_{\mathcal{G}})$, $r_{\mathcal{G}} = 3, 2, 1.5$ fm, are shown in Fig. 17. In Fig. 18, we show the correlation function corresponding to 1% η', 19% ω, 60% $\mathcal{M}(r^*; 9.20 \text{ fm}, 0.656, 2.86)$ and 20% $\mathcal{G}(r^*; 1.5 \text{ fm})$ contributions, as expected for the pairs of charged pions from the UrQMD simulations; the errors are taken from the DIRAC pNi 2001 data. To demonstrate the sensitivity to the relative ω contribution, f_ω, we show in this figure also the correlation functions calculated with f_ω varied by $\sim 30\%$. One can conclude that the different shape of the ω contribution as compared with the shapes of the short-distance ones ($\mathcal{M}$ and $\mathcal{G}$) allows one, in principle, to determine f_ω — the most critical parameter required to calculate the finite-size $\pi^+\pi^-$ correction factors. To estimate the statistics required to determine f_ω better

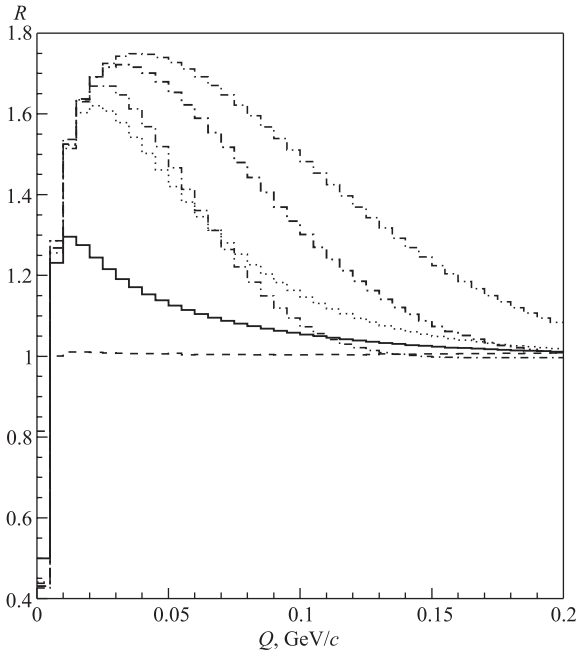

Fig. 17. The $\pi^-\pi^-$ correlation functions. The histograms in the increasing order of the peak values correspond to the r^* distributions η', ω, $\mathcal{M}(r^*; 9.20\ \text{fm}, 0.656, 2.86)$, $\mathcal{G}(r^*; 3\ \text{fm})$, $\mathcal{G}(r^*; 2\ \text{fm})$ and $\mathcal{G}(r^*; 1.5\ \text{fm})$, respectively

than to 30%, we have fitted the correlation function in Fig. 18 by

$$\mathcal{R}(Q) = N\left\{\lambda\left[f_{\eta'}\mathcal{R}^{--}_{\eta'}(Q) + f_\omega\mathcal{R}^{--}_{\omega}(Q) + f_{\mathcal{G}}\mathcal{R}^{--}_{\mathcal{G}}(Q; r_{\mathcal{G}}) + \right.\right.$$
$$\left.\left. + (1 - f_{\eta'} - f_\omega - f_{\mathcal{G}})\mathcal{R}^{--}_{\mathcal{M}}(Q; r_{\mathcal{M}}, \alpha, \beta)\right] + (1 - \lambda)\right\}(1 + bQ). \quad (163)$$

The parameter N cares for possible normalization mismatch, the correlation strength parameter λ takes into account the contribution of LL emitters, particle misidentification as well as coherence effects, and the slope parameter b cares for a possible mismatch in the Q dependence of the reference sample in the denominator of the correlation function. Equation (163) does not take into account a decrease of the fractions $f_{\eta'}$ and f_ω with increasing Q which can amount to $\sim 20\%$ in the interval 0–200 MeV/c [29].

The dependence of the correlation function on the parameters $r_{\mathcal{G}}$, $r_{\mathcal{M}}$, α, β is calculated with the help of quadratic interpolation. For example, to calculate the $r_{\mathcal{G}}$ dependence, three values of this parameter are chosen and the corresponding

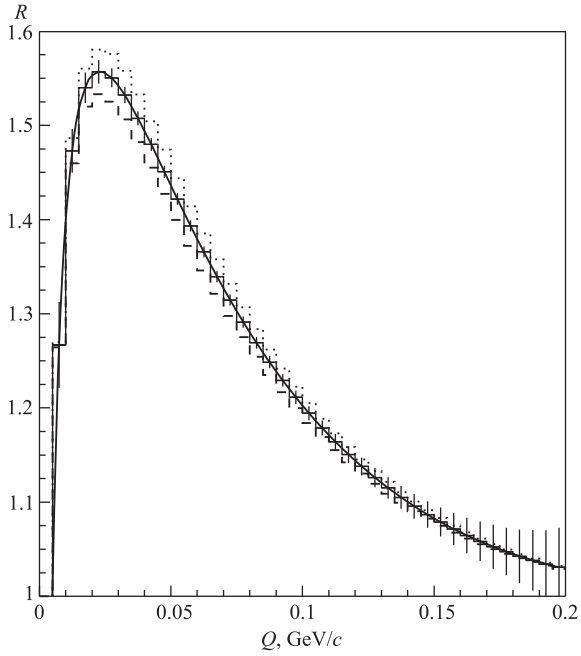

Fig. 18. The $\pi^-\pi^-$ correlation functions. The middle histogram and the fit curve correspond to 1% η', 19% ω, 60% $\mathcal{M}(r^*;\, 9.20\ \text{fm}, 0.656, 2.86)$ and 20% $\mathcal{G}(r^*; 1.5\ \text{fm})$ contributions. The errors are taken from the DIRAC pNi 2001 data [29]. The upper and lower histograms correspond to the 1% η', $(19 \pm 6)\%$ ω contributions and the unchanged ratio 3:1 of the $\mathcal{M}$ and $\mathcal{G}$ contributions (unchanged form of the short-distance contribution)

correlation functions $\mathcal{R}^{--}_{\mathcal{G}}(Q; r^i_{\mathcal{G}})$, $i = 1, 2, 3$, are used to interpolate to the correlation function at a given value of $r_{\mathcal{G}}$ according to (82) with the substitutions $\mathcal{R}_{\mathrm{RQMD}} \to \mathcal{R}^{--}_{\mathcal{G}}$ and $s_r \to r_{\mathcal{G}}$. Similarly, the quadratic interpolation in the three-parameter space $r_{\mathcal{M}}$, α, β requires the calculation of 3^3 correlation functions $\mathcal{R}^{--}_{\mathcal{M}}(Q; r^i_{\mathcal{M}}, \alpha^j, \beta^k)$, $i, j, k = 1, 2, 3$.

The fit recovers the input parameters with rather small parabolic errors, particularly, $f_\omega = 0.189 \pm 0.048$. It appears, however, that the real error, corresponding to the increase of the χ^2 by one unit, is one order of magnitude larger. Thus, to achieve the error in f_ω smaller than 30%, one has to collect the statistics of $\sim 5 \cdot 10^7$ $\pi^-\pi^-$ pairs. The fit results corresponding to such a statistics are shown in Table 5, fits 1–6. Comparing fits 1–3, one may see that they are practically insensitive to the nearly flat η' contribution to the correlation function, except for $\sim 20\%$ drop in the first 5 MeV/c bin. Since the drop contribution of $0.2 \cdot 0.01$ is much smaller than the correlation function error of 0.02 in the first bin, the 0.01

Table 5. **The results of the fits according to (163) of the $\pi^-\pi^-$ correlation function corresponding to the mixture of the 1% η', 19% ω, 60% $\mathcal{M}(r_\mathcal{M},\alpha,\beta)$, and 20% $\mathcal{G}(r_\mathcal{G})$ contributions with $r_\mathcal{G}=1.5$ fm, $r_\mathcal{M}=9.2$ fm, $\alpha=0.656$, $\beta=2.863$. The errors correspond to the statistics of $5\cdot10^7$ $\pi^-\pi^-$ pairs from pNi interactions in the conditions of the DIRAC experiment. Only the parabolic errors are shown, absent error means a fixed parameter**

FIT i	1	2	3	4	5	6
N	1.000 ±0.001	0.999 ±0.001	1.000 ±0.001	1.002 ±0.001	0.998 ±0.001	1.017 ±0.001
λ	1.001 ±0.004	0.993 ±0.003	0.999 ±0.004	0.973 ±0.003	1.024 ±0.003	0.984 ±0.003
$r_\mathcal{M}$, fm	9.253 ±0.048	9.239 ±0.049	9.161 ±0.048	7.381 ±0.045	10.844 ±0.065	6.322 ±0.032
α	0.657 ±0.003	0.651 ±0.003	0.655 ±0.003	0.611 ±0.002	0.746 ±0.004	0.561 ±0.001
β	2.864 ±0.010	2.893 ±0.010	2.853 ±0.009	2.717 ±0.008	2.813 ±0.013	3.001 ±0.006
$r_\mathcal{G}$, fm	1.495 ±0.016	1.492 ±0.016	1.496 ±0.015	1.505 ±0.022	1.554 ±0.013	1.5
$f_\mathcal{G}$	0.202 ±0.003	0.199 ±0.003	0.200 ±0.003	0.147 ±0.004	0.261 ±0.003	0
f_ω	0.187 ±0.004	0.190 ±0.005	0.184 ±0.005	0.131	0.238	0.234 ±0.004
$f_{\eta'}$	0.010 ±0.004	0	0.01	0.01	0.01	0.01
b, $(\mathrm{GeV}/c)^{-1}$	0.001 ±0.008	0.000 ±0.008	0.000 ±0.007	-0.033 ±0.008	0.036 ±0.008	–0.162 ±0.006
χ^2	0.01	0.02	0.01	1.01	1.01	33.9

shift in $f_{\eta'}$ in fit 2 ($f_{\eta'}=0$) leaves the parameters and χ^2 practically unchanged, except for the compensating ~0.01 shift in the correlation strength parameter λ. Comparing further fits 3–5, one can conclude that the true error in f_ω, corresponding to the increase of χ^2 by one unit, composes $\sim25\%$ (~0.05). Finally, fit 6 ($f_\mathcal{G}=0$) shows that the oversimplified description of the short-distance contribution could lead to $\sim25\%$ systematic shift of f_ω.

To infer the fraction f_ω^{+-} for $\pi^+\pi^-$ pairs at $Q\to0$ from the fitted $f_\omega^{\pm\pm}$ for identical charged pions, one has to take into account its Q dependence as well as the fact that, due to a lower multiplicity of the pairs of identical charged pions, the fraction $f_\omega^{\pm\pm}$ is $\sim40\%$ higher than f_ω^{+-} [29].

CONCLUSIONS

We have developed a practical formalism allowing one to quantify the effect of a finite space-time extent of particle emission region on the two-particle production in continuous and discrete spectrum. We have shown that one can usually neglect the nonequal emission times in the pair c.m. system, the space-time coherence and the residual charge. The developed formalism is in the basis of the femtoscopy techniques allowing one to measure space-time characteristics of particle production as well as the low-energy strong interaction between specific particles. We have applied it to the problem of lifetime measurement of hadronic atoms produced by a high-energy beam in a thin target, particularly, to the measurement of pionium lifetime in the DIRAC experiment at CERN. Based on the transport code simulations, we have calculated the so-called correction factors that can be used to take into account the finite size of the production region by multiplying the point-like Coulomb production cross sections of the free and bound $\pi^+\pi^-$ pairs. We have shown that the short-distance contribution is of minor importance for the lifetime measurement since it leads to practically the same and nearly constant correction factors for free and bound pairs which cancel in the breakup probability. The most important is the fraction f_ω of $\pi^+\pi^-$ pairs containing a pion from ω decay and the other pion from any short-lived source, except for pion pairs from one and the same ω decay. Besides leading to slightly different global shifts of the correction factors, it also affects their Q- and n-dependence. The resulting correction to the «point-like» pionium lifetime composes $\sim -7.5\%$. Assuming rather conservative 30% uncertainty in f_ω, due to the uncertainty in the ω production and a simplified treatment of the correction (e.g., the neglect of f_ω variation in the analyzed Q interval), one arrives at $\sim 5\%$ uncertainty in the extracted pionium lifetime. It is shown that this uncertainty could be diminished if the high statistics data on correlations of identical charged pions were collected in the DIRAC experiment. The statistics required to determine f_ω to 10% and control the finite-size effect on the lifetime to $\sim 2\%$ composes $\sim 3 \cdot 10^8$ $\pi^-\pi^-$ pairs. The uncertainty in f_ω can be also reduced by tuning the transport simulations with the help of experimental data on particle (resonance) spectra and femtoscopic correlations in proton–nucleus collisions at the beam energy of ~ 20 GeV. The lifetime uncertainty can be essentially reduced in future experiments using the multilayer targets [2] since it will be basically determined by the uncertainty in the calculated number N_A of produced atoms only; even for the conservative 30% uncertainty in f_ω, the corresponding uncertainty in the lifetime will be $\sim 1\%$ only. The above estimates of the finite-size correction to the pionium lifetime and its uncertainty are based on a 1-dimensional fit of the Q distribution in the interval $(4, 15)$ MeV/c. One may expect their underestimation due to the neglected increase of the slope of Q distribution for $Q > Q_T^{\rm cut} = 4$ MeV/c. On the other hand, one may expect

their reduction when extending the fit interval down to $Q = 0$ and performing a more constrained 2-dimensional fit of the (Q_T, Q_L) distribution. The effect of the finite-size uncertainty on the breakup probability of other hadronic atoms remains to be studied. For πK and πp atoms, it is expected similar to the one for $\pi^+\pi^-$ atoms since $\sim 50\%$ decrease of the ω contribution is compensated by about the same decrease of the Bohr radius $|a|$ thus retaining a similar finite-size Coulomb FSI effect $\sim \langle r^* \rangle^{\text{SL}}/a$. As for K^+K^-, K^-p, and $\bar{p}p$ atoms, there is no ω contribution to the corresponding hadron pairs though, due to the smaller Bohr radii, its effect can be partly substituted by the contribution of ϕ meson and other sufficiently narrow resonances.

Acknowledgements. The author thanks Vladimir Lyuboshitz, Leonid Nemenov, Jan Smolík, and Valery Yazkov for useful discussions. This work was supported by the Grant Agency of the Czech Republic under contracts 202/01/0779, 202/04/0793 and 202/07/0079.

Appendix A
NONEQUAL EMISSION TIMES

We consider here the role of nonequal emission times in the Bethe–Salpeter amplitude $\psi_{\widetilde{q}}(x) = \mathrm{e}^{i\tilde{q}x/2} + \Delta\psi^{(+)}_{\widetilde{q}}(x)$, where the correction $\Delta\psi$ to the plane wave is given in (10). We will consider the amplitude in the pair c.m. system, in which the plane wave $\mathrm{e}^{i\tilde{q}x/2} = \mathrm{e}^{-i\mathbf{k}^*\mathbf{r}^*}$ is independent of the emission times. First, we will prove the integral relation between the Bethe–Salpeter amplitude and the corresponding nonrelativistic wave function, derived on the condition $k^{*2} \ll \mu^2$ [12]:

$$\psi^{(+)}_{\widetilde{q}}(x) = \int d^3\mathbf{r}'\delta_{k^*}(\mathbf{r}^* - \mathbf{r}', t^*)\psi_{-\mathbf{k}^*}(\mathbf{r}'), \tag{A.1}$$

$$\delta_{k^*}(\mathbf{r}^* - \mathbf{r}', t^*) = \frac{1}{(2\pi)^3}\int d^3\kappa\, \mathrm{e}^{-i\kappa(\mathbf{r}^* - \mathbf{r}')} \exp\left(-i\frac{\boldsymbol{\kappa}^2 - \mathbf{k}^{*2}}{2m(t^*)}|t^*|\right), \tag{A.2}$$

where $m(t^* > 0) = m_2$ and $m(t^* < 0) = m_1$.

We start by splitting the product of the propagators into four terms, each containing only two poles in the complex κ_0 plane, situated in the opposite upper and lower half-planes. Taking into account that in the pair c.m. system $\mathbf{P} = 0$ and that the pair energy coincides with its effective mass: $P_0 = m_{12}$, we get

$$\begin{aligned}
&\{(\kappa^2 - {m_1}^2 + i0)[(P-\kappa)^2 - {m_2}^2 + i0]\}^{-1} = \\
&= [(\kappa_0 - \widetilde{\omega}_1 + i0)(\kappa_0 + \widetilde{\omega}_1 - i0)(\kappa_0 - m_{12} - \widetilde{\omega}_2 + i0)(\kappa_0 - m_{12} + \widetilde{\omega}_2 - i0)]^{-1} = \\
&\quad = [{m_{12}}^2 - (\widetilde{\omega}_1 - \widetilde{\omega}_2)^2]^{-1}\{[(\kappa_0 - \widetilde{\omega}_1 + i0)(\kappa_0 + \widetilde{\omega}_1 - i0)]^{-1} + \\
&\quad\quad + [(\kappa_0 - m_{12} - \widetilde{\omega}_2 + i0)(\kappa_0 - m_{12} + \widetilde{\omega}_2 - i0)]^{-1} - \\
&\quad\quad\quad - [(\kappa_0 - \widetilde{\omega}_1 + i0)(\kappa_0 - m_{12} + \widetilde{\omega}_2 - i0)]^{-1} - \\
&\quad\quad\quad\quad - [(\kappa_0 + \widetilde{\omega}_1 - i0)(\kappa_0 - m_{12} - \widetilde{\omega}_2 + i0)]^{-1}\},
\end{aligned} \tag{A.3}$$

where $\widetilde{\omega}_i = ({m_i}^2+\kappa^2)^{1/2}$. Assuming now that the amplitude $f^S \equiv f^S(\kappa_0, m_{12}-\kappa_0)$ is an analytical function in the complex κ_0 plane, we can integrate over κ_0 using the residue theorem. Consider first $t^* > 0$. In this case the integration contour has to be closed in the upper half-plane, equation (10) then giving

$$\Delta\psi^{(+)}_{\widetilde{q}}(x) = \frac{1}{\pi^2} m_{12}\, \mathrm{e}^{-i[m_{12}+({m_1}^2-{m_2}^2)/m_{12}]t^*/2} \int \frac{d^3\kappa\, \mathrm{e}^{-i\kappa\mathbf{r}^*}}{{m_{12}}^2 - (\widetilde{\omega}_1-\widetilde{\omega}_2)^2} \times$$
$$\times \left[\mathrm{e}^{-i\widetilde{\omega}_1 t^*} f(-\widetilde{\omega}_1, m_{12}+\widetilde{\omega}_1) \left(\frac{1}{m_{12}+\widetilde{\omega}_1+\widetilde{\omega}_2} - \frac{1}{2\widetilde{\omega}_1} \right) - \right.$$
$$\left. - \mathrm{e}^{i(m_{12}-\widetilde{\omega}_2)t^*} f(m_{12}-\widetilde{\omega}_2, \widetilde{\omega}_2) \left(\frac{1}{m_{12}-\widetilde{\omega}_1-\widetilde{\omega}_2+i0} + \frac{1}{2\widetilde{\omega}_2} \right) \right]. \quad \text{(A.4)}$$

Since we are interested in the limit of small particle momenta in the pair c.m. system: $k^{*2} \ll \mu^2$ and since the integral (A.4) is dominated by $\kappa^2 \approx \mathbf{k}^{*2}$, we can use the following nonrelativistic approximations (recall that $\mu = m_1 m_2/(m_1+m_2)$ is the reduced mass of the two-particle system):

$$m_{12} \doteq m_1 + m_2 + \frac{\mathbf{k}^{*2}}{2\mu}, \quad m_{12} + \frac{{m_1}^2 - {m_2}^2}{m_{12}} \doteq 2\left(m_1 + \frac{m_2}{m_1+m_2} \frac{\mathbf{k}^{*2}}{2\mu} \right), \quad \text{(A.5)}$$

$$\widetilde{\omega}_i \doteq m_i + \frac{\kappa^2}{2m_i},\ {m_{12}}^2 - (\widetilde{\omega}_1-\widetilde{\omega}_2)^2 \doteq 4m_1 m_2,\ m_{12} - \widetilde{\omega}_1 - \widetilde{\omega}_2 \doteq \frac{\mathbf{k}^{*2}-\kappa^2}{2\mu}.$$

Retaining in the integral (A.4) only the dominant pole term $\sim [m_{12}-\widetilde{\omega}_1-\widetilde{\omega}_2+i0]^{-1}$, we get

$$\Delta\psi^{(+)}_{\widetilde{q}}(x) = \frac{1}{2\pi^2} \int \frac{d^3\kappa\, \mathrm{e}^{-i\kappa\mathbf{r}^*}}{\kappa^2 - \mathbf{k}^{*2} - i0} \exp\left(-i\frac{\kappa^2-\mathbf{k}^{*2}}{2m_2} t^* \right) f(m_{12}-\widetilde{\omega}_2, \widetilde{\omega}_2). \quad \text{(A.6)}$$

Using now the equalities $\Delta\psi^{(+)}_{\widetilde{q}}(\mathbf{r}^*, t^*=0) \equiv \Delta\psi_{-\mathbf{k}^*}(\mathbf{r}^*)$ and $\delta^{(3)}(\kappa-\kappa') = (2\pi)^{-3}\int d^3\mathbf{r}' \exp[i(\kappa-\kappa')\mathbf{r}']$, we can write:

$$\Delta\psi^{(+)}_{\widetilde{q}}(x) = \frac{1}{2\pi^2} \int d^3\kappa' \delta^{(3)}(\kappa-\kappa') \frac{d^3\kappa\, \mathrm{e}^{-i\kappa\mathbf{r}^*}}{\kappa'^2 - \mathbf{k}^{*2} - i0} \times$$
$$\times \exp\left(-i\frac{\kappa^2-\mathbf{k}^{*2}}{2m_2} t^* \right) f(m_{12}-\widetilde{\omega}'_2, \widetilde{\omega}'_2) =$$
$$= \int d^3\mathbf{r}' \int \frac{d^3\kappa}{(2\pi)^3} \mathrm{e}^{-i\kappa(\mathbf{r}^*-\mathbf{r}')} \exp\left(-i\frac{\boldsymbol{\kappa}^2-\mathbf{k}^{*2}}{2m(t^*)} t^* \right) \times$$
$$\times \frac{1}{2\pi^2} \int \frac{d^3\kappa' \mathrm{e}^{-i\kappa'\mathbf{r}'}}{\kappa'^2 - \mathbf{k}^{*2} - i0} f(m_{12}-\widetilde{\omega}'_2, \widetilde{\omega}'_2) \equiv$$
$$\equiv \int d^3\mathbf{r}' \delta_{k^*}(\mathbf{r}^*-\mathbf{r}', t^*) \Delta\psi_{-\mathbf{k}^*}(\mathbf{r}'), \quad \text{(A.7)}$$

where the δ_{k^*} function is given in (A.2). Noting that the δ_{k^*} function in the integral (A.7) acts on the plane wave $\mathrm{e}^{-i\mathbf{k}^*\mathbf{r}'}$ as a δ function, we finally arrive at the integral relation in (A.1) for $t^* > 0$. The prove of this relation in the case of $t^* < 0$ is done in a similar way, the integration κ_0 contour being now closed in the lower half-plane. The result is the same as in (A.4)–(A.7), up to the substitutions $m_2 \to -m_1$ in the time-dependent phase factor and $\widetilde{\omega}_2 \to m_{12} - \widetilde{\omega}_1$ in the arguments of the scattering amplitude f.

At $t^* = 0$, the function $\delta_{k^*}(\mathbf{r}^* - \mathbf{r}', 0) = \delta^{(3)}(\mathbf{r}^* - \mathbf{r}')$ and, at $t^* > 0$,

$$\delta_{k^*}(\mathbf{r}^* - \mathbf{r}', t^*) = \left(\frac{m_2}{2\pi i t^*}\right)^{3/2} \exp\left[i\left(\frac{k^{*2}t^*}{2m_2} + \frac{(\mathbf{r}^* - \mathbf{r}')^2 m_2}{2t^*}\right)\right]. \qquad \text{(A.8)}$$

For negative t^* values, the substitution $m_2 \to -m_1$ has to be done in (A.8). It is clear from (A.8) that, at small k^* ($k^* \ll m(t^*)r^*/|t^*|$), the function $\delta_{k^*}(\mathbf{r}^* - \mathbf{r}', t^*)$ practically coincides with the δ function $\delta^{(3)}(\mathbf{r}^* - \mathbf{r}')$ on condition (73).

Since the particles start to feel each other only after both of them are created, it is clear that a large difference in the emission times generally leads to a suppression of particle interaction at small k^*: $|\Delta\psi^{(+)}_{\widetilde{q}}(x)| \leqslant |\Delta\psi_{-\mathbf{k}^*}(\mathbf{r}^*)|$; $\Delta\psi^{(+)}_{\widetilde{q}}(x) \to 0$ at $|t^*| \to \infty$. Particularly instructive is the case when one of the two particles is very heavy, say $m_2 \gg m_1$. Then the two-particle interaction is suppressed provided the light particle is emitted prior the emission of the heavy one ($m(t^* < 0) = m_1$ in (A.2)). Otherwise, the large mass $m(t^* > 0) = m_2$ prevents the suppression even if the light particle is emitted much later than the heavy one. Below we consider the effect of nonequal emission times on two-particle production in some detail.

We start with the FSI due to the short-range forces only. Inserting the spherical wave (85) into the integral relation (A.1) or (A.7), we get [12]

$$\Delta\psi^{(+)}_{\widetilde{q}}(x) = \frac{f(k^*)}{r^*}\left\{i\sin(k^*r^*) + \frac{1-i}{2}\left[\mathrm{E}_1(z_-)\,\mathrm{e}^{ik^*r^*} + \mathrm{E}_1(z_+)\,\mathrm{e}^{-ik^*r^*}\right]\right\}, \qquad \text{(A.9)}$$

where $z_\pm = (m(t^*)/2|t^*|)^{1/2}\,(r^* \pm (k^*|t^*|/m(t^*)))$ and $\mathrm{E}_1(z) = \sqrt{2/\pi}\int\limits_0^z dy\,\mathrm{e}^{iy^2}$ is the Fresnel integral. Note that the length $k^*|t^*|/m(t^*) \equiv l_{k^*}$ can be interpreted classically, for large k^*r^*, as a distance traveled by the first emitted particle until the creation moment of the second one. The absolute value of the factor $(r^* \pm l_{k^*})$ in the argument z_+ (z_-) thus corresponds to the maximal (minimal) possible distance between the particles in their c.m. system at the later of the two creation moments. The effect of nonequal emission times however does not reduce to the modification of the distance r^*, it survives even at $k^* = 0$. This effect vanishes in the limit of small $|t^*|$, when $z_- \gg 1$, $\mathrm{E}_1(z_\pm) \to (1+i)/2$ and (A.9) reduces to the spherical wave (85). In the opposite limit of large $|t^*|$,

when $\left[m(t^*)r^{*2}/(2|t^*|)\right]^{1/2} \ll 1$, the interaction is suppressed and the scattered wave $\Delta\psi^{(+)}_{\tilde{q}}(x)$ tends to zero for arbitrary k^* values.

In the simple static Gaussian model of independent one-particle emitters described by the amplitude (51), the applicability condition (73) of the *equal-time* approximation can be roughly written in the form (74). Clearly, the latter condition is not satisfied for very slow particles emitted by the emitters of a long lifetime. This is demonstrated in Figs. 3 and 4 for the FSI contribution in the $\pi^0\pi^0$ correlation function.

Note that the change of the character of the effect of nonequal times at $v \approx 0.6$ and its increase with the increasing velocity is not expected from condition (74). The increase of the effect for relativistic particles ($v \to 1$) is specific for the systems of not very large sizes and lifetimes $\tau_0 \sim r_0$, when the population of the light-cone region $\mathbf{r} \sim \mathbf{v}t$ is not negligible. Indeed, in this region the arguments of the Fresnel integrals at $k^* = 0$ can be small even at large γ: $z_\pm \approx (\gamma m|r_L - t|/2)^{1/2}$, leading to the modification of the spherical wave.

Consider finally the effect of nonequal emission times on the correlations of two charged particles. Since, at not very large $|t^*|$, the function $\delta_{k^*}(\mathbf{r}^* - \mathbf{r}', t^*)$ is close to the δ function, we can neglect the terms of higher powers of (r'/a) in (A.1)*. The nonequal time correction is thus mainly generated by the subleading term $\sim r^*/a$ and so can be expected rather small, similar to the case of strong FSI, where it arises from a small finite-size contribution $\sim f/r^*$. It concerns also the case of hadronic atoms since the Schrödinger equation at a small negative energy $-\epsilon_b = -\kappa^2/(2\mu)$ practically coincides with that in continuous spectrum at zero energy. As a result, for $r^* \ll \kappa^{-1} \doteq n|a|$ (n being the main atomic quantum number), the r^* dependence of the corresponding wave functions at a given orbital angular momentum is the same.

Appendix B
DECAY RATE AND NORMALIZATION

The decay rate (partial width) Γ^β_n of a bound α-channel state decay into the β channel is given by the square of the wave function ψ^β_{n0} in (146) (at a distance $r^* > d$), multiplied by the product of the surface $4\pi r^{*2}$ and the relative velocity $v_\beta = k^*_\beta/\mu_\beta$:

$$\Gamma^\beta_n = 4\pi r^{*2}\frac{k^*_\beta}{\mu_\beta}|\psi^\beta_{n0}|^2 = 4\pi\frac{k^*_\beta}{\mu_\alpha}|N'(n)|^2\frac{(K^{\beta\alpha})^2}{1+(k^*_\beta K^{\beta\beta})^2}. \qquad \text{(B.1)}$$

*The account of these terms is however important at large time separations to guarantee vanishing of the Coulomb interaction at $|t^*| \to \infty$.

Note that for two identical bosons in the channel β, the twice as large square of the symmetrized wave function is compensated by twice as small surface so that the result is the same as for two nonidentical particles. In the considered two-channel case, the β channel is the only open one, so the decay rate coincides with the inverse lifetime (total width) of the bound α-channel state which can be calculated from the imaginary part of the energy $E_n = -{\kappa_n}^2/(2\mu_\alpha)$:

$$1/\tau_n \equiv \Gamma_n = -2\mathrm{Im}\, E_n \equiv 2\mathrm{Re}\,\kappa_n \mathrm{Im}\,\kappa_n/\mu_\alpha. \tag{B.2}$$

Using (140), one has (neglecting $\mathrm{Im}\, A^{\alpha\alpha}$ as compared with the $\mathrm{Re}\, A^{\alpha\alpha}$ in the correction terms)

$$\mathrm{Re}\,\kappa_n = \kappa_n^c \left[1 + 2\mathrm{Re}\, A^{\alpha\alpha}\kappa_n^c + O\Big((2\mathrm{Re}\, A^{\alpha\alpha}\kappa_n^c)^2\Big)\right], \tag{B.3}$$

$$\mathrm{Im}\,\kappa_n = 2\mathrm{Im}\, A^{\alpha\alpha}(\kappa_n^c)^2 \left\{1 + 2[\phi(n)-1]\mathrm{Re}\, A^{\alpha\alpha}\kappa_n^c - 4\pi^2 O\Big(\frac{\mathrm{Re}\, A^{\alpha\alpha}}{a}\Big)^2\right\},$$

$$\Gamma_n = \frac{4}{\mu_\alpha}\left\{1 + 2\phi(n)\mathrm{Re}\, A^{\alpha\alpha}\kappa_n^c - 4\pi^2 O\Big(\frac{\mathrm{Re}\, A^{\alpha\alpha}}{a}\Big)^2\right\}(\kappa_n^c)^3\, \mathrm{Im}\, A^{\alpha\alpha}. \tag{B.4}$$

Using the relation $(\kappa_n^c)^3 = \pi|\psi_{n0}^{\mathrm{coul}}|^2$ and (143) for $\mathrm{Im}\, A^{\alpha\alpha}$, one finally gets, in agreement with [50, 54]:

$$\Gamma_n = 4\pi\frac{k_\beta^*}{\mu_\alpha}|\psi_{n0}^{\mathrm{coul}}|^2 \left\{1 + 2\phi(n)\frac{\mathrm{Re}\, A^{\alpha\alpha}}{n|a|} - 4\pi^2 O\left(\left(\frac{\mathrm{Re}\, A^{\alpha\alpha}}{a}\right)^2\right)\right\} \times \\ \times \frac{(K^{\beta\alpha})^2}{1 + (k_\beta^* K^{\beta\beta})^2}. \tag{B.5}$$

Inserting (B.1) and (B.5) into the equality $\Gamma_n = \Gamma_n^\beta$, one proves the relation (147) between the normalization factors $\mathcal{N}'(n)$ and $\psi_{n0}^{\mathrm{coul}}(0)$.

In the case of two or more open decay channels, the two-channel (α, β) matrix $\hat{K}$ is no more real, particularly, in the presence of one additional channel j, one has:

$$K^{\alpha\alpha} = \mathcal{K}^{\alpha\alpha} + \frac{ik_j^*(\mathcal{K}^{j\alpha})^2}{1 - ik_j^*\mathcal{K}^{jj}},$$

$$K^{\beta\alpha} = \mathcal{K}^{\beta\alpha} + \frac{ik_j^*\mathcal{K}^{j\beta}\mathcal{K}^{j\alpha}}{1 - ik_j^*\mathcal{K}^{jj}}, \tag{B.6}$$

$$K^{\beta\beta} = \mathcal{K}^{\beta\beta} + \frac{ik_j^*(\mathcal{K}^{j\beta})^2}{1 - ik_j^*\mathcal{K}^{jj}},$$

where $\mathcal{K}^{\lambda\lambda'}$ are the elements of a real three-channel matrix $\mathcal{K}$. Note that in the case of a two-pion system ($\alpha = \pi^+\pi^-$, $\beta = \pi^0\pi^0$), the third channel is $j = \gamma\gamma$ so that the elements $\mathcal{K}^{j\beta}$ and $\mathcal{K}^{jj}$ can be safely neglected. Then, only the element $K^{\alpha\alpha}$ acquires the imaginary part: $K^{\alpha\alpha} = \mathcal{K}^{\alpha\alpha} + ik_j^*(\mathcal{K}^{j\alpha})^2$.

Generally, one has to account for the possible imaginary parts of the elements of the two-channel K matrix, as well as for a possibility of a pure imaginary value of the momentum k_β^* in the case of a closed channel β ($k_\beta^{*2} < 0$, $k_\beta^* = i(-k_\beta^{*2})^{1/2}$, $\Gamma_n^\beta = 0$). Then

$$\begin{aligned}\operatorname{Re} A^{\alpha\alpha} &= \operatorname{Re} K^{\alpha\alpha} - \left\{\operatorname{Im} k_\beta^* \operatorname{Re}(K^{\beta\alpha})^2 + \operatorname{Re} k_\beta^* \operatorname{Im}(K^{\beta\alpha})^2 + \right. \\ &\left. + \left|k_\beta^*\right|^2 \left[\operatorname{Re} K^{\beta\beta} \operatorname{Re}(K^{\beta\alpha})^2 + \operatorname{Im} K^{\beta\beta} \operatorname{Im}(K^{\beta\alpha})^2\right]\right\} \left|1 - ik_\beta^* K^{\beta\beta}\right|^{-2}, \quad \text{(B.7)}\end{aligned}$$

$$\begin{aligned}\operatorname{Im} A^{\alpha\alpha} &= \operatorname{Im} K^{\alpha\alpha} - \left\{\operatorname{Im} k_\beta^* \operatorname{Im}(K^{\beta\alpha})^2 - \operatorname{Re} k_\beta^* \operatorname{Re}(K^{\beta\alpha})^2 + \right. \\ &\left. + \left|k_\beta^*\right|^2 \left[\operatorname{Re} K^{\beta\beta} \operatorname{Im}(K^{\beta\alpha})^2 + \operatorname{Im} K^{\beta\beta} \operatorname{Re}(K^{\beta\alpha})^2\right]\right\} \left|1 - ik_\beta^* K^{\beta\beta}\right|^{-2} = \\ &= k_\beta^* \left|\frac{K^{\beta\alpha}}{1 - ik_\beta^* K^{\beta\beta}}\right|^2 \theta\left(k_\beta^{*2}\right) + \sum_j k_j \left|\frac{Df_c^{j\alpha}}{1 - ik_\beta^* K^{\beta\beta}}\right|^2 = \\ &= \frac{\mu_\alpha}{4\pi|N'(n)|^2} \left[\Gamma_n^\beta + \sum_j \Gamma_n^j\right], \quad \text{(B.8)}\end{aligned}$$

where $\theta(x) = 1$ for $x \geqslant 0$, $\theta(x) = 0$ for $x < 0$. The second expression for $\operatorname{Im} A^{\alpha\alpha}$ in (B.8) follows from a straightforward though lengthy matrix algebra and, the last one — from an obvious generalization of (B.1) using the relation $K^{\beta\alpha} = Df_c^{\beta\alpha}$. Inserting the last equality in (B.8) into (B.4), one proves (147) for the case of any number of open decay channels.

REFERENCES

1. *Adeva B. et al.* (*DIRAC Collab.*). Lifetime Measurement of $\pi^+\pi^-$ Atoms to Test Low-Energy QCD Predictions. Proposal to the SPSLC, CERN/SPSLC 95-1. Updated 10 Nov. 1995.
2. *Adeva B. et al.* (*DIRAC Collab.*). Lifetime Measurement of $\pi^+\pi^-$ and $\pi^\pm K^\mp$ Atoms to Test Low-Energy QCD. CERN-SPSC-2004-009, SPSC-P-284 Add. 4. 2004.
3. *Adeva B. et al.* (*DIRAC Collab.*) // J. Phys. G. 2004. V. 30. P. 1929.
4. *Adeva B. et al.* (*DIRAC Collab.*) // Phys. Lett. B. 2005. V. 619. P. 50.
5. *Nagels M. N. et al.* // Nucl. Phys. B. 1979. V. 147. P. 189.

6. *Pislak S. et al.* (*E865 Collab.*) // Phys. Rev. Lett. 2001. V. 87. P. 221801.

7. *Batley J. R. et al.* (*NA48/2 Collab.*) // Phys. Lett. B. 2006. V. 633. P. 173.

8. *Colangelo G., Gasser J., Leutwyler H.* // Nucl. Phys. B. 2001. V. 603. P. 125.

9. *Knecht M. et al.* // Nucl. Phys. B. 1995. V. 457. P. 513;
Knecht M. et al. // Nucl. Phys. B. 1996. V. 471. P. 445.

10. *Nemenov L.* // Yad. Fiz. 1985. V. 41. P. 980.

11. *Lyuboshitz V. L.* // Yad. Fiz. 1988. V. 48. P. 1501; Sov. J. Nucl. Phys. 1988. V. 48. P. 956.

12. *Lednicky R., Lyuboshitz V. L.* // Yad. Fiz. 1982. V. 35. P. 1316; Sov. J. Nucl. Phys. 1982. V. 35. P. 770;
Lednicky R., Lyuboshitz V. L. // Proc. of Workshop on Part. Correlations and Interferometry in Nuclear Collisions. Nantes, France, 1990. P. 42.

13. *Lednicky R.* // Proc. of Workshop on Hadronic Atoms. ITP, University of Bern, Oct. 14–15, 1999; hep-ph/9911339.

14. *Afanasyev L., Voskresenskaya O.* // Phys. Lett. B. 1999. V. 453. P. 302.

15. *Podgoretsky M. I.* // Fiz. Elem. Chast. At. Yad. 1989. V. 20. P. 628; Sov. J. Part. Nucl. 1989. V. 20. P. 266.

16. *Lorstad B.* // J. Mod. Phys. A. 1989. V. 4. P. 2861.

17. *Boal D. H., Gelbke C.-K., Jennings B. K.* // Rev. Mod. Phys. 1990. V. 62. P. 553.

18. *Wiedemann U. A., Heinz U.* // Phys. Rep. 1999. V. 319. P. 145.

19. *Csörgö T.* // Heavy Ion Phys. 2002. V. 15. P. 1.

20. *Lednicky R.* // Phys. At. Nucl. 2004. V. 67. P. 71.

21. *Lisa M. et al.* // Ann. Rev. Nucl. Part. Sci. 2005. V. 55. P. 357.

22. *Lednicky R.* // Braz. J. Phys. 2007. V. 37. P. 939.

23. *Erazmus B. et al.* // Nucl. Phys. A. 1995. V. 583. P. 395;
Martin L. et al. // Nucl. Phys. A. 1996. V. 604. P. 69;
Lednicky R. // Nukleonika. 1998. V. 43. P. 345.

24. *Schweber S. S., Bethe H. A., Hoffmann F.* Mesons and Fields. V. 1. Fields. N. Y.: Row, Peterson and Comp., 1955. Sec. 25.6.

25. *Landau L. D., Lifshitz E. M.* Quantum Mechanics: Nonrelativistic Theory. 3rd Ed. Oxford: Pergamon Press, 1977. Sec. 136.

26. *Migdal A. B.* // Zh. Eksp. Theor. Fiz. 1955. V. 28. P. 3; 10; Sov. Phys. JETP. 1955. V. 1. P. 2; 7.

27. *Anisovich V. V., Dakhno L. G., Makarov M. M.* // Yad. Fiz. 1980. V. 32. P. 1521; Sov. J. Nucl. Phys. 1980. V. 32. P. 788.

28. *Bass S. A. et al.* // Prog. Part. Nucl. Phys. 1998. V. 41. P. 225.

29. *Smolik J.* PhD Thesis. Prague: Charles Univ., 2005.

30. *Akkelin S. V., Lednicky R., Sinyukov Yu. M.* // Phys. Rev. C. 2002. V. 65. P. 064904.

31. *Lednicky R. et al.* // Phys. Rev. C. 2000. V. 61. P. 034901.

32. *Ridky J.* // Fortschr. Phys. 1988. V. 36. P. 707.

33. *Sinyukov Yu. M. et al.* // Phys. Lett. B. 1998. V. 432. P. 248.

34. *Pratt S.* // Phys. Rev. Lett. 1984. V. 53. P. 1219;
Pratt S. // Phys. Rev. D. 1986. V. 33. P. 1314;
Pratt S., Csörgö T., Zimanyi J. // Phys. Rev. C. 1990. V. 42. P. 2646.

35. *Makhlin A. N., Sinyukov Yu. M.* // Yad. Fiz. 1987. V. 46. P. 637;
Makhlin A. N., Sinyukov Yu. M. // Z. Phys. C. 1988. V. 39. P. 69.
Sinyukov Yu. M. // Nucl. Phys. A. 1989. V. 498. P. 151c.

36. *Podgoretsky M. I.* // Sov. J. Nucl. Phys. 1983. V. 37. P. 272;
Lednicky R. JINR Commun. B2-3-11460. Dubna, 1978;
Grassberger P. // Nucl. Phys. B. 1977. V. 120. P. 231.

37. *Bertsch G.F., Danielewicz P., Herrmann M.* // Phys. Rev. C. 1994. V. 49. P. 442;
Pratt S. Quark Gluon Plasma 2 / Ed. R. C. Hwa. Singapore, 1995. P. 700;
Chapman S., Scotto P., Heinz U. // Phys. Rev. Lett. 1995. V. 74. P. 4400.

38. *Csörgö T., Pratt S.* // Proc. of the Relativistic Heavy-Ion Physics at Present and Future Accelerators. Budapest, 1991; KFKI-1991-28/A. P. 75.

39. *Adams J. et al.* (*STAR Collab.*) // Phys. Rev. C. 2005. V. 71. P. 044906.

40. *Brown D. A., Danielewicz P.* // Phys. Rev. C. 1998. V. 57. P. 2474;
Brown D. A. et al. // Phys. Rev. C. 2005. V. 72. P. 054902;
Chung P., Danielewicz P. // Intern. J. Mod. Phys. E. 2008. V. 16. P. 3286.

41. *Abelev B. I. et al.* (*STAR Collab.*) // Phys. Rev. C. 2006. V. 74. P. 054902.

42. *Lednicky R. et al.* // Phys. Lett. B. 1996. V. 373. P. 30.

43. *Adams J. et al.* (*STAR Collab.*) // Phys. Rev. Lett. 2003. V. 91. P. 262302.

44. *Csanad M. et al.* // J. Phys. G. 2004. V. 30. P. S1079.

45. *Gmitro M. et al.* // Czech. J. Phys. B. 1986. V. 36. P. 1281.

46. *Ananthanarayan B. et al.* // Phys. Rep. 2001. V. 353. P. 207.

47. *Adams J. et al.* (*STAR Collab.*) // Phys. Rev. C. 2006. V. 74. P. 064906.

48. *Lednicky R., Lyuboshitz V. V., Lyuboshitz V. L.* // Phys. At. Nucl. 1998. V. 61. P. 2050.

49. *Lednicky R., Progulova T. B.* // Z. Phys. C. 1992. Bd. 55. S. 295.

50. *Rasche G., Woolcock W. S.* // Nucl. Phys. A. 1982. V. 381. P. 405.

51. *Amirkhanov I. et al.* // Phys. Lett. B. 1999. V. 452. P. 155.

52. *Gashi A., Rasche G., Woolcock W. S.* // Phys. Lett. B. 2001. V. 513. P. 269.

53. *Jackson J. D., Blatt J. O.* // Rev. Mod. Phys. 1950. V. 22. P. 77.

54. *Moor U., Rasche G., Woolcock W. S.* // Nucl. Phys. A. 1995. V. 587. P. 747.